Electronic Supporting Information

For
Catalytic Synergy Using Al(III) and Group 1 Metals to Accelerate Epoxide and Anhydride Ring Opening Copolymerizations

Wilfred T. Diment [a], Georgina L. Gregory [a], Ryan W. F. Kerr [a], Andreas Phanopoulos [a], Antoine Buchard [b], Charlotte K. Williams[a]*

[a]Chemistry Research Laboratory, Department of Chemistry, University of Oxford, 12 Mansfield Road, Oxford, OX1 3TA, UK.

[b] Department of Chemistry, University of Bath, Claverton Down, Bath BA2 7AY, UK

General Procedures and Materials

All manipulations were carried out in a nitrogen filled glovebox, or dual manifold nitrogen-vacuum Schlenk line. Solvents used for synthesis were collected from a solvent purification system (SPS), degassed with freeze-pump-thaw cycles and stored over 3 Å molecular sieves under an inert atmosphere, unless otherwise stated. All materials were stored under a nitrogen atmosphere, in a glovebox. Triethyl aluminium (93%) was purchased from Sigma-Aldrich and was used as received. Group 1 acetate salts were purchased from Sigma Aldrich or Acros Organics and were dried at 100 °C for 16 hours before use.

All epoxides (cyclohexene oxide (CHO, Acros Organics), propylene oxide (PO, Sigma Aldrich), vinyl-cyclohexene oxide (vCHO, Sigma Aldrich), *tert*-butyl glycidyl ether (tBGE, Sigma Aldrich), allyl glycidyl ether (AGE, Sigma Aldrich) and styrene oxide (SO, Sigma Aldrich)) were purified by stirring over calcium hydride followed by fractional distillation. Purification of phthalic anhydride (PA, Sigma Aldrich) was achieved though stirring in dry toluene. The supernatant was filtered, and the toluene subsequently removed *in vacuo*. The resultant white powder recrystallised from hot (60 °C) chloroform and subsequently sublimed under vacuum at 80 °C. Norbornene anhydride (NBA, Acros Organics) was purified through recrystallisation from dry ethyl acetate, followed by sublimation at 80 °C. Tricyclic anhydride (TCA) was synthesised according to a literature procedure, and was purified through recrystallisation from hexane followed by sublimation at 80 °C.[1]

The pro-ligand, [$L_{van}H_2$], was synthesised through the Schiff base condensation reaction of *o*-vanillin with 2,2-dimethyl-1,3-propanediamine.[2] Synthesis of the salen pro-ligand, [$L_{sal}H_2$], was achieved following a literature procedure.[3]

Methods

NMR Spectroscopy: ^{1}H NMR and [27]Al spectra were obtained using a Bruker Avance III HD 400 NMR spectrometer. ^{13}C{^{1}H} NMR were obtained with either Bruker AV III HD 500 MHz NMR, Bruker NEO 600 MHz with broadband helium cryprobe, or Bruker AVIII 700 MHz with inverse TCI 1H/13C/15N cryoprobe spectrometers.

GPC analysis: Carried out using a Shimadzu LC-20AD instrument, equipped with a Refractive Index (RI) detector and two PSS SDV 5 μm linear M columns. The eluent used was HPLC-grade THF, heated to 30 °C, and with a flow rate of 1.0 mL min^{-1}.

MALDI-ToF spectrometry: Carried out on a Bruker Autoflex Speed MALDI-ToF spectrometer. Samples were prepared by preparing a 1:4:1 solution of polymer (10 mg mL^{-1} in THF), dithranol (10 mg mL^{-1} in THF) and KTFA (10 mg mL^{-1} in THF). This solution was spotted twice on a MALDI plate and allowed to dry completely before analysis was undertaken.

Elemental analysis was carried out by Elemental Microanalysis Ltd, Hameldown Road, Okehampton Business Park, Exeter Road, Okehampton, Devon, EX20 1UB.

X-Ray Crystallography: Crystallographic data were collected, and structures solved, by Dr. Ryan Kerr and Dr. Andreas Phanopoulos. Air sensitive crystalline samples were isolated in a nitrogen filled glovebox and immersed in fluorinated oil. Crystalline samples were mounted on a MiTeGen Micromount, and cooled to 150 K with dry nitrogen using an Oxford Cryosystem.[4] Data was collected using an Oxford Diffraction Supernova diffractometer using Cu K$_\alpha$ (λ = 1.5417 Å) or Mo K$_\alpha$ (λ = 0.7107 Å) radiation. The resulting reflection data was processed with CrysAlis Pro.[5] The crystal structures were solved using the SHELXT program and least-square refined using the SHELXL program within the Olex2 system suite.[6-8]

Synthesis of Complexes

Synthesis of L$_{van}$AlOAc

The synthesis of L$_{van}$AlOAc was conducted using a modified literature preparation.[9] Under inert conditions, AlEt$_3$ (191 mg, 1.67 mmol) was added to a stirred solution of L$_{van}$H$_2$ (550 mg, 1.48 mmol) in THF (5 mL) at room temperature, and stirred for 2 hours. Subsequently, glacial acetic acid (85 μL, 1.48 mmol) was added, and the reaction was stirred for 16 hours at room temperature, resulting in the formation of a yellow precipitate. The precipitate was isolated *via* centrifuge, and subsequently washed with THF (1 x 10 mL) and hexane (1 x 10 mL) before being dried under vacuum, to give L$_{van}$AlOAc as a pale yellow precipitate (496 mg, 1.09 mmol, 74%). The NMR spectra were consistent with those previously reported.[9]

Synthesis of L$_{van}$AlNa(OAc)$_2$ (1)

Under inert conditions, NaOAc (17 mg, 0.21 mmol) was added to a stirred solution of L$_{van}$AlOAc (95 mg, 0.21 mmol) in chloroform (5 mL) at room temperature, and stirred for 16 hours. The solvent was removed, and the crude product purified by recrystallisation from a saturated solution of dichloromethane layered with hexane, to give complex **1** as pale yellow crystals. (72 mg, 0.13 mmol, 64%). Diffraction quality crystals were obtained through the same recrystallisation method.

^{1}H NMR (CD$_2$Cl$_2$, 400 MHz, 298 K): δ 7.94 (2H, s, H^e), 6.81 (2H, d, J = 7.6 Hz, H^d), 6.65 (2H, d, J = 7.6 Hz, H^b), 6.60 (2H, t, J = 7.6 Hz, H^c), 3.70 (4H, s, H^f), 3.23 (6H, s, H^a), 1.57 (6H, s, H^h), 1.15 (6H, s, H^g) ppm. **^{13}C NMR** (CD$_2$Cl$_2$, 176 Hz, 298 K): δ 174.2 (C^l), 167.5 (C^h), 155.7 (C^g), 150.8 (C^b), 125.6 (C^e), 119.5 (C^f), 114.4 (C^d or C^c), 114.5 (C^d or C^c), 74.3 (C^i), 55.5 (C^a), 35.2 (C^j), 25.0 (C^m), 24.7 (C^k) ppm. **^{27}Al NMR** (CD$_2$Cl$_2$, 104 MHz, 298 K): δ -1.0 ppm. **Anal. Calc.** (C$_{25}$H$_{30}$AlNaN$_2$O$_8$); C, 55.97; H, 5.64; N, 5.22 %. Found: C, 56.25; H, 5.48; N, 5.29 %.

Synthesis of L$_{van}$AlK(OAc)$_2$ (2)

Under inert conditions, KOAc (18 mg, 0.18 mmol) was added to a stirred solution of L$_{van}$AlOAc (85 mg, 0.18 mmol) in chloroform at room temperature, and stirred for 16 hours. Subsequently, the solution was filtered, and the solvent removed under vacuum to give **2** as a pale yellow powder (102 mg, 0.18 mmol, 98%). Diffraction quality crystals were grown from a saturated solution of **2** in chlorform, layered with hexane.

^{1}H NMR (CDCl$_3$, 400 MHz, 298 K): δ 7.90 (2H, s, H^e), 6.78 (2H, dd, J = 7.9, 1.2 Hz, H^d), 6.63 (2H, d, J = 7.9 Hz, H^b), 6.52 (2H, t, J = 7.9 Hz, H^c), 3.75 (4H, s, H^f), 3.39 (6H, s, H^a), 1.53 (6H, s, H^h), 1.20 (6H, s, H^g) ppm. **^{13}C NMR** (CDCl$_3$, 151 MHz, 298 K): δ 173.5 (C^l), 166.7 (C^h), 156.4 (C^g), 151.1 (C^b), 125.2 (C^e), 120.0 (C^f), 114.1 (C^d), 113.7 (C^c), 74.0 (C^i), 55.2 (C^a), 35.6 (C^j), 24.9 (C^k), 24.2 (C^m) ppm. **^{27}Al NMR** (CDCl$_3$, 104 MHz, 298 K): δ -1.2 ppm. **Anal. Calc.** (C$_{25}$H$_{30}$AlKN$_2$O$_8$); C, 54.34; H, 5.47; N, 5.07 %. Found: C, 54.70; H, 5.59; N, 4.74 %.

Synthesis of L$_{van}$AlRb(OAc)$_2$ (3)

Under inert conditions, RbOAc (16 mg, 0.11 mmol) was added to a stirred solution of L$_{van}$AlOAc (55 mg, 0.11 mmol) in chloroform at room temperature, and stirred for 16 hours. Subsequently, the solution was filtered, and the solvent removed under vacuum. The crude product was washed with toluene (1 x 10 mL), and subsequently dried under vacuum to give **3** as a pale yellow powder (57 mg, 0.95 mmol, 86%). Diffraction quality crystals were grown from a saturated solution of **3** in chloroform, layered with hexane.

^{1}H NMR (CDCl$_3$, 400 MHz, 298 K): δ 7.92 (2H, s, H^e), 6.79 (2H, d, J = 7.9 Hz, H^d), 6.66 (2H, d, J = 7.9 Hz, H^b), 6.53 (2H, t, J = 7.9 Hz, H^c), 3.73 (4H, s, H^f), 3.46 (6H, s, H^a), 1.59 (6H, s, H^h), 1.18 (6H, s, H^g) ppm. **^{13}C NMR** (CDCl$_3$, 126 MHz, 298 K): δ 173.9 (C^l), 167.0 (C^h), 156.4 (C^g), 151.1 (C^b), 125.3 (C^e), 120.0 (C^f), 114.4 (C^d). 114.0 (C^c), 73.4 (C^i), 55.0 (C^a), 35.7 (C^j), 25.1 (C^k), 23.8

(C^m) ppm. **^{27}Al NMR** (CDCl$_3$, 104 MHz, 298 K): δ -2.1 ppm. **Anal. Calc.** (C$_{25}$H$_{30}$AlRbN$_2$O$_8$); C, 50.13; H, 5.05; N, 4.68 %. Found: C, 50.17; H, 4.8.; N, 4.61 %.

Synthesis of L$_{van}$AlCs(OAc)$_2$ (4)

Under inert conditions, CsOAc (39 mg, 0.20 mmol) was added to a stirred solution of L$_{van}$AlOAc (95 mg, 0.20 mmol) in chloroform at room temperature, and stirred for 16 hours. Subsequently the solvent removed under vacuum to give **4** as a pale yellow powder (131 mg, 0.20 mmol, 99%). Diffraction quality crystals were grown from a saturated solution of **4** in chloroform, layered with hexane.

^{1}H NMR: (CDCl$_3$, 400 MHz, 298 K): δ 7.94 (2H, s, H^e), 6.80 (2H, d, J = 7.9 Hz, H^d), 6.71 (2H, d, J = 7.9 Hz, H^b), 6.54 (2H, t, J = 7.9 Hz, H^c), 3.71 (4H, s, H^f), 3.51 (6H, s, H^a), 1.58 (6H, s, H^h), 1.18 (6H, s, H^g) ppm. **^{13}C NMR** (CDCl$_3$, 126 MHz, 298 K): δ 174.1 (C^l) 167.4 (C^h), 156.4 (C^g), 151.1 (C^b), 125.6 (C^e), 120.2 (C^f), 114.6 (C^d). 114.2 (C^c), 72.8 (C^i), 54.8 (C^a), 35.7 (C^j), 25.5 (C^k), 23.9 (C^m) ppm. **^{27}Al NMR** (CDCl$_3$, 104 MHz, 298 K): δ -2.5 ppm. **Anal. Calc.** (C$_{25}$H$_{30}$AlCsN$_2$O$_8$); C, 46.45; H, 4.68; N, 4.33 %. Found: C, 46.85; H, 4.55; N, 4.38 %.

Synthesis of L$_{sal}$Al(OAc)

[L$_{sal}$AlEt] was synthesised following an adapted literature procedure.[10] Under inert conditions, AlEt$_3$ (113 mg, 0.99 mmol) was added to a stirred solution of [L$_{sal}$H$_2$] (493 mg, 0.92 mmol) in hexane (5 mL) at room temperature, and stirred for 16 hours, resulting in the formation [L$_{sal}$AlEt] as a yellow precipitate. The precipitate was isolated *via* centrifuge, and a crude yield was recorded (137 mg, 0.23 mmol, 25%). The crude product was subsequently dissolved in toluene before glacial acetic acid (15 μL, 0.23 mmol) was added, and the reaction was stirred for 16 hours at room temperature, resulting in the formation of a yellow precipitate. The precipitate was isolated *via* centrifuge, and subsequently washed with hexane (1 x 10 mL)

before being dried under vacuum, to give [L_{sal}Al(OAc)] as a pale yellow precipitate (0.117 g, 0.19 mmol, 83%).

¹H NMR: (CDCl$_3$, 400 MHz, 298 K): δ 8.11 (2H, s, H^e), 7.48 (2H, d, J = 2.6 Hz, H^b), 7.06 (2H, d, J = 2.6 Hz, H^d), 3.53 (2H, d, J = 11.5 Hz, H^f or H^g), 3.32 (2H, d, J = 11.5 Hz, H^f or H^g), 1.90 (3H, s, H^j), 1.40 (9H, s, H^c), 1.30 (9H, s, H^d), 1.15 (3H, s, H^h), 0.98 (3H, s, H^i) ppm. **¹³C NMR** (CDCl$_3$, 176 MHz, 298 K): δ 186.7 (C^p), 170.0 (C^k), 163.9 (C^h), 140.8 (C^c), 137.4 (C^e), 130.6 (C^d), 127.5 (C^f), 118.5 (C^g), 67.9 (C^l), 36.8 (C^m), 35.4 (C^n), 34.1 (C^i), 31.6 (C^a), 29.7 (C^j), 26.3 (C^n or C^o), 25.7 (C^n or C^o), 20.5 (C^q) ppm. **²⁷Al NMR** (CDCl$_3$, 104 MHz, 298 K): δ 16.3 ppm. **Anal. Calc.** (C$_{25}$H$_{30}$AlNaN$_2$O$_8$); C, 71.81; H, 8.96; N, 4.53 %. Found: C, 70.43; H, 8.92; N, 4.13 %.

Synthesis of L$_{van}$AlK(OBz)$_2$ (5)

The synthesis of L$_{van}$AlOBz was carried out in an analogous manner to L$_{van}$AlOAc, with benzoic acid used in place of acetic acid. under inert conditions, benzoic acid (57 mg, 0.47 mmol) was added to a stirred solution of L$_{van}$AlEt (198 mg, 0.47 mmol) in THF (5 mL) and heated for 16 hours at 60 °C, resulting in the formation of a yellow precipitate. The precipitate was isolated *via* centrifuge and washed with hexane (1 x 5 mL) to yield L$_{van}$AlOBz as a yellow powder (202 mg, 0.39 mmol, 84%), and was used without further purification. Under inert conditions, KOBz (35 mg, 0.22 mmol) was added to a stirred solution of L$_{van}$AlOBz (113 mg, 0.22 mmol) in dry chloroform at room temperature, and stirred for 16 hours. Subsequently, the reaction solution was filtered, and the solvent removed under vacuum to give **5** as a pale yellow powder (127 mg, 0.19 mmol, 86%). A ¹H NMR was taken of the crude product to confirm formation. Diffraction quality crystals were grown from a saturated solution of **5** in THF layered with hexane. This complex was not utilised in catalysis and so further characterisation was not undertaken.

¹H NMR: (CDCl$_3$, 400 MHz, 298 K): δ 8.01 (2H, s, H^e), 7.73 (4H, d, J = 7.4 Hz, H^h), 7.31 (2H, t, H^j), 7.23 (4H, t, J = 7.4 Hz, H^i), 6.71 (2H, d, J = 7.7 Hz, H^d or H^b), 6.45 (2H, d, J = 7.7 Hz, H^d or H^b), 6.37 (2H, t, J = 7.7 Hz, H^c), 3.96 (4H, s, H^f), 3.30 (6H, s, H^a), 1.35 (6H, s, H^g) ppm.

Representative Polymerization

Inside a nitrogen filled glovebox, the catalyst and desired monomers were added to a dried vial equipped with a magnetic stirrer bar. The vial was sealed with a melamine-cap containing a Teflon inlay, and further sealed with first Parafilm M and then electrical insulation tape. This sealed vial was then heated to 100 °C for the time stated. Aliquoting was performed by first cooling the polymerisation vial in a cold water bath, before removing *ca.* 10 μL of the polymerisation mixture with a syringe in the glovebox. The polymerisations were quenched by exposing the reaction mixture to air, followed by removal of volatiles. A ¹H NMR spectrum of the crude product was measured in CDCl$_3$. GPC samples were prepared by dissolving *ca.* 10 mg of the crude product in 1 mL HPLC grade THF and filtered before use. Polymers were purified by precipitation from methanol and dried under vacuum at 40 °C.

Figure S1. ^{1}H NMR Spectrum (400 MHz, 298 K, CD$_2$Cl$_2$(*)) of complex **1**.

Figure S2. ^{13}C NMR Spectrum (400 MHz, 298 K, CD$_2$Cl$_2$(*)) of complex **1**.
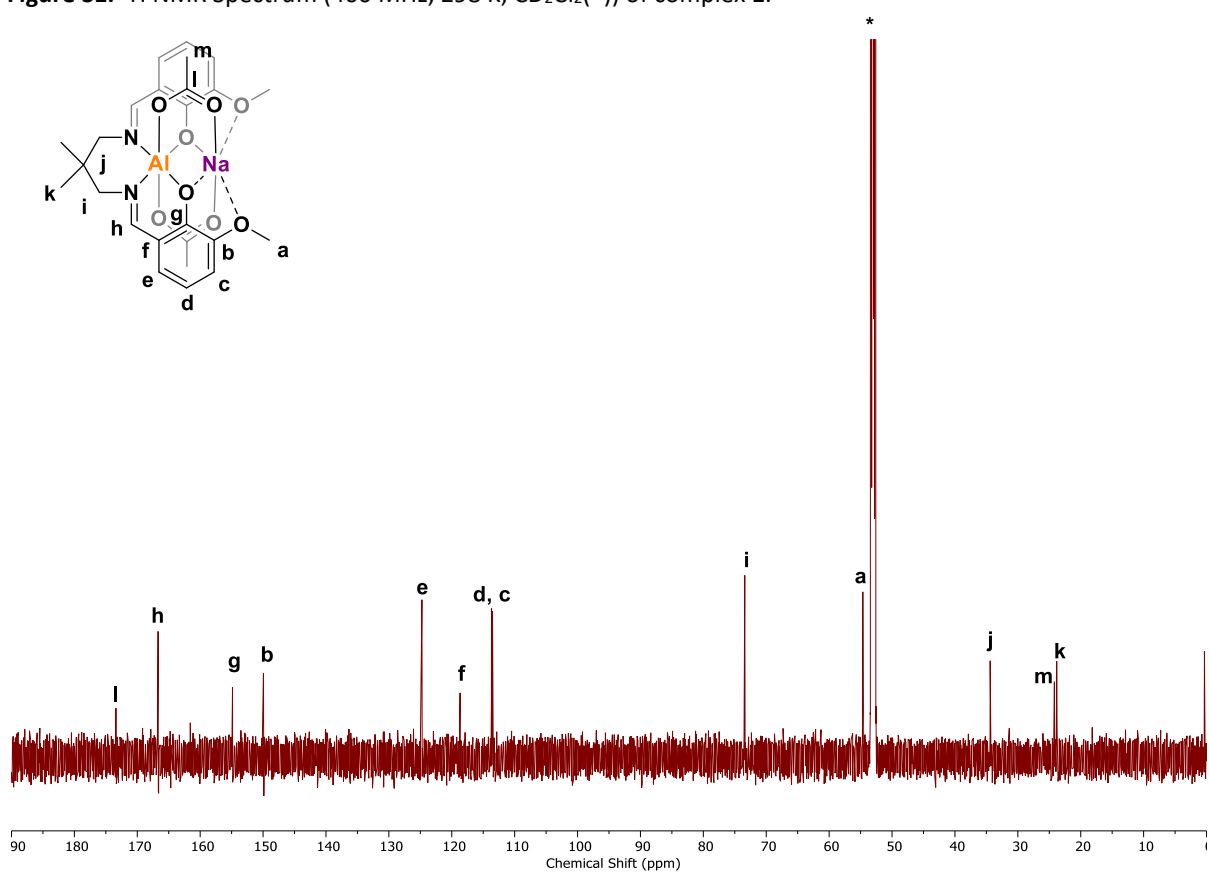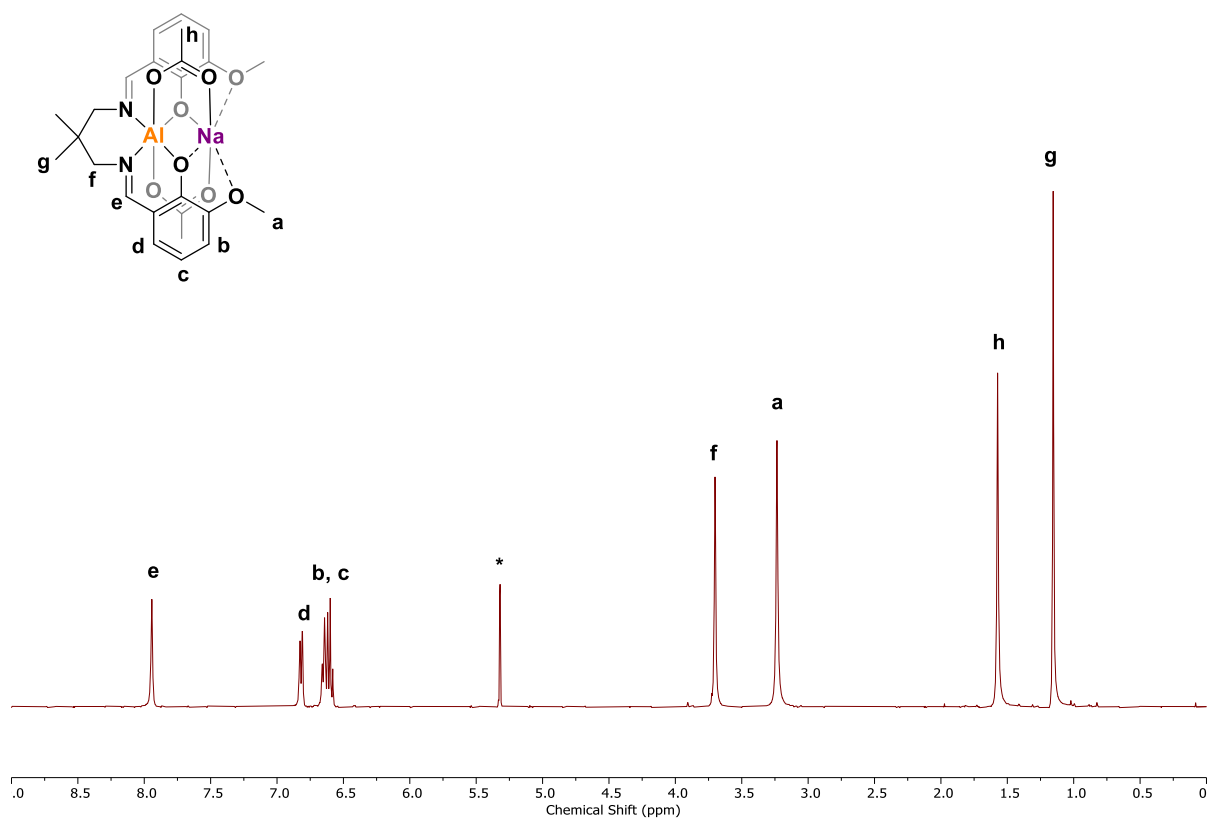
Figure S3. ^{27}Al NMR Spectrum (104 MHz, 298 K, CD_2Cl_2) of complex **1**.

Figure S4. ^{1}H COSY NMR Spectrum (400 MHz, 298 K, CD_2Cl_2) of complex **1**.

Figure S5. ^1H-^{13}C HSQC NMR Spectrum (298 K, CD_2Cl_2) of complex **1**.

Figure S6. ^1H-^{13}C HMBC NMR Spectrum (298 K, CD_2Cl_2) of complex **1**.

Figure S7. ^{1}H NMR Spectrum (400 MHz, 298 K, CDCl$_3$(*)) of complex **2**.
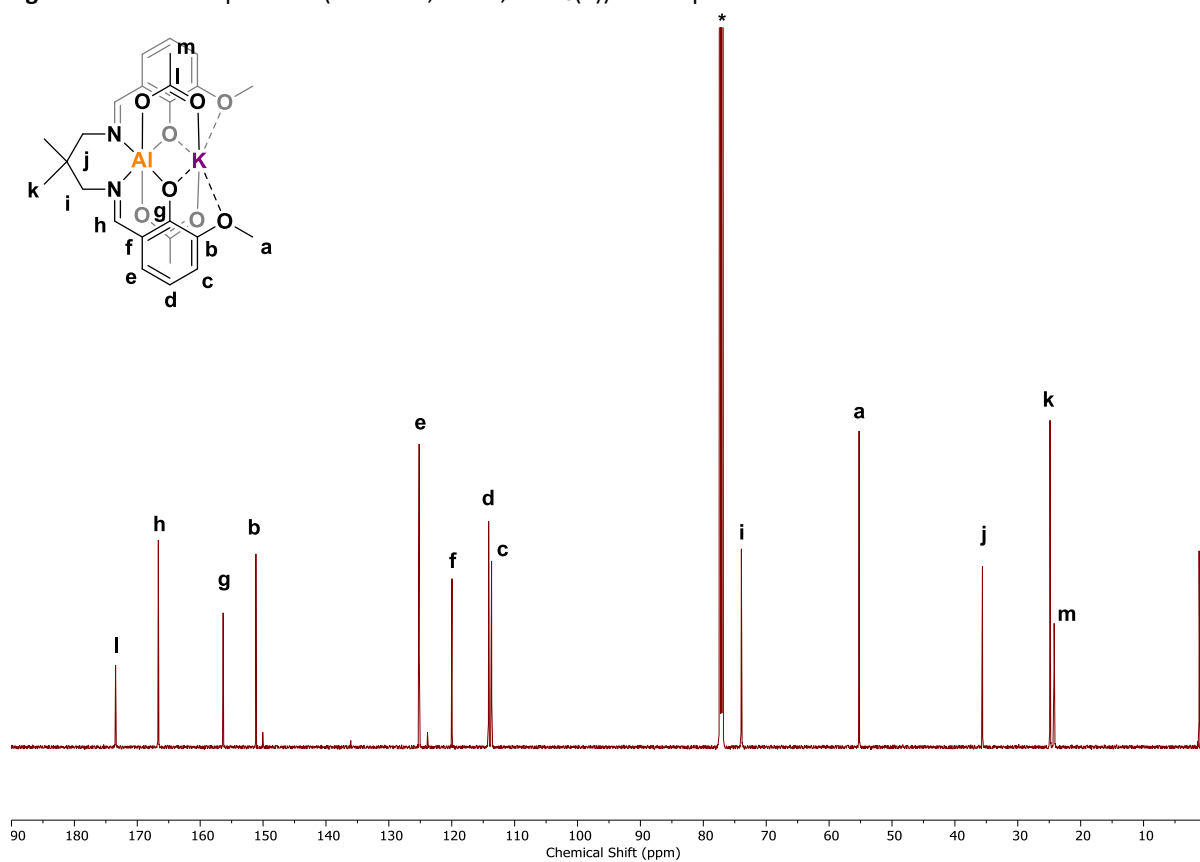
Figure S8. ^{13}C NMR Spectrum (151 MHz, 298 K, CDCl$_3$(*)) of complex **2**.
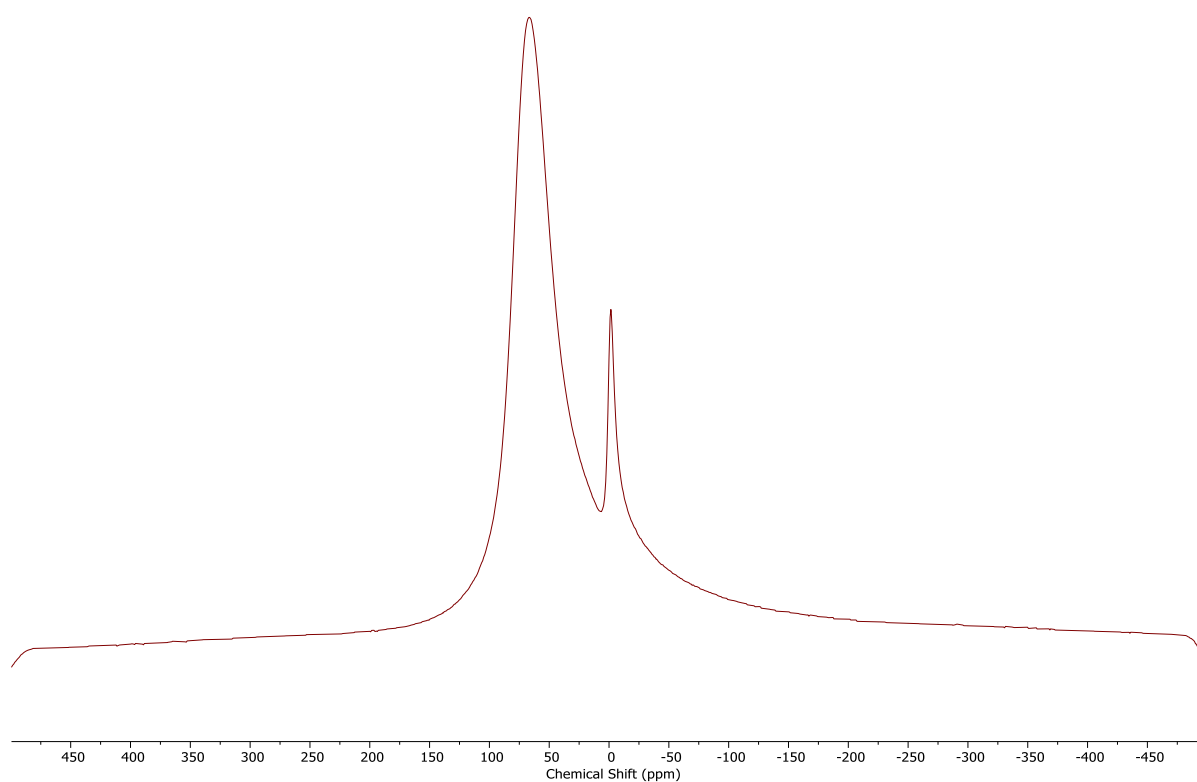
Figure S9. ^{27}Al NMR Spectrum (104 MHz, 298 K, CDCl$_3$) of complex **2**.
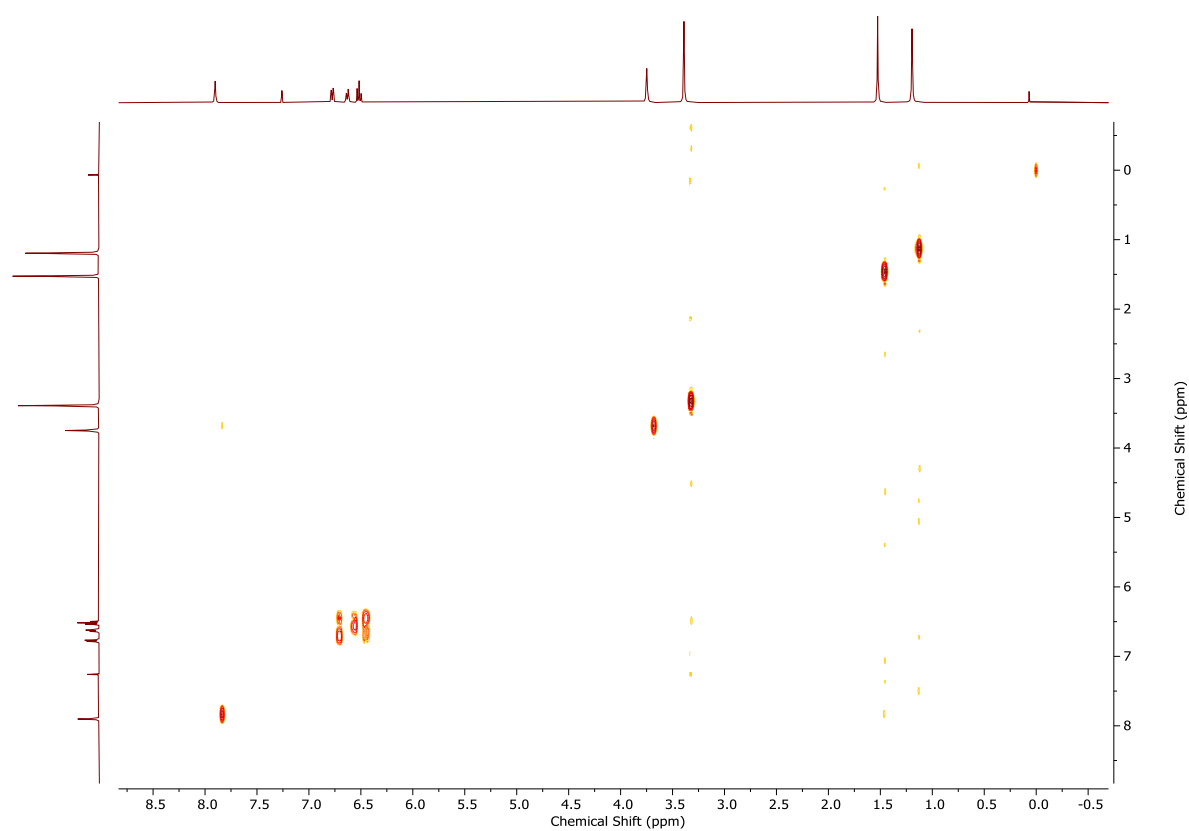
Figure S10. ^{1}H COSY NMR Spectrum (400 MHz, 298 K, CDCl$_3$) of complex **2**.
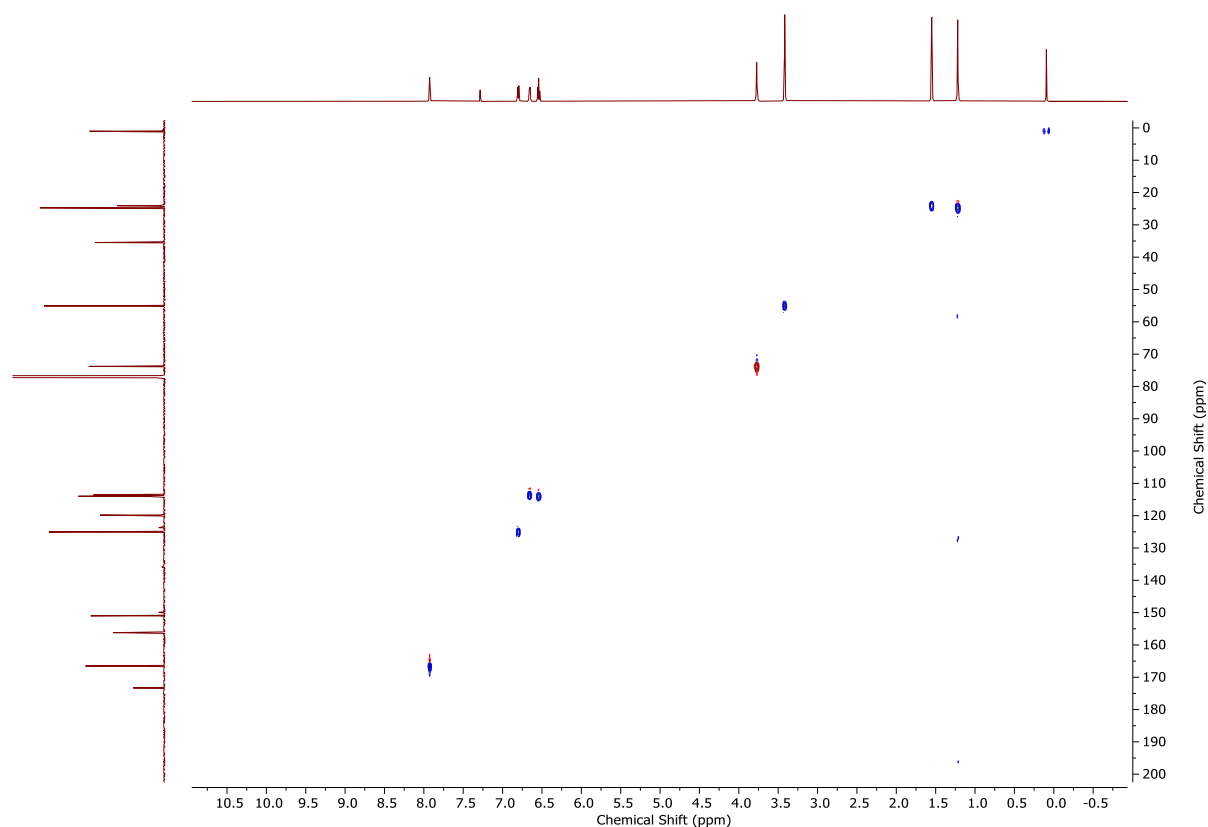
Figure S11. ^{1}H-^{13}C HSQC NMR Spectrum (298 K, CDCl$_3$) of complex **2**.
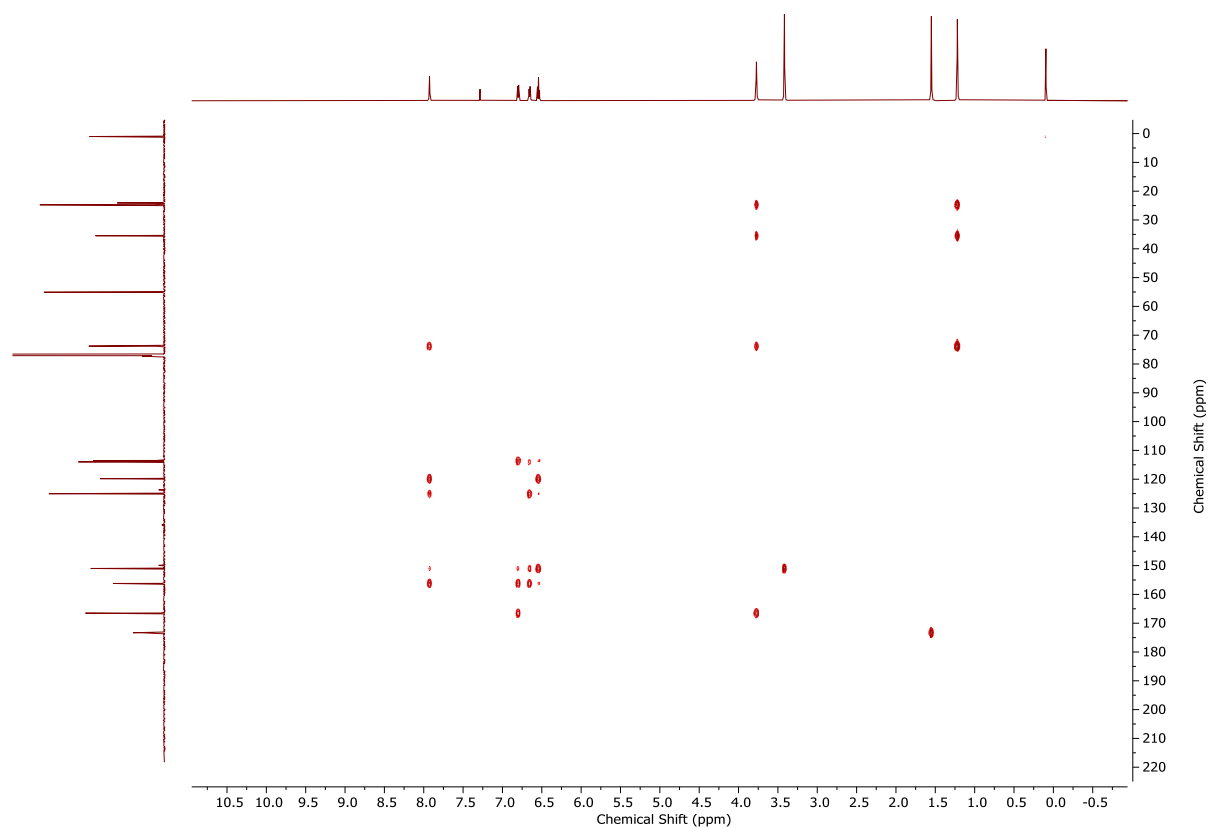
Figure S12. ^{1}H-^{13}C HMBC NMR Spectrum (298 K, CDCl$_3$) of complex **2**.

Figure S13. ^{1}H NMR Spectrum (400 MHz, 298 K, CDCl$_3$(*)) of complex **3**.

Figure S14. ^{13}C NMR Spectrum (400 MHz, 298 K, CDCl$_3$(*)) of complex **3**.
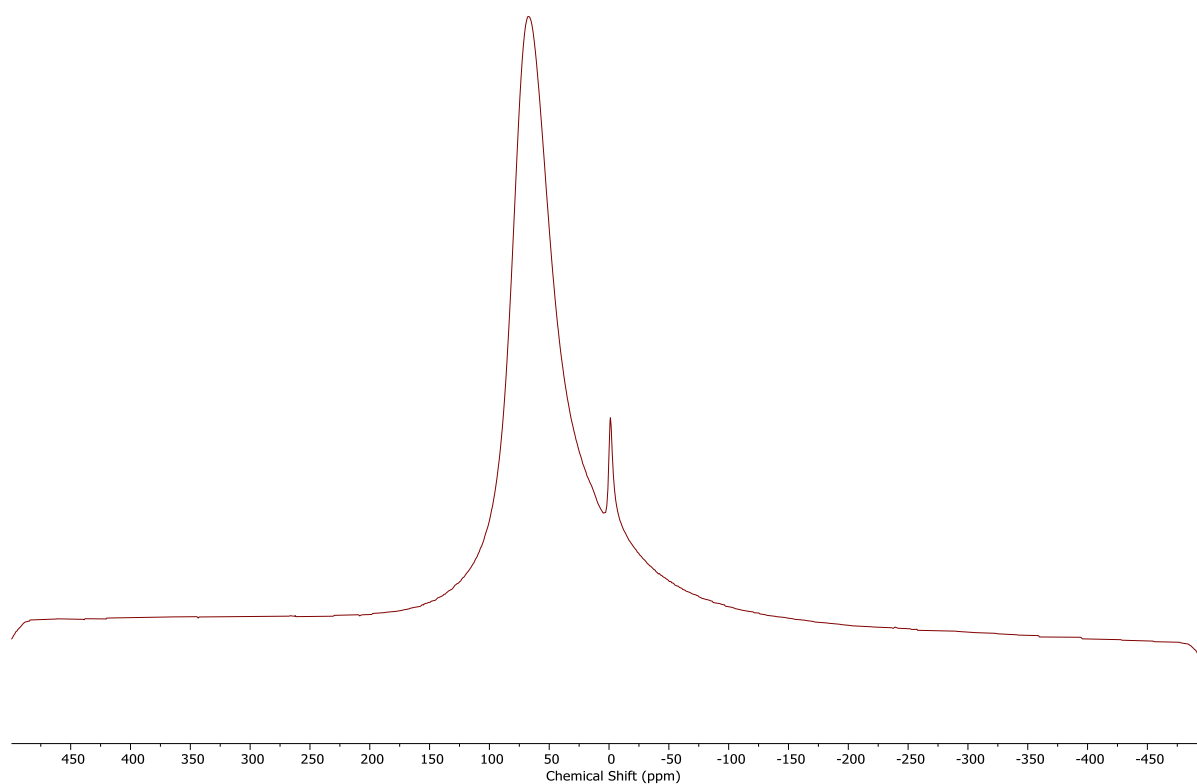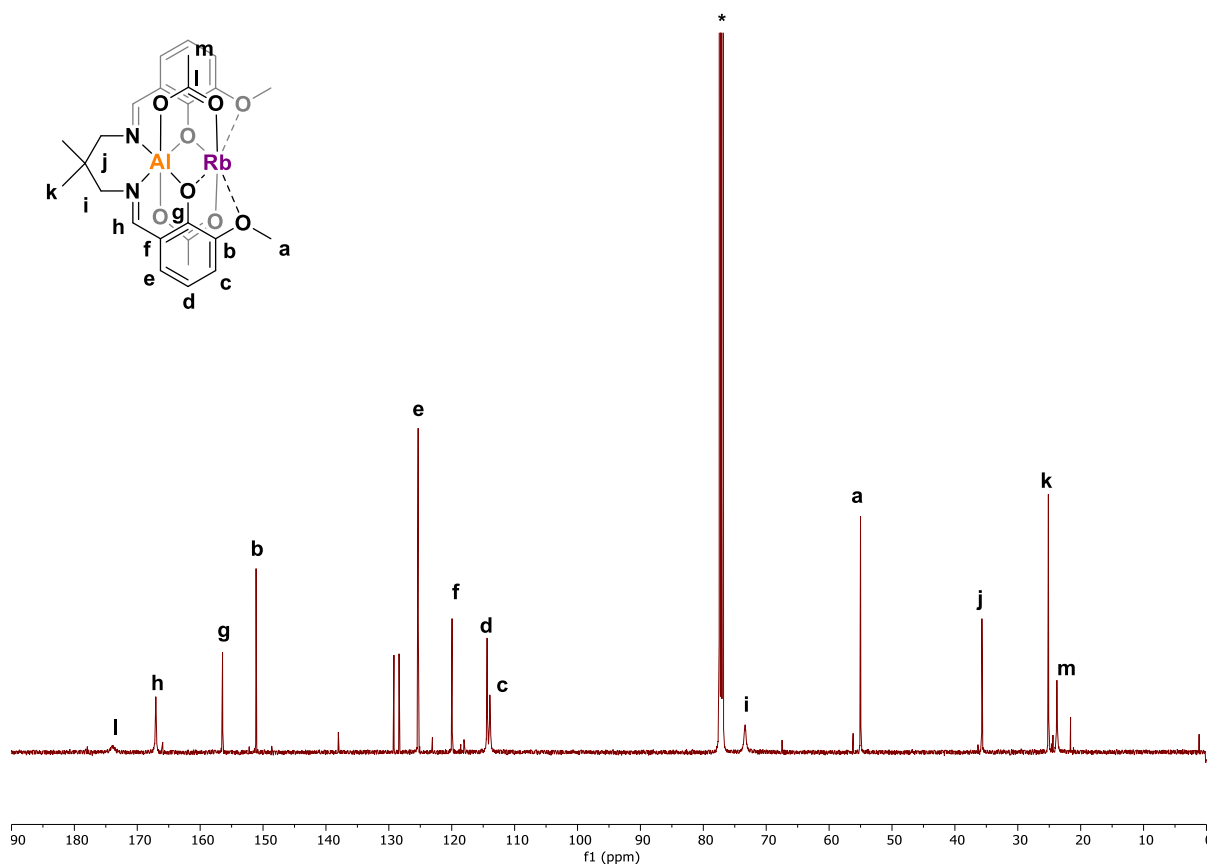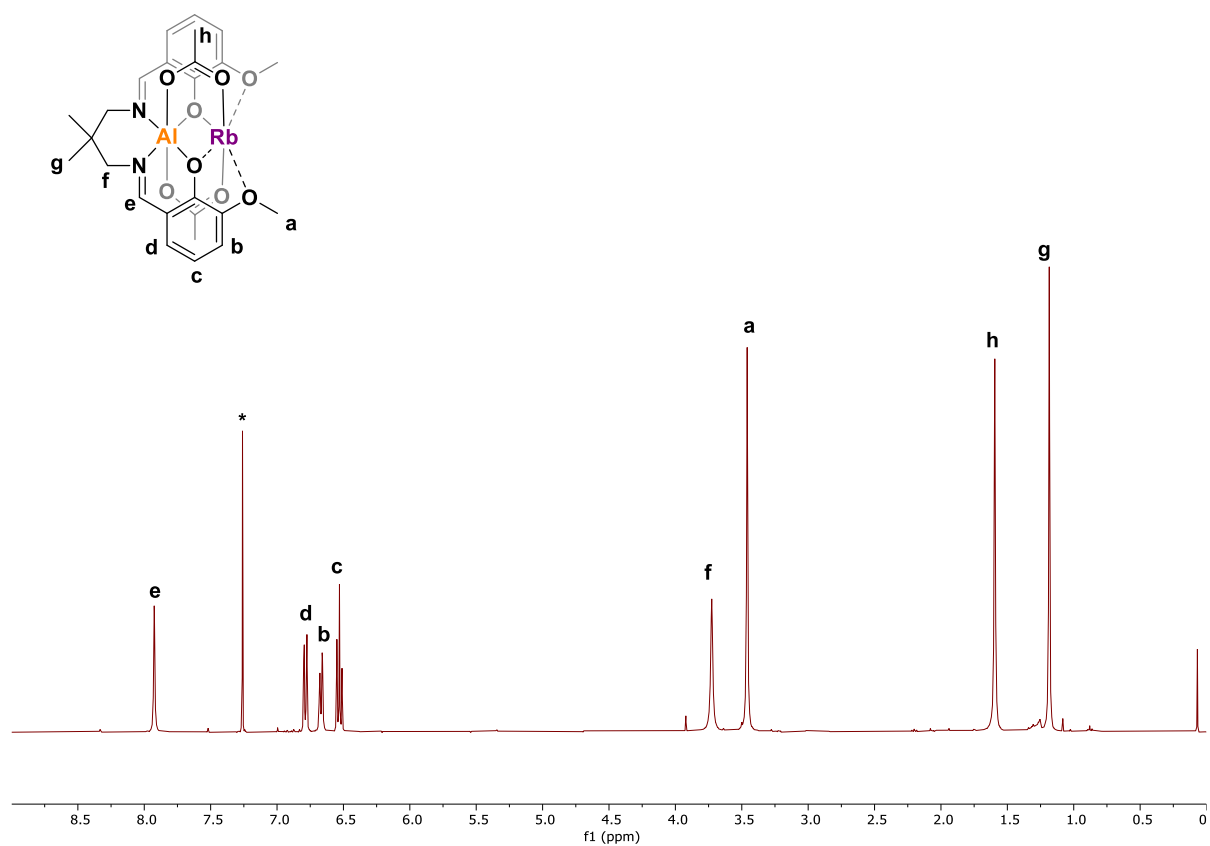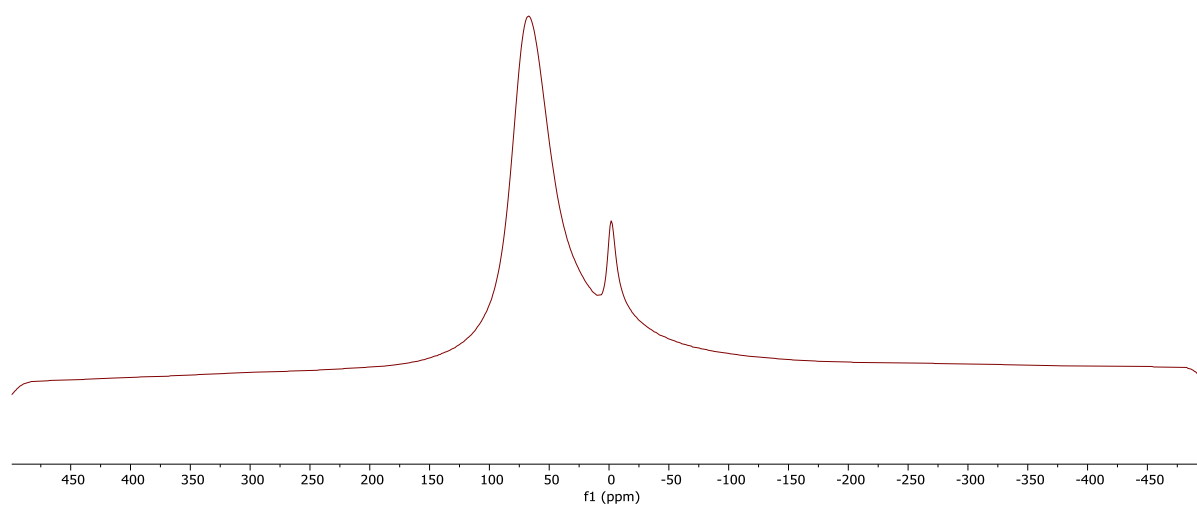
Figure S15. ^{27}Al NMR Spectrum (104 MHz, 298 K, CDCl$_3$) of complex **3**.
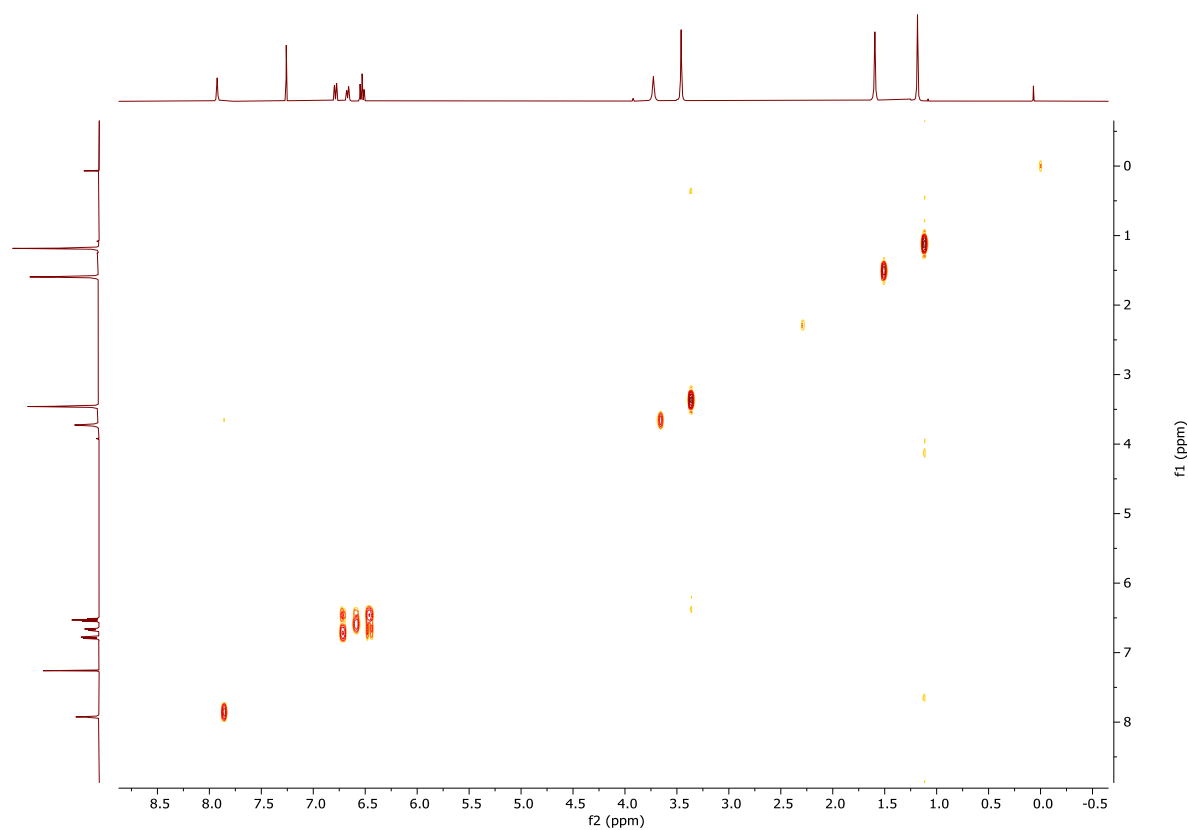
Figure S16. ^{1}H COSY NMR Spectrum (400 MHz, 298 K, CDCl$_3$) of complex **3**.
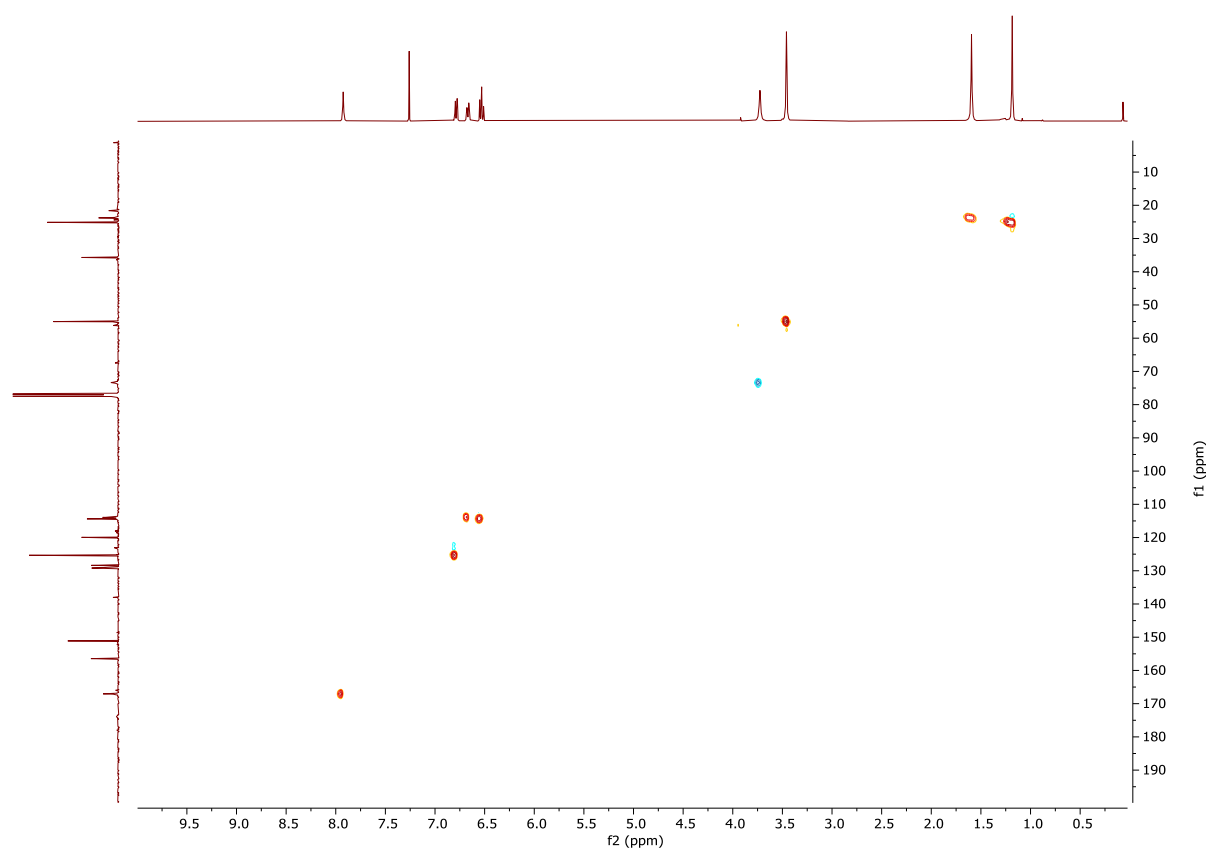
Figure S17. ¹H-¹³C HSQC NMR Spectrum (298 K, CDCl₃) of complex **3**.
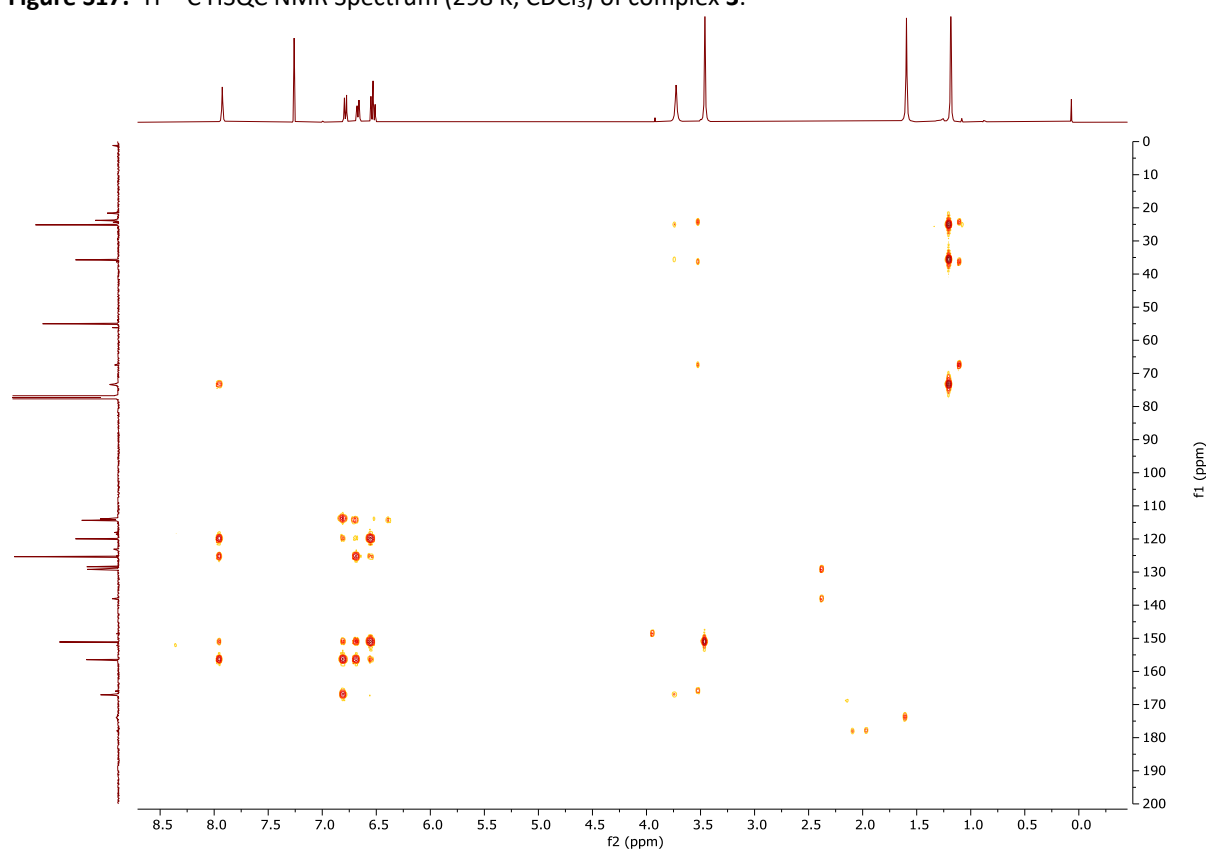
Figure S18. ¹H-¹³C HMBC NMR Spectrum (298 K, CDCl₃) of complex **3**.
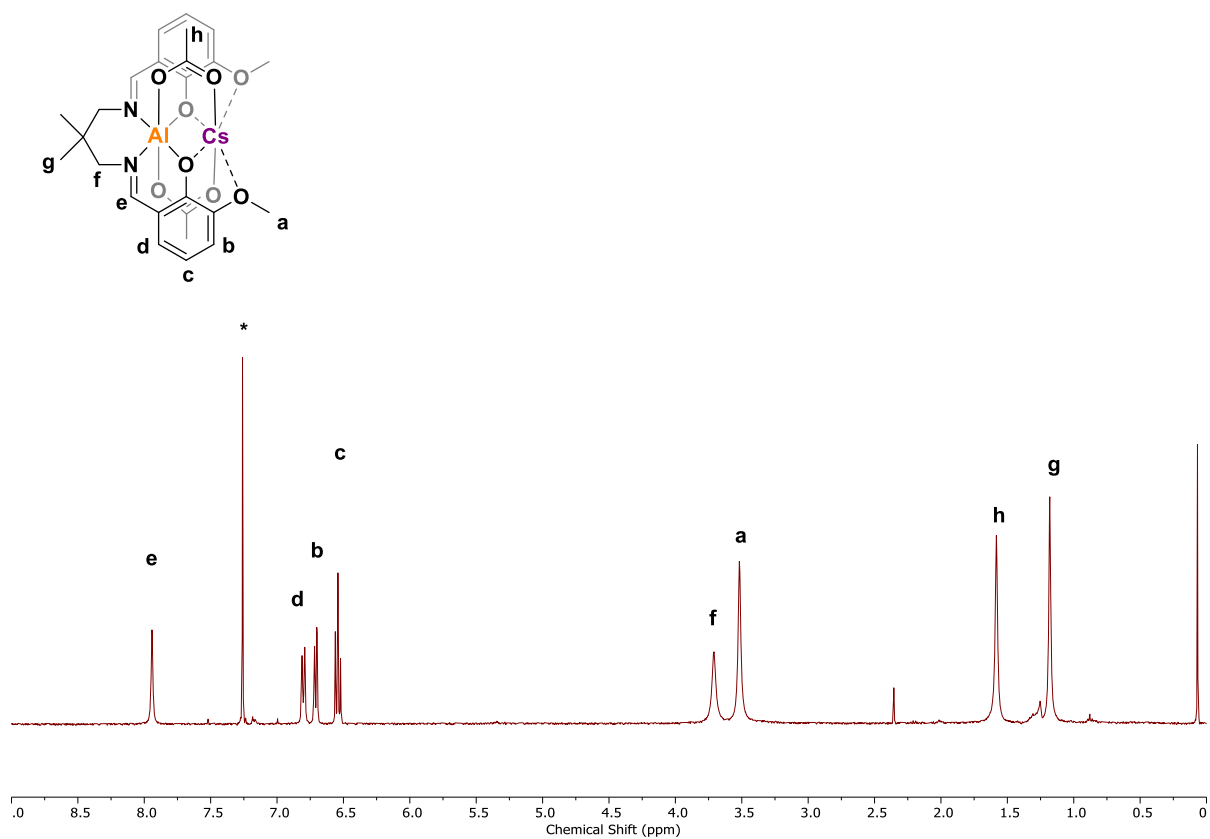
Figure S19. ^{1}H NMR Spectrum (400 MHz, 298 K, CDCl$_3$(*)) of complex **4**.
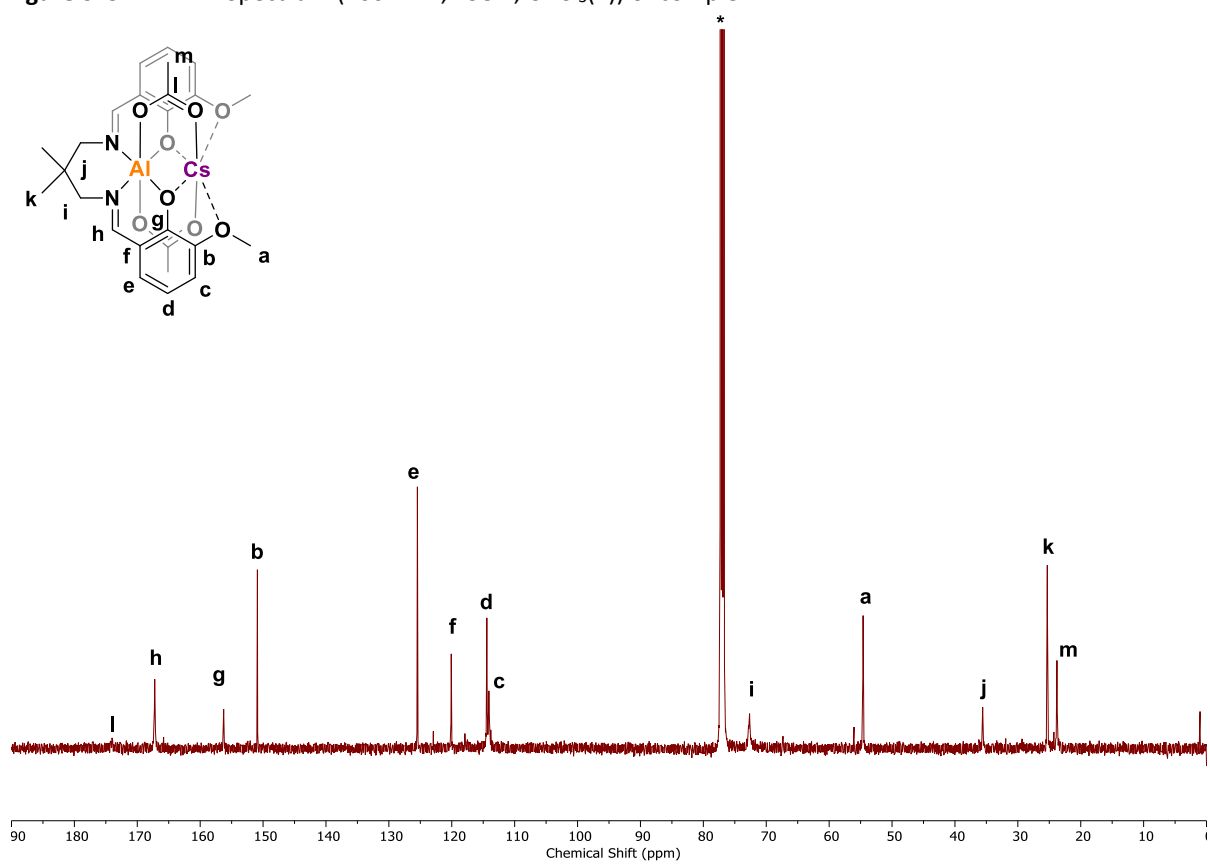
Figure S20. ^{13}C NMR Spectrum (126 MHz, 298 K, CDCl$_3$(*)) of complex **4**.
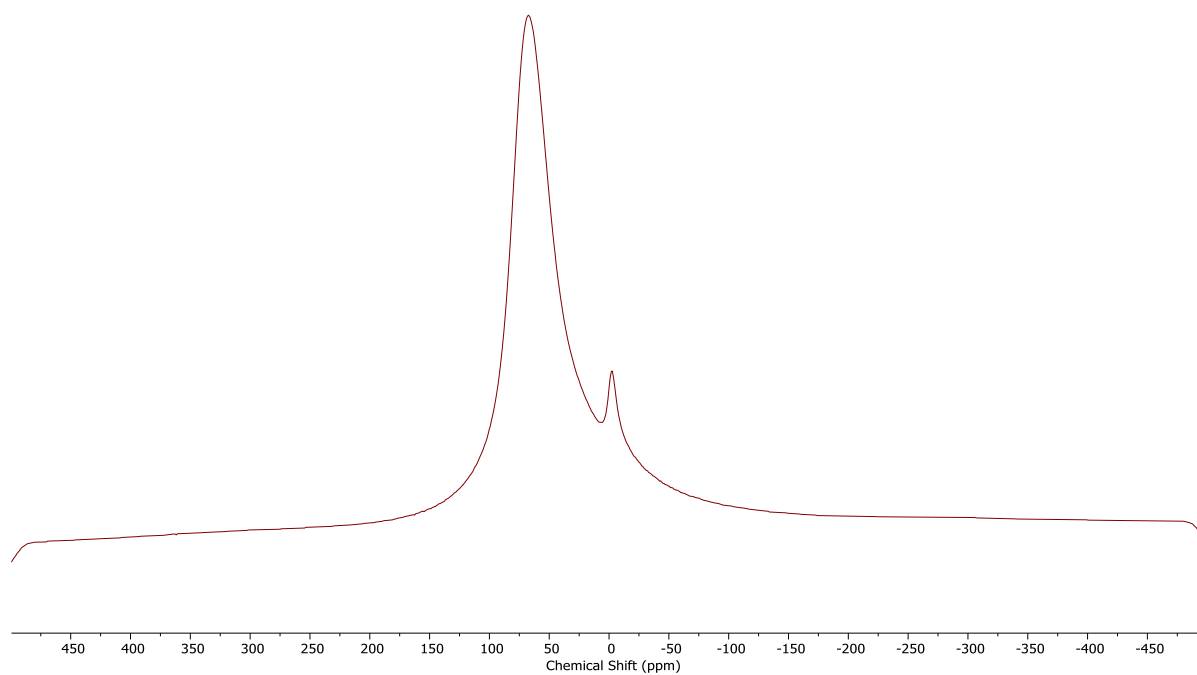
Figure S21. ^{27}Al NMR Spectrum (104 MHz, 298 K, CDCl$_3$) of complex **4**.
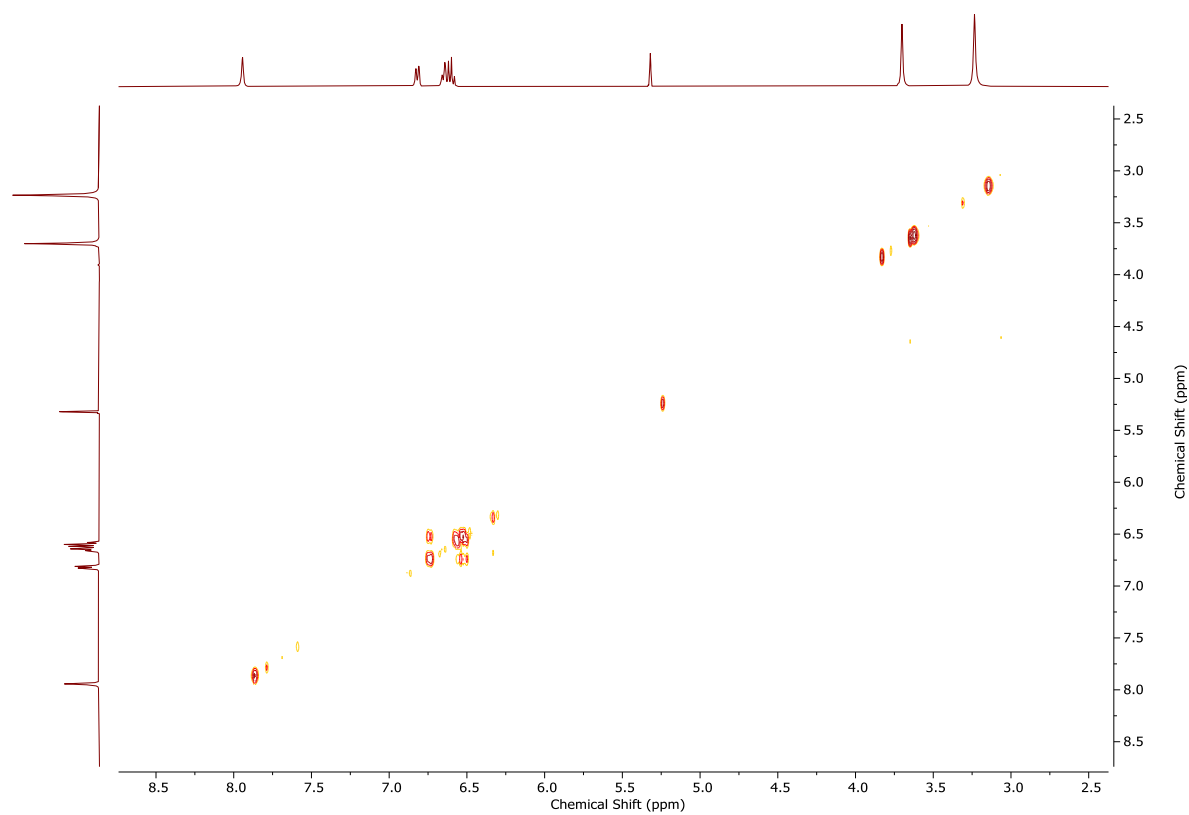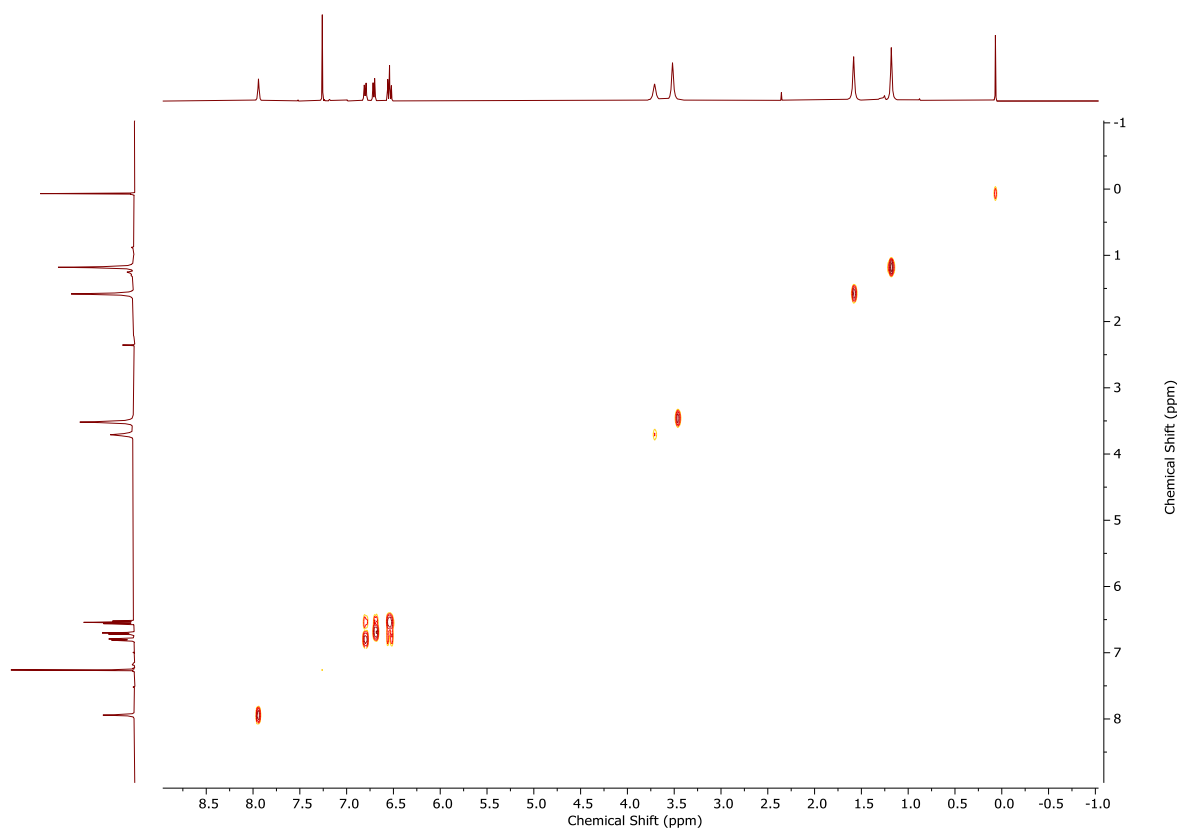

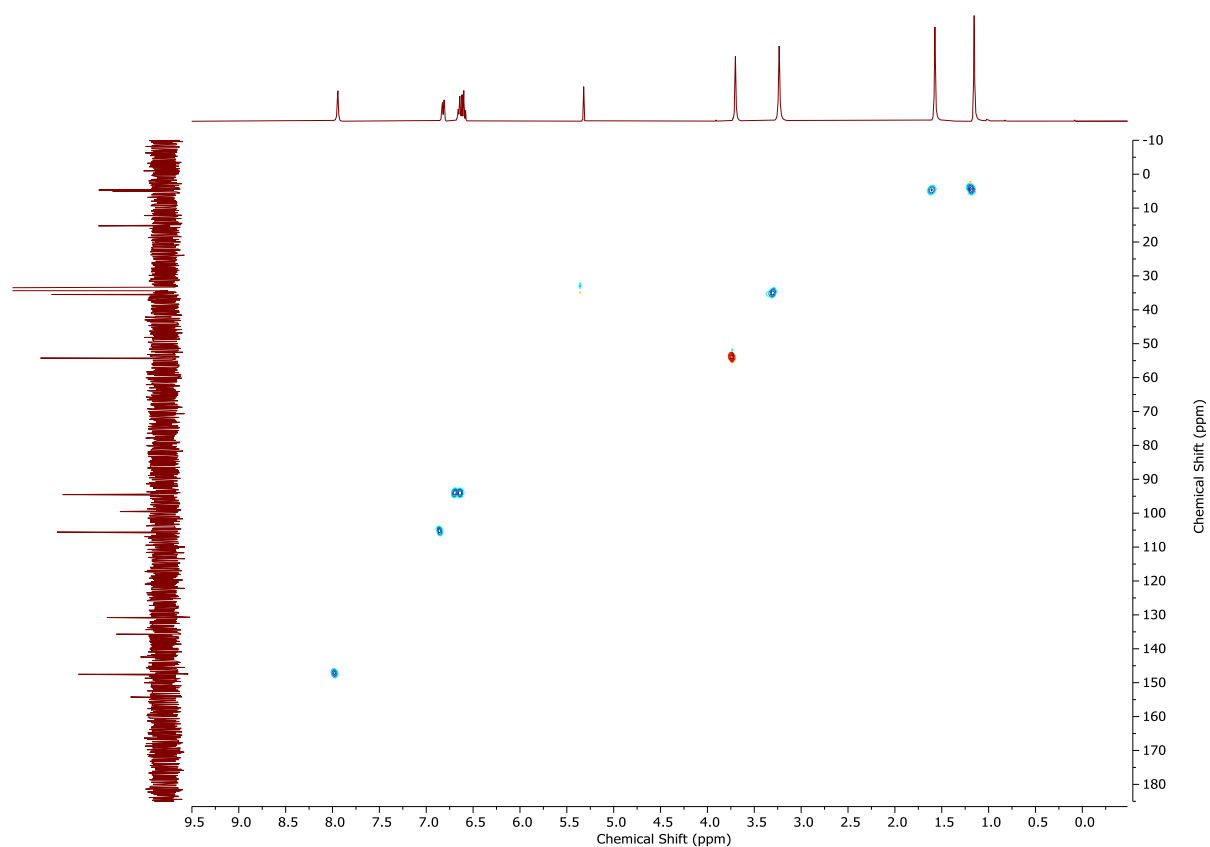**Figure S22.** ^{1}H COSY NMR Spectrum (400 MHz, 298 K, CDCl$_3$) of complex **4**.
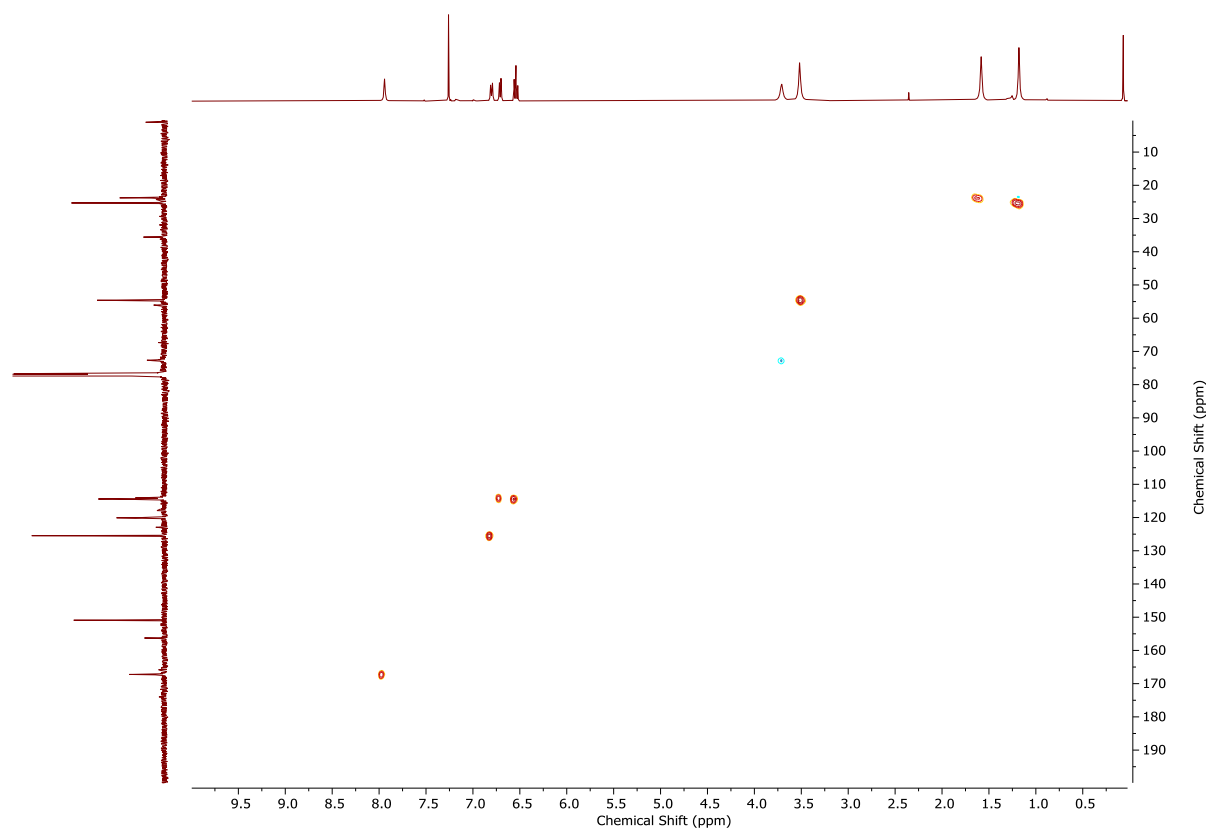
Figure S23. ^{1}H-^{13}C HSQC NMR Spectrum (298 K, CDCl$_3$) of complex **4**.
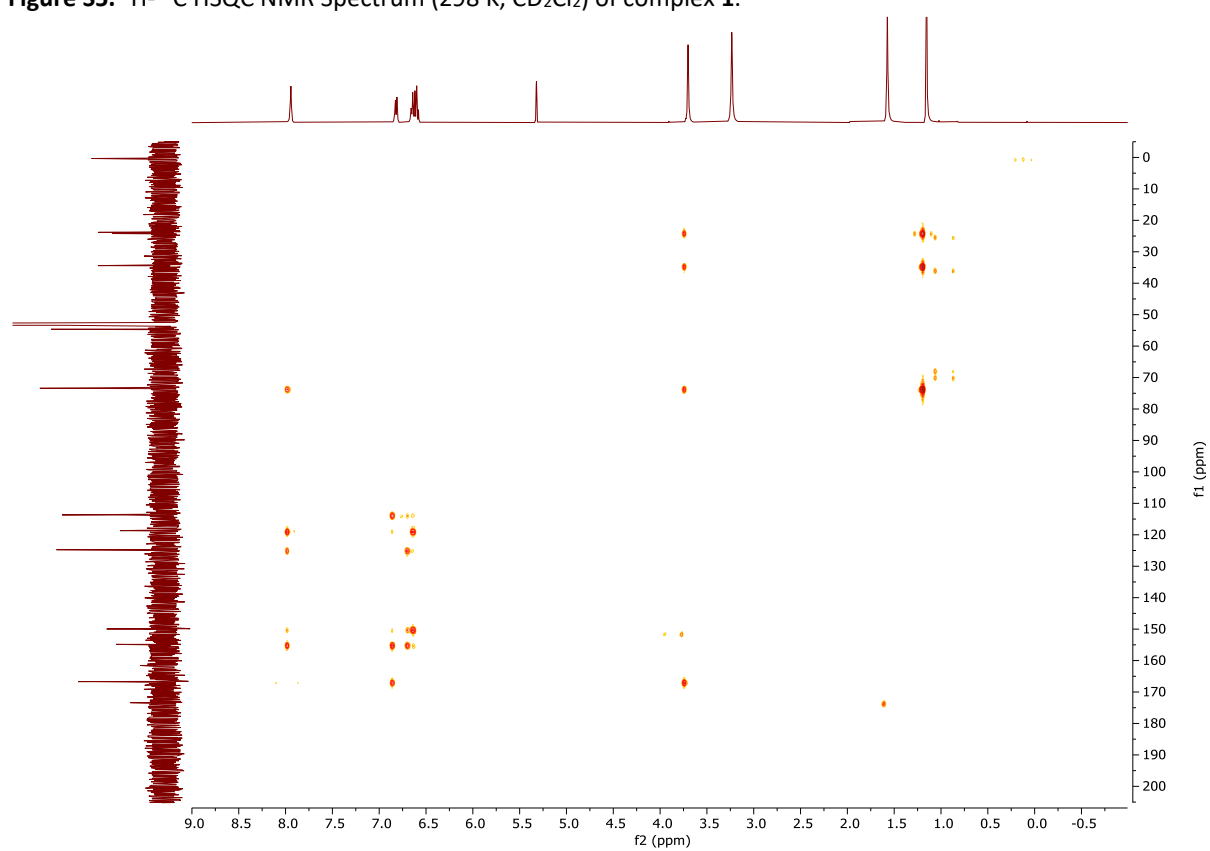

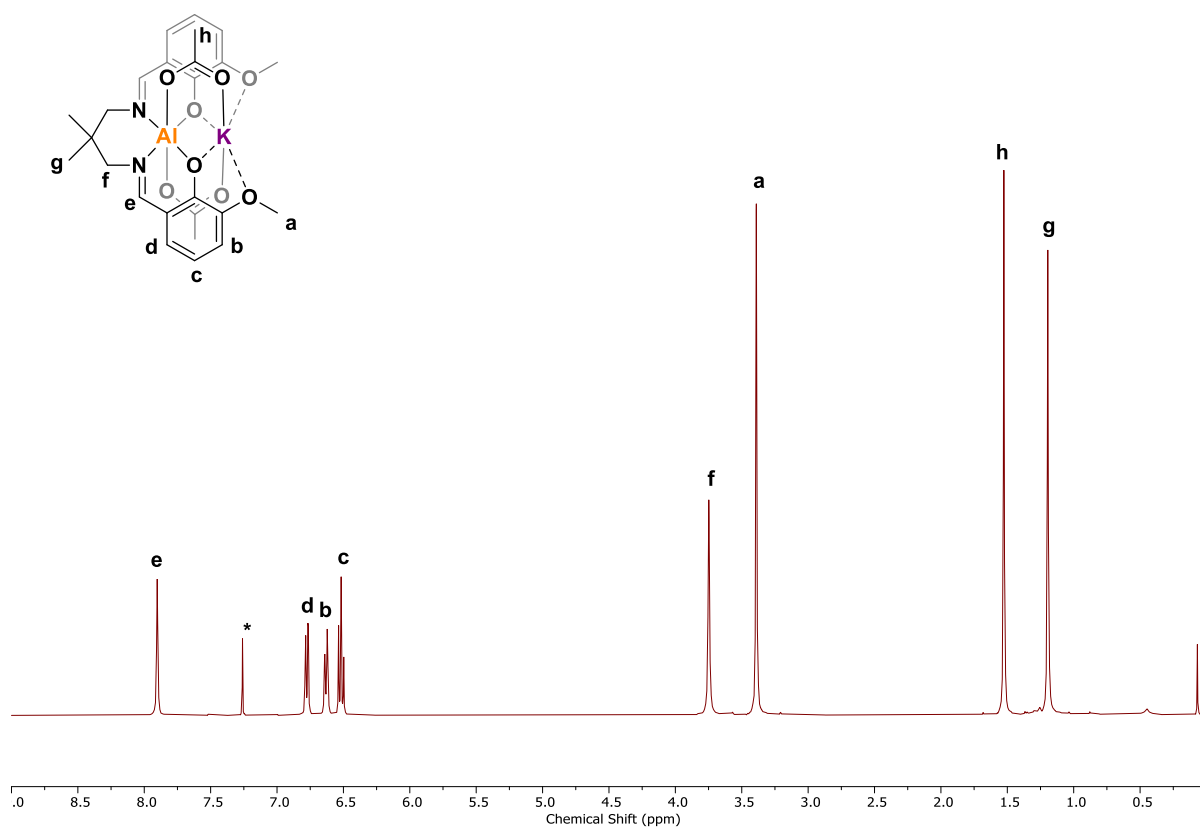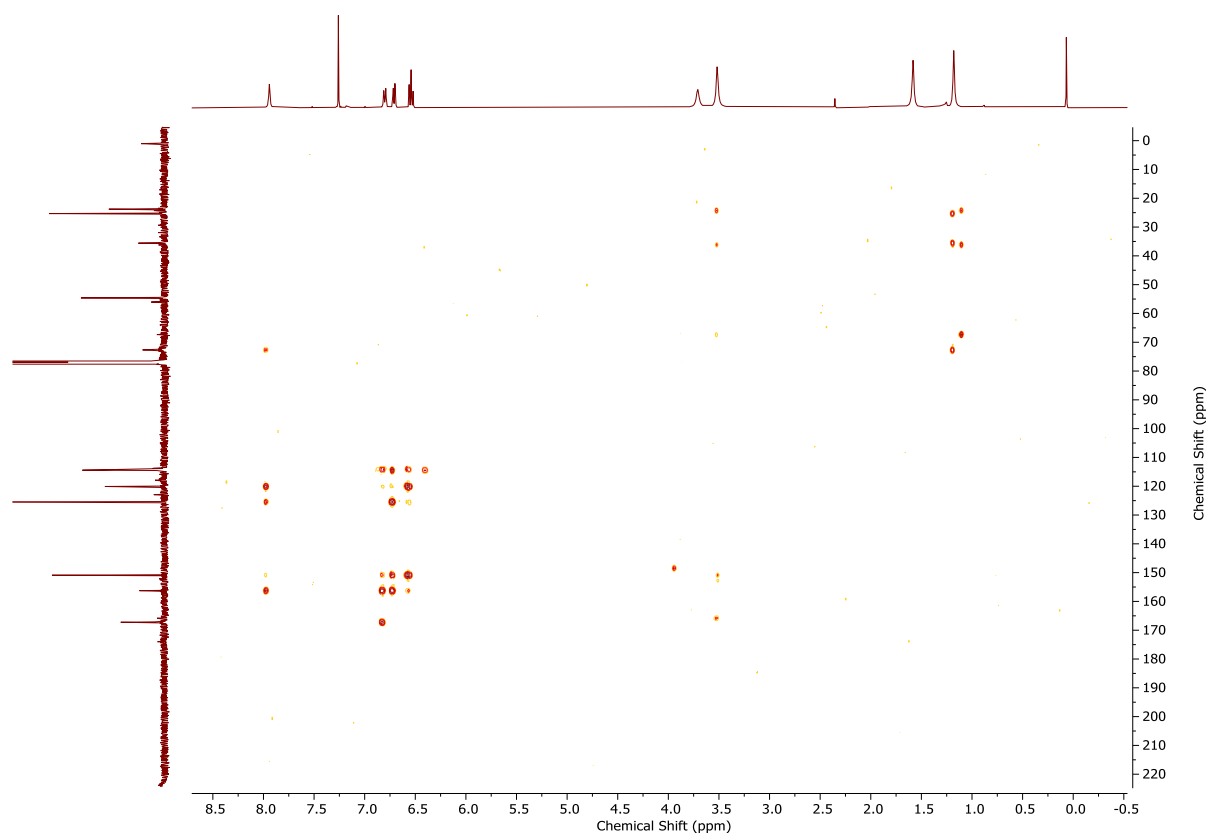**Figure S24.** ^{1}H-^{13}C HMBC NMR Spectrum (298 K, CDCl$_3$) of complex **4**.
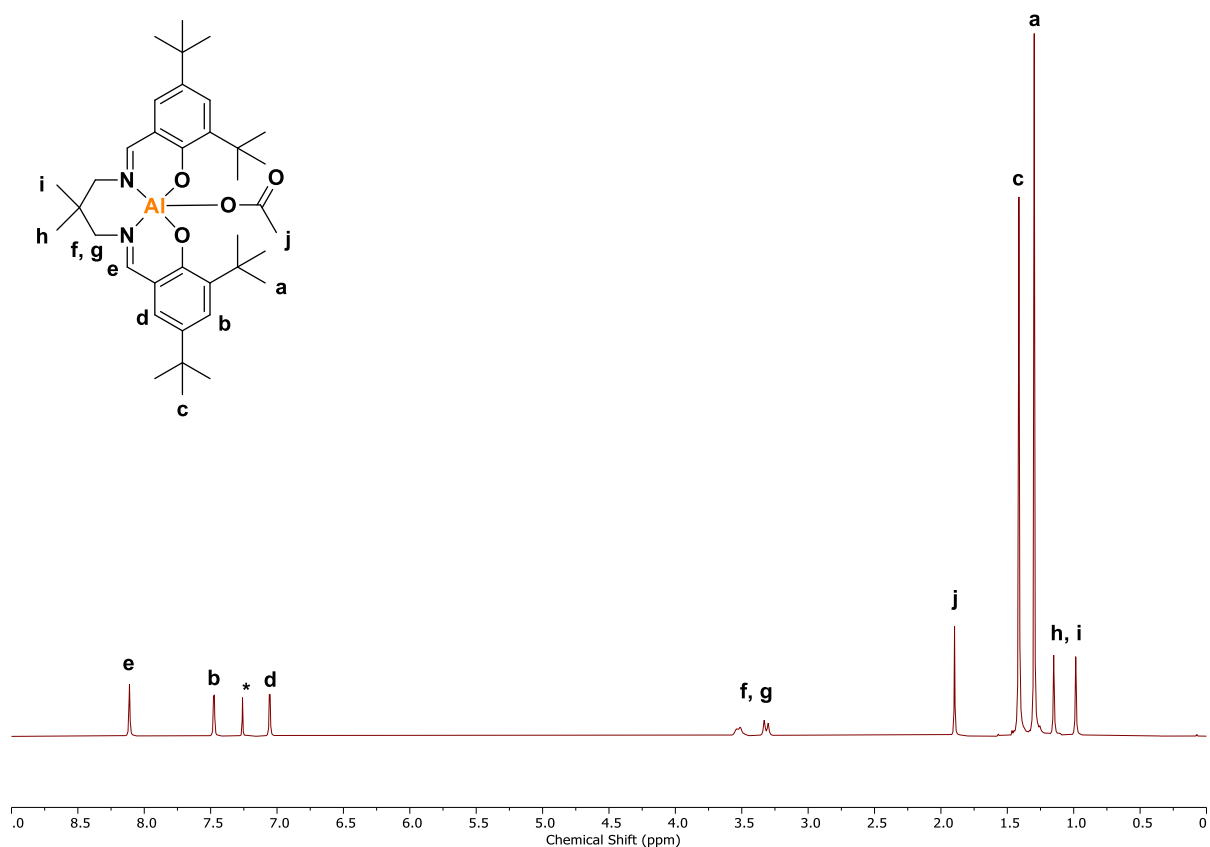
Figure S25. ^{1}H NMR Spectrum (400 MHz, 298 K, CDCl$_3$(*)) of [L$_{sal}$Al(OAc)].
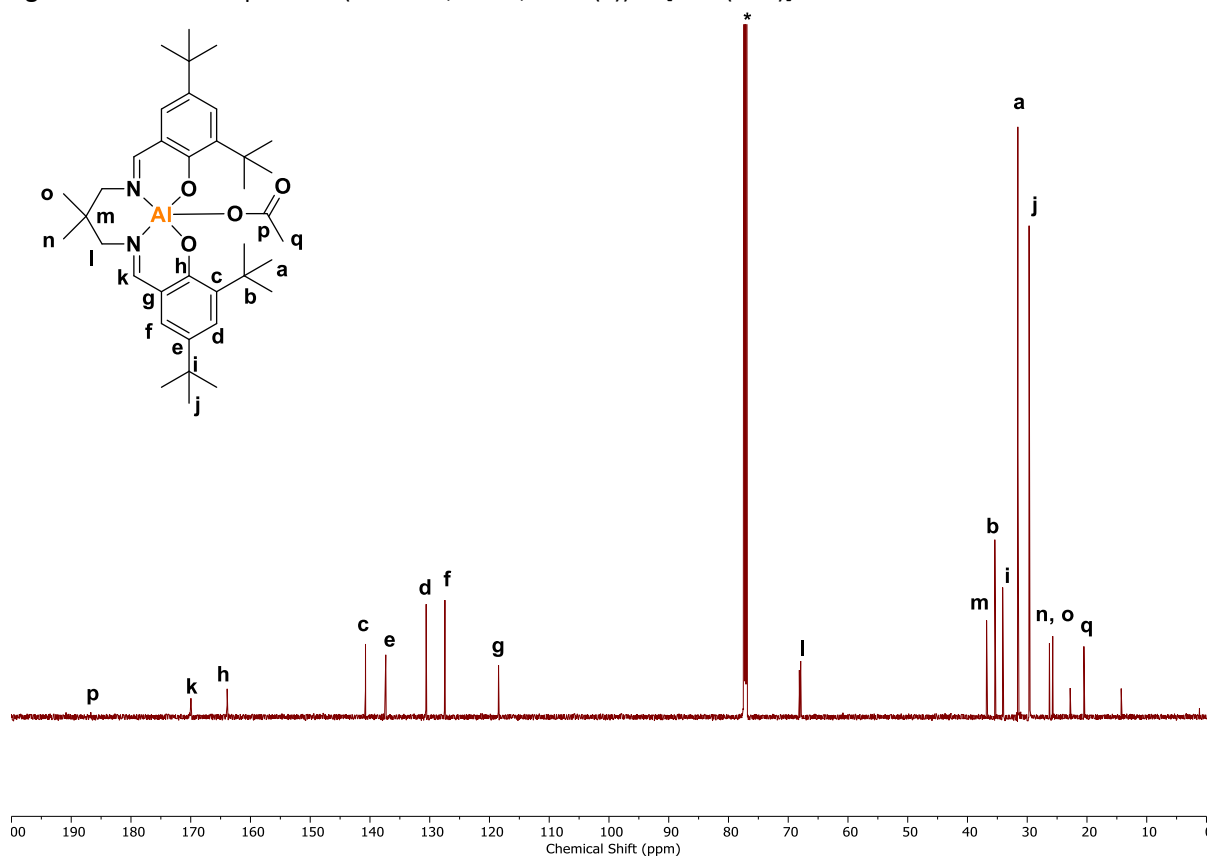
Figure S26. ^{13}C NMR Spectrum (176 MHz, 298 K, CDCl$_3$(*)) of [L$_{sal}$Al(OAc)].
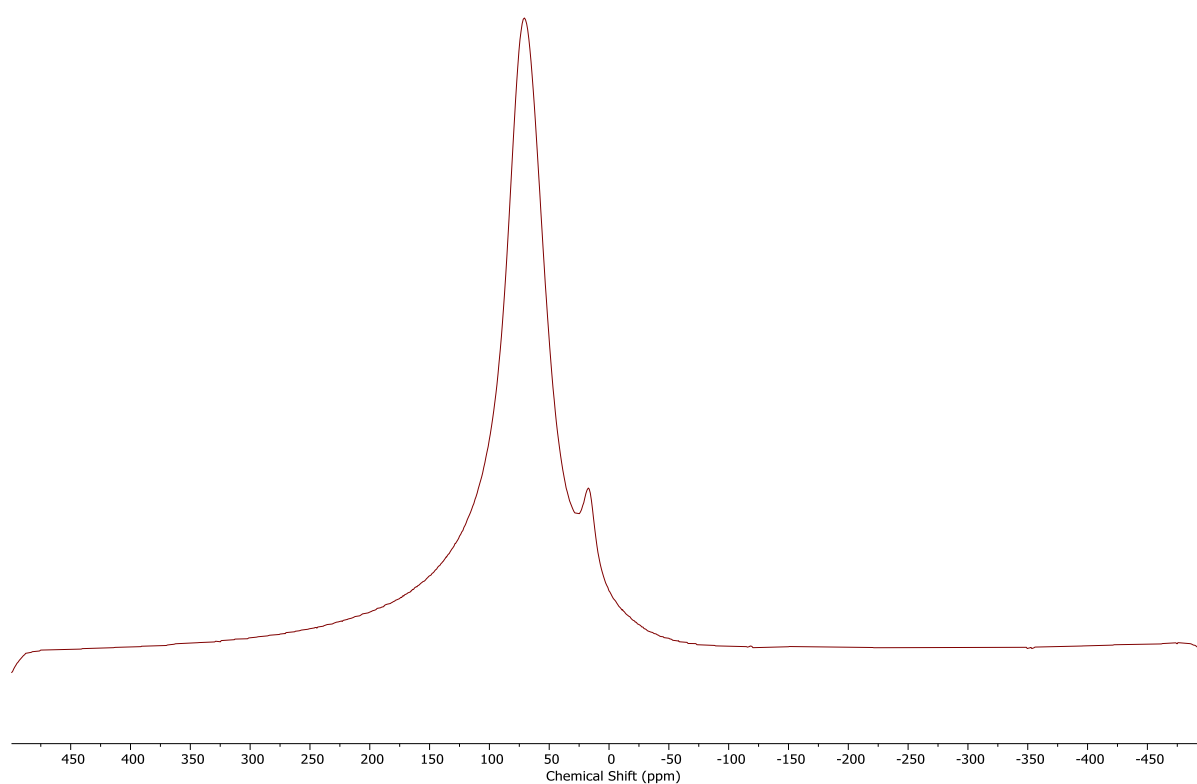
Figure S27. ^{27}Al NMR Spectrum (104 MHz, 298 K, CDCl$_3$) of [L$_{sal}$Al(OAc)].
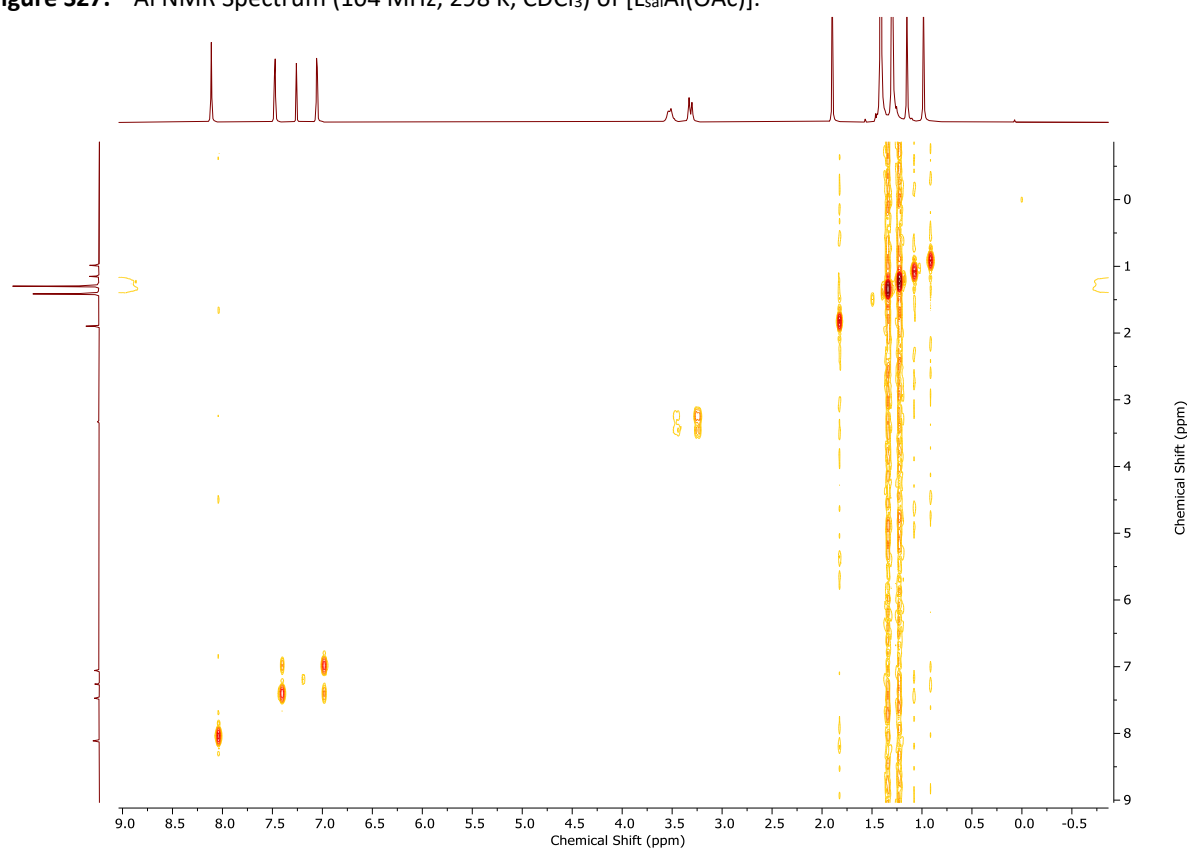
Figure S28. ^{1}H COSY NMR Spectrum (400 MHz, 298 K, CDCl$_3$) of [L$_{sal}$Al(OAc)].
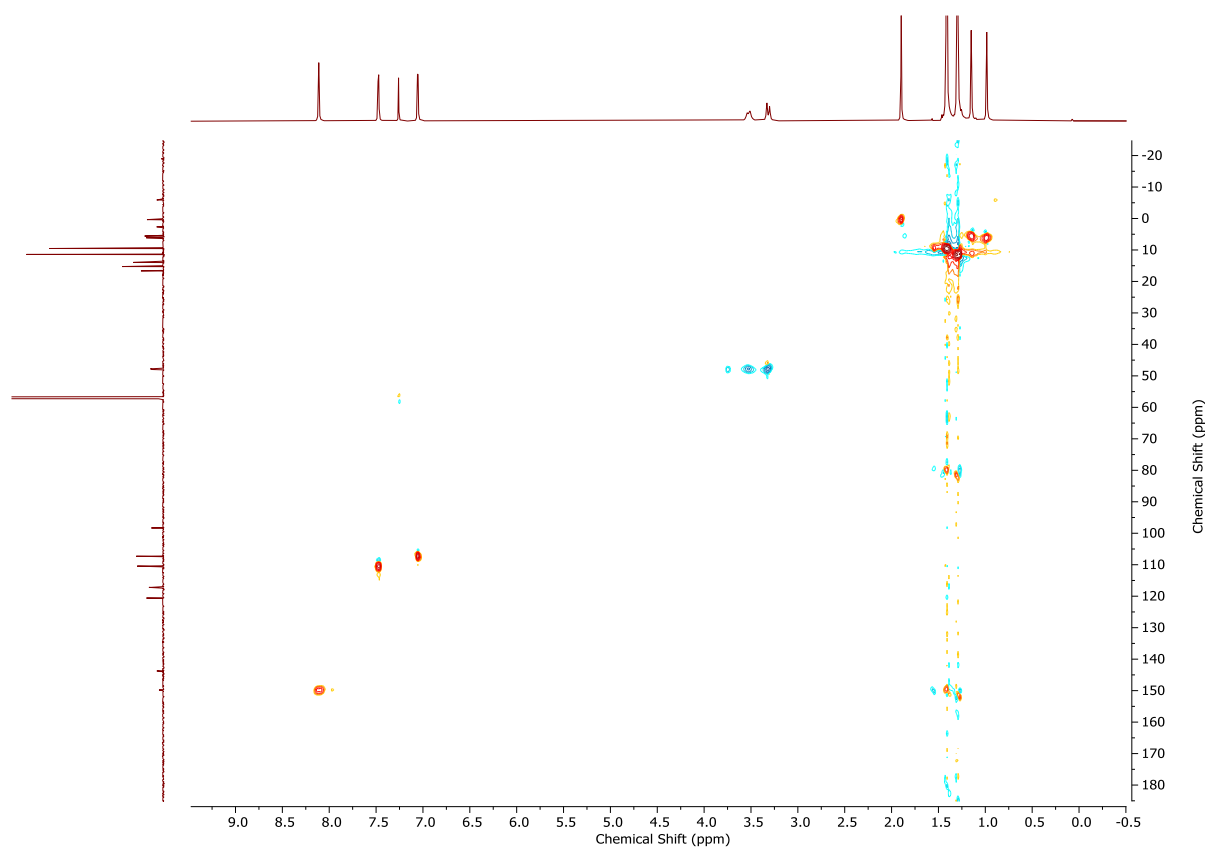
Figure S29. ^1H-^{13}C HSQC NMR Spectrum (298 K, CDCl$_3$) of [L$_{sal}$Al(OAc)].
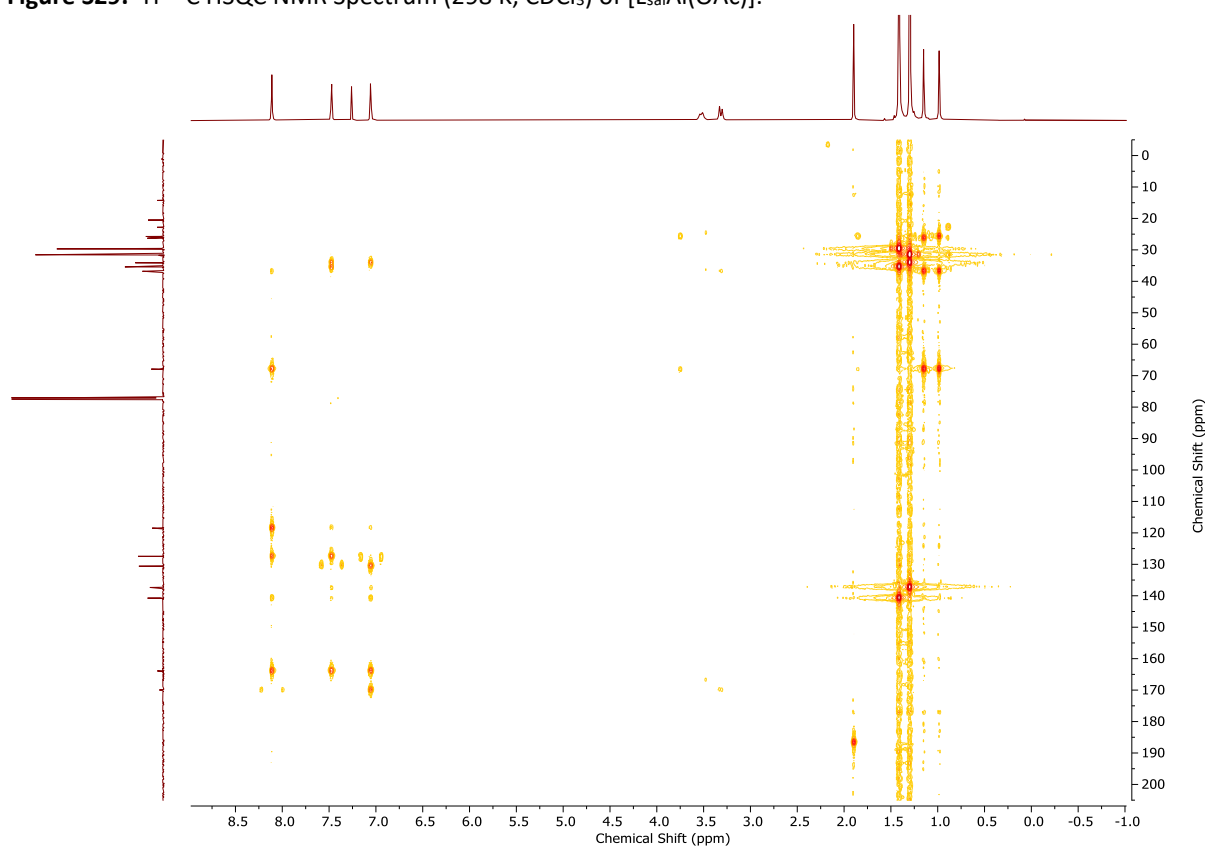
Figure S30. ^1H-^{13}C HMBC NMR Spectrum (298 K, CDCl$_3$) of [L$_{sal}$Al(OAc)].
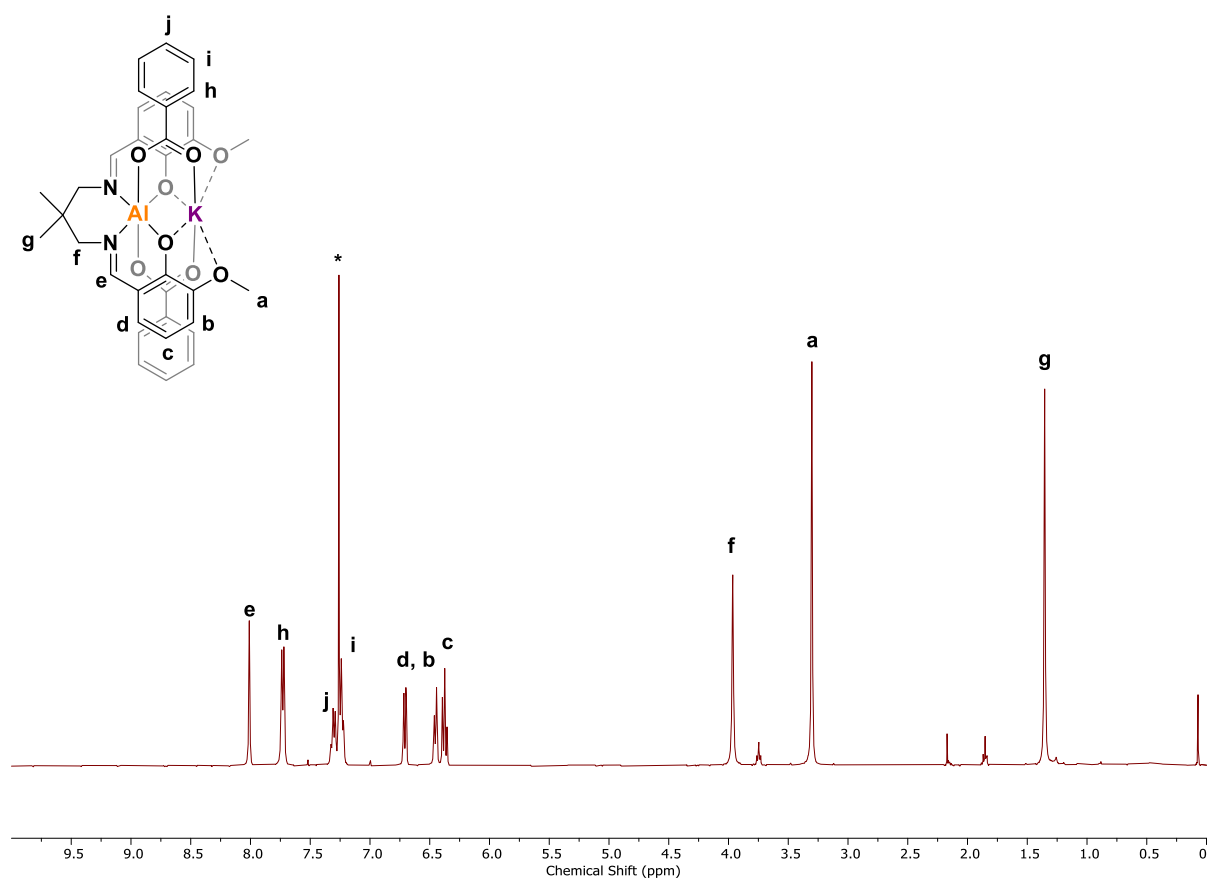
Figure S31. ^{1}H NMR (400 MHz, 298 K, CDCl$_3$ (*)) of complex **5**.

Crystallographic Data for Complexes 1, 3, 4 and 5.
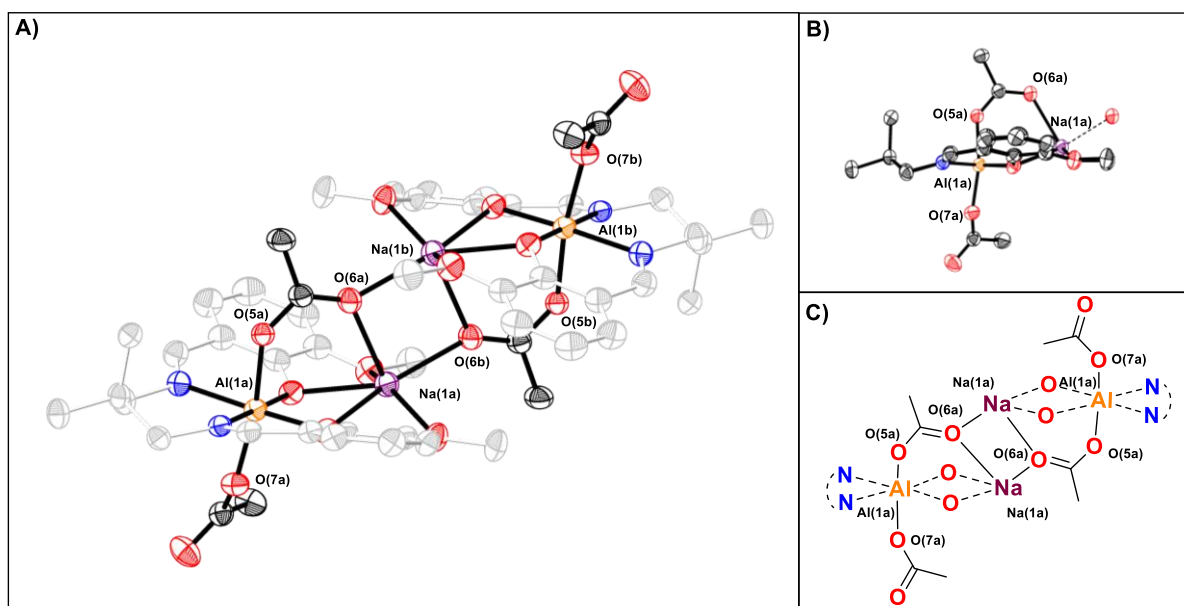
Figure S32. Molecular structure of complex **1**. Obtained from X-ray diffraction experiments with thermal ellipsoids presented at 50% probability and H atoms omitted for clarity (Atom colour scheme: Al (orange), Na (purple), O (red), N (blue), C (greyscale/black). A) Structure of the dimer, showing acetate co-ligands bridging between two molecules of the complex. B) Structure of one half of the dimer, showing a 'bowl' confirmation ligand, and aluminate centre. Note that the two molecules within the dimer are related by symmetry in the crystal structure. C) Schematic showing key binding of both metals and acetate groups.
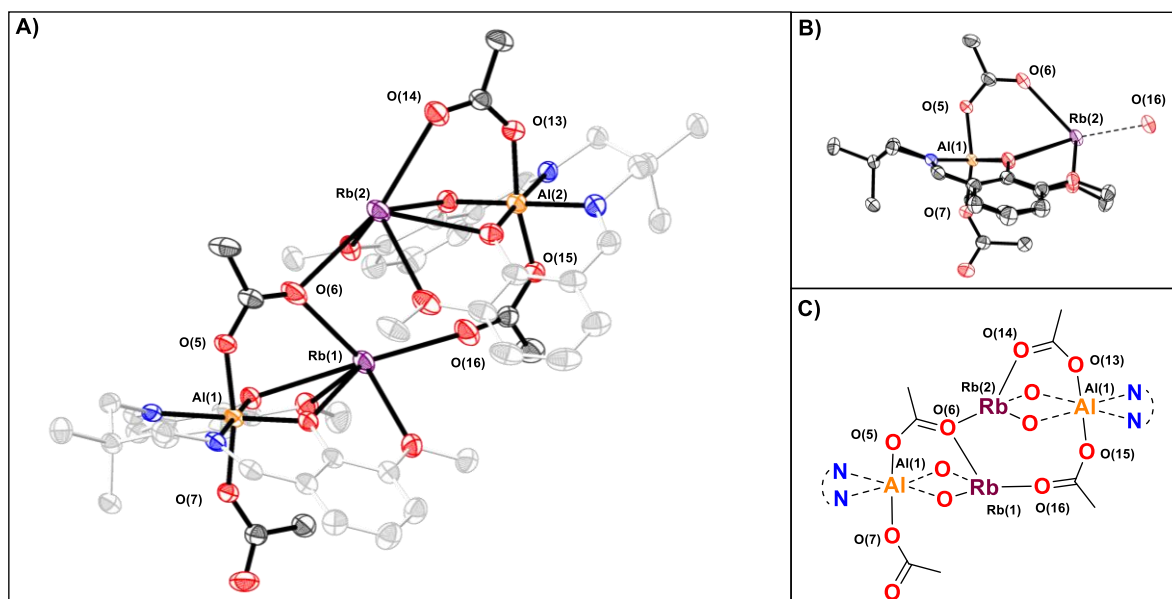
Figure S33. Molecular structure of complex **3**. Obtained from X-ray diffraction experiments with thermal ellipsoids presented at 50% probability and H atoms omitted for clarity (Atom colour scheme: Al (orange), Rb (purple), O (red), N (blue), C (greyscale/black). A) Structure of the dimer, showing acetate co-ligands bridging between two molecules of the complex. B) Structure of one half of the dimer, showing a 'bowl' confirmation ligand, and aluminate centre C) Schematic showing key binding of both metals and acetate groups.
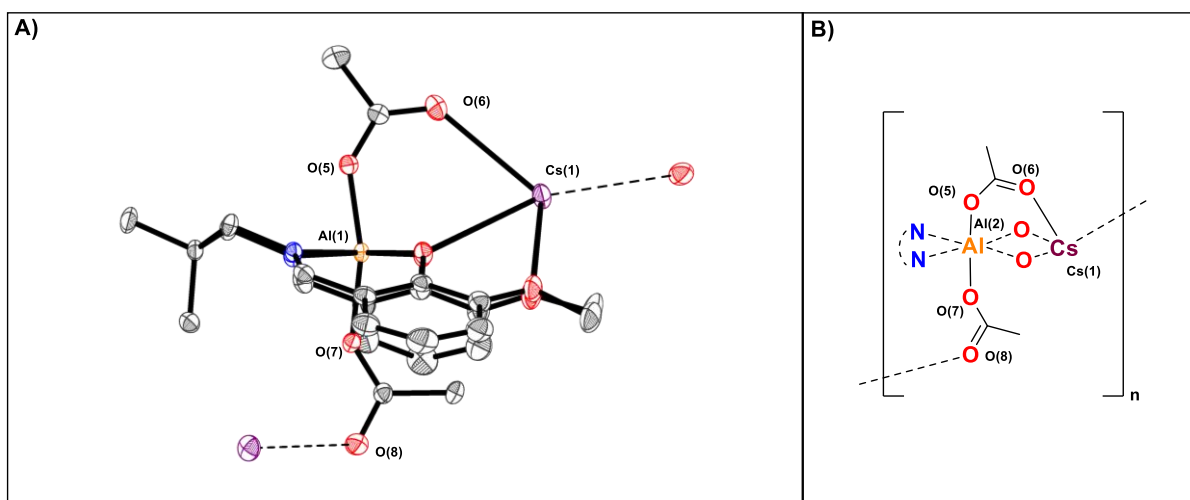
Figure S34. Molecular structure of complex **4**. Obtained from X-ray diffraction experiments, with thermal ellipsoids presented at 50% probability and H atoms omitted for clarity (Atom colour scheme: Al (orange), Cs (purple), O (red), N (blue), C (black). A) Structure of the monomeric unit, showing acetate co-ligands bridging between molecules in the extended polymeric crystal structure. B) Schematic showing key binding of both metals and acetate groups
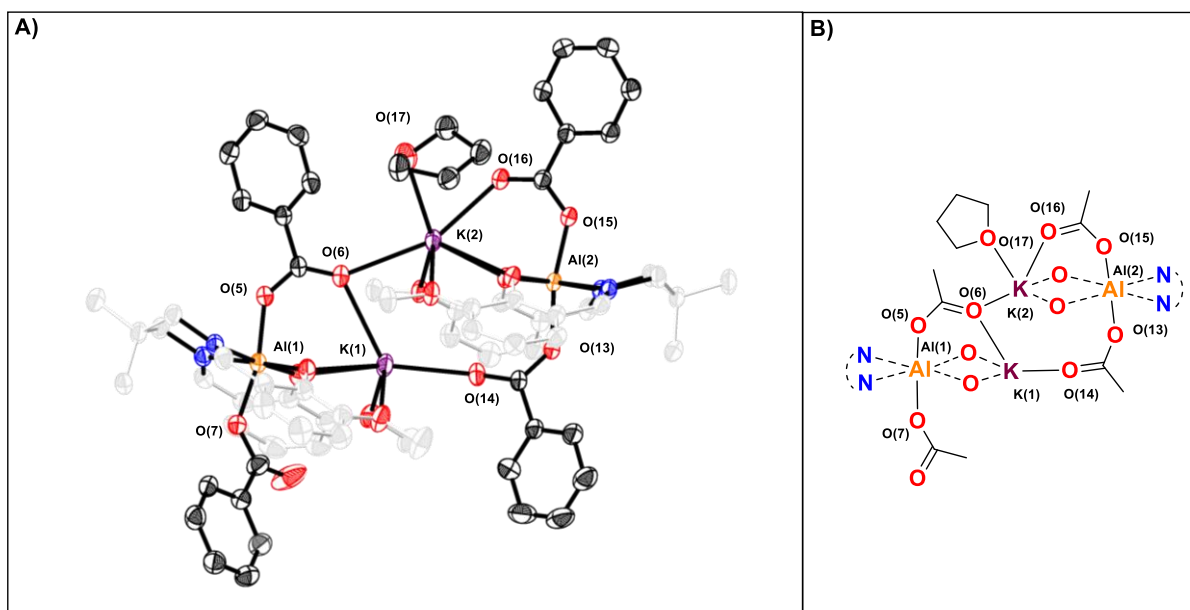
Figure S35. Molecular structure of complex **5.** Obtained from X-ray diffraction experiments, with thermal ellipsoids presented at 50% probability and H atoms omitted for clarity (Atom colour scheme: Al (orange), K (purple), O (red), N (blue), C (greyscale/black). A) Structure of the dimer, showing benzoate co-ligands bridging between two molecules of the complex, and a molecule of THF bound to K(2). B) Schematic showing key binding of both metals, benzoate groups, and THF coordination.

Table S1. Selected bond lengths and angles for complex **1**.

Bond	Bond Length (Å)	Bond	Bond Angle (°)
Al(1a) – Na(1a)	3.284	O(7a) – Al(1a) – O(5a)	169.21(7)
Al(1a) – N(1a)	2.059(18)	N(1a) – Al(1a) – N(2a)	92.10(7)
Al(1a) – N(2a)	2.0350(17)	N(1a) – Al(1a) – O(2a)	90.35(7)
Al(1a) – O(2a)	1.8494(15)	N(2a) – Al (1a) – O(3a)	91.06(7)
Al(1a – O(3a)	1.8481(15)	O(2a) – Al(1a) – O(3a)	86.44(6)
Al(1a) – O(5a)	1.8967(15)	O(1a) – Na(1a) – O(2a)	64.95(5)
Al(1a) – O(7a)	1.8694(16)	O(2a) – Na(1a) – O(3a)	64.76(5)
Na(1a) – O(1a)	2.5018(17)	O(3a) – Na(1a) – O(4a)	64.69(5)
Na(1a) – O(2a)	2.3521(16)	O(6a) – Na(1a) – O(1a)	86.40(6)
Na(1a) – O(3a)	2.3756(15)	O(6a) – Na(1a) – O(2a)	145.34(7)
Na(1a) – O(4a)	2.5013(18)	O(6a) – Na(1a) – O(6b)	88.74(6)
Na(1a) – O(6a)	2.4098(17)		
Na(1a) – O(6b)	2.2934(16)		

Table S2. Selected bond lengths and angles for complex **2**.

Bond	Bond Length (Å)	Bond	Bond Angle (°)
Al(1) – K(1)	3.665	O(7) – Al(1) – O(5)	167.84(10)
Al(1) – N(1)	2.077(2)	N(1) – Al(1) – N(2)	90.84(10)
Al(1) – N(2)	2.038(2)	N(1) – Al(1) – O(2)	89.49(9)
Al(1) – O(2)	1.842(2)	N(2) – Al(1) – O(3)	90.13(9)
Al(1) – O(3)	1.854(2)	O(2) – Al(1) – O(3)	89.57(9)
Al(1) – O(5)	1.905(2)	O(1) – K(1) – O(2)	57.79(6)
Al(1) – O(7)	1.869(2)	O(2) – K(1) – O(3)	56.95(6)
K(1) – O(1)	2.718(2)	O(3) – K(1) – O(4)	56.31(6)
K(1) – O(2)	2.7220(19)	O(1) – K(1) – O(6)	117.58(7)
K(1) – O(3)	2.738(2)	O(2) – K(1) – O(6)	71.81(6)
K(1) – O(4)	2.853(2)	O(6) – K(1) – O(16)	119.62(7)
K(1) – O(6)	2.673(2)	O(13) – Al(2) – O(15)	169.18(10)
K(1) – O(16)	2.582(2)	N(3) – Al(2) – N(4)	89.64(10)
Al(2) – K(2)	3.519	N(3) – Al(2) – O(10)	87.84(9)
Al(2) – N(3)	2.067(2)	N(4) – Al(2) – O(11)	89.24(10)
Al(2) – N(4)	2.040(2)	O(10) – Al(2) – O(11)	93.25(9)
Al(2) – O(10)	1.853(2)	O(9) – K(2) – O(10)	57.91(6)
Al(2) – O(11)	1.843(2)	O(10) – K(2) – O(11)	60.70(6)
Al(2) – O(13)	1.871(2)	O(11) – K(2) – O(12)	57.68(6)
Al(2) – O(15)	1.907(2)	O(9) – K(2) – O(14)	120.95(7)
K(2) – O(9)	2.781(2)	O(10) – K(2) – O(14)	74.83(6)
K(2) – O(10)	2.668(2)	O(6) – K(2) – O(14)	155.60(7)
K(2) – O(11)	2.649(2)		
K(2) – O(12)	2.809(2)		
K(2) – O(14)	2.662(2)		
K(2) – O(6)	2.728(2)		

Table S3. Selected bond lengths and angles for complex **3**.

Bond	Bond Length (Å)	Bond	Bond Angle (°)
Al(1) – Rb(1)	3.819	O(7) – Al(1) – O(5)	167.42(7)
Al(1) – N(1)	2.0445(18)	N(1) – Al(1) – N(2)	90.17(7)
Al(1) – N(2)	2.0900(17)	N(1) – Al(1) – O(2)	89.92(7)
Al(1) – O(2)	1.8632(15)	N(2) – Al(1) – O(3)	89.37(7)
Al(1) – O(3)	1.8456(15)	O(2) – Al(1) – O(3)	90.56(6)
Al(1) – O(5)	1.9103(16)	O(1) – Rb(1) – O(2)	54.45(4)
Al(1) – O(7)	1.8678(15)	O(2) – Rb(1) – O(3)	54.45(4)
Rb(1) – O(1)	2.9229(16)	O(3) – Rb(1) – O(4)	55.44(4)
Rb(1) – O(2)	2.8828(14)	O(1) – Rb(1) – O(6)	110.30(5)
Rb(1) – O(3)	2.8780(13)	O(2) – Rb(1) – O(6)	67.54(5)
Rb(1) – O(4)	2.8018(15)	O(6) – Rb(1) – O(16)	122.50(5)
Rb(1) – O(6)	2.7858(19)	O(13) – Al(2) – O(15)	167.69(7)
Rb(1) – O(16)	2.6979(17)	N(3) – Al(2) – N(4)	89.55(7)
Al(2) – Rb(2)	3.678	N(3) – Al(2) – O(10)	89.44(7)
Al(2) – N(3)	2.0450(19)	N(4) – Al(2) – O(11)	87.96(7)
Al(2) – N(4)	2.0728(18)	O(10) – Al(2) – O(11)	93.01(7)
Al(2) – O(10)	1.8418(15)	O(9) – Rb(2) – O(10)	55.55(4)
Al(2) – O(11)	1.8561(15)	O(10) – Rb(2) – O(11)	57.17(4)
Al(2) – O(13)	1.8720(16)	O(11) – Rb(2) – O(12)	55.38(4)
Al(2) – O(15)	1.8936(16)	O(9) – Rb(2) – O(14)	113.89(5)
Rb(2) – O(9)	2.8800(16)	O(10) – Rb(2) – O(14)	70.76(5)
Rb(2) – O(10)	2.7934(16)	O(6) – Rb(2) – O(14)	161.57(5)
Rb(2) – O(11)	2.8135(14)		
Rb(2) – O(12)	2.8872(16)		
Rb(2) – O(14)	2.7746(17)		
Rb(2) – O(6)	2.8786(16)		

Table S4. Selected bond lengths and angles for complex **4**.

Bond	Bond Length (Å)	Bond	Bond Angle (°)
Al(1) – Cs(1)	3.979	O(7) – Al(1) – O(5)	165.76(7)
Al(1) – N(1)	2.065(2)	N(1) – Al(1) – N(2)	90.90(8)
Al(1) – N(2)	2.0451(19)	N(1) – Al(1) – O(2)	89.04(7)
Al(1) – O(2)	1.8417(16)	N(2) – Al(1) – O(3)	89.48(7)
Al(1) – O(3)	1.8453(16)	O(2) – Al(1) – O(3)	90.54(7)
Al(1) – O(5)	1.8719(17)	O(1) – Cs(1) – O(2)	50.82(4)
Al(1) – O(7)	1.9084(16)	O(2) – Cs(1) – O(3)	50.45(4)
Cs(1) – O(1)	3.0356(18)	O(3) – Cs(1) – O(4)	50.64(4)
Cs(1) – O(2)	3.0694(15)	O(1) – Cs(1) – O(6)	107.28(6)
Cs(1) – O(3)	3.0763(15)	O(2) – Cs(1) – O(6)	65.57(5)
Cs(1) – O(4)	3.0975(18)	O(6) – Cs(1) – O(8)	127.57(5)
Cs(1) – O(6)	2.9220(19)		
Cs(1) – O(8)	3.0478(17)		

Table S5. Selected bond lengths and angles for complex **5**.

Bond	Bond Length (Å)	Bond	Bond Angle (°)
Al(1) – K(1)	3.5995(6)	O(7) – Al(1) – O(5)	166.72(6)
Al(1) – N(1)	2.0646(15)	N(1) – Al(1) – N(2)	90.64(6)
Al(1) – N(2)	2.0584(16)	N(1) – Al(1) – O(2)	88.45(6)
Al(1) – O(2)	1.8519(14)	N(2) – Al(1) – O(3)	90.18(6)
Al(1) – O(3)	1.8364(12)	O(2) – Al(1) – O(3)	90.85(6)
Al(1) – O(5)	1.9060(15)	O(1) – K(1) – O(2)	57.90(4)
Al(1) – O(7)	1.8784(14)	O(2) – K(1) – O(3)	58.54(4)
K(1) – O(1)	2.7808(16)	O(3) – K(1) – O(4)	57.45(4)
K(1) – O(2)	2.6588(13)	O(1) – K(1) – O(6)	111.08(5)
K(1) – O(3)	2.7137(14)	O(2) – K(1) – O(6)	67.27(4)
K(1) – O(4)	2.7698(18)	O(6) – K(1) – O(14)	122.00(5)
K(1) – O(6)	2.8365(15)	O(13) – Al(2) – O(15)	168.42(6)
K(1) – O(14)	2.6320(14)	N(3) – Al(2) – N(4)	89.11(6)
Al(2) – K(2)	3.6286(6)	N(3) – Al(2) – O(10)	89.27(6)
Al(2) – N(3)	2.0383(15)	N(4) – Al(2) – O(11)	90.03(6)
Al(2) – N(4)	2.0743(16)	O(10) – Al(2) – O(11)	91.55(6)
Al(2) – O(10)	1.8399(13)	O(9) – K(2) – O(10)	57.08(4)
Al(2) – O(11)	1.8432(12)	O(10) – K(2) – O(11)	57.78(4)
Al(2) – O(13)	1.9152(14)	O(11) – K(2) – O(12)	56.73(4)
Al(2) – O(15)	1.8982(14)	O(9) – K(2) – O(16)	104.05(5)
K(2) – O(9)	2.7923(15)	O(10) – K(2) – O(16)	65.59(4)
K(2) – O(10)	2.7330(12)	O(6) – K(2) – O(16)	156.19(5)
K(2) – O(11)	2.7296(13)	O(16) – K(2) – O(17)	79.95(5)
K(2) – O(12)	2.8129(14)		
K(2) – O(16)	2.6571(15)		
K(2) – O(6)	2.8076(14)		
K(2) – O(17)	3.146(2)		

Table S6. Summary of Crystallographic Refinement Data for complexes **1 - 5**.

Complex	1	2	3	4	5
Local Code	013rwfk20	063ap20	014rwfk20	016rwfk20	021rwfk21
CCDC Deposition Number	2096248	2096249	2096250	2096251	2096252
Crystal data					
Chemical formula	$C_{25}H_{30}AlN_2NaO_8\cdot 2(CH_2Cl_2)$	$C_{50}H_{60}Al_2K_2N_4O_{16}\cdot CHCl_3$	$C_{50}H_{60}Al_2N_4O_{16}Rb_2\cdot CHCl_3$	$C_{25}H_{30}AlCsN_2O_8\cdot CHCl_3$	$C_{74}H_{76}Al_2K_2N_4O_{17}$
M_r	706.33	1224.54	1317.28	765.77	1425.54
Crystal system, space group	Triclinic, $P\bar{1}$	Triclinic, $P\bar{1}$	Triclinic, $P\bar{1}$	Monoclinic, $P2_1/c$	Monoclinic, $P2_1/n$
a, b, c (Å)	10.7960 (5), 11.9409 (8), 14.6196 (7)	12.4551 (6), 15.8089 (10), 16.1748 (8)	12.5460 (3), 15.7343 (4), 16.4513 (5)	14.9518 (2), 12.8871 (1), 16.7675 (2)	15.0779 (2), 30.1479 (4), 17.5249 (3)
α, β, γ (°)	66.034 (5), 84.098 (4), 69.361 (5)	65.273 (5), 82.478 (4), 76.607 (5)	64.372 (3), 82.396 (2), 76.638 (2)	90, 98.577 (1), 90	90, 114.699 (2), 90
V (Å³)	1609.86 (17)	2812.1 (3)	2846.84 (15)	3194.72 (6)	7237.5 (2)
Z	2	2	2	4	4
Radiation type	Cu $K\alpha$	Mo $K\alpha$	Cu $K\alpha$	Cu $K\alpha$	Cu $K\alpha$
μ (mm^{-1})	4.17	0.41	4.42	12.03	1.98
Crystal size (mm)	0.17 × 0.14 × 0.05	0.17 × 0.11 × 0.08	0.36 × 0.20 × 0.12	0.26 × 0.18 × 0.18	0.49 × 0.13 × 0.07
Data collection					
Absorption correction	Multi-scan *CrysAlis PRO* 1.171.39.46 (Rigaku Oxford Diffraction, 2018) Empirical absorption correction using spherical harmonics, implemented in SCALE3 ABSPACK scaling algorithm.				
T_{min}, T_{max}	0.893, 1.000	0.969, 1.000	0.731, 1.000	0.670, 1.000	0.778, 1.000
No. of measured, independent and observed [$I > 2\sigma(I)$] reflections	12886, 6670, 5365	21284, 13911, 8926	30073, 11825, 10423	15348, 6656, 6283	44644, 14927, 11897
R_{int}	0.031	0.040	0.032	0.028	0.051
$(\sin\theta/\lambda)_{max}$ (Å^{-1})	0.631	0.696	0.631	0.632	0.630
Refinement					
$R[F^2 > 2\sigma(F^2)]$, $wR(F^2)$, S	0.043, 0.121, 1.03	0.061, 0.129, 1.05	0.032, 0.088, 1.03	0.028, 0.073, 1.05	0.043, 0.114, 1.02
No. of reflections	6670	13911	11825	6656	14927
No. of parameters	404	715	715	404	900
No. of restraints	1	0	0	3	0
$\Delta\rangle_{max}, \Delta\rangle_{min}$ (e Å^{-3})	0.50, -0.34	0.38, -0.39	0.67, -0.50	0.70, -1.29	0.58, -0.28
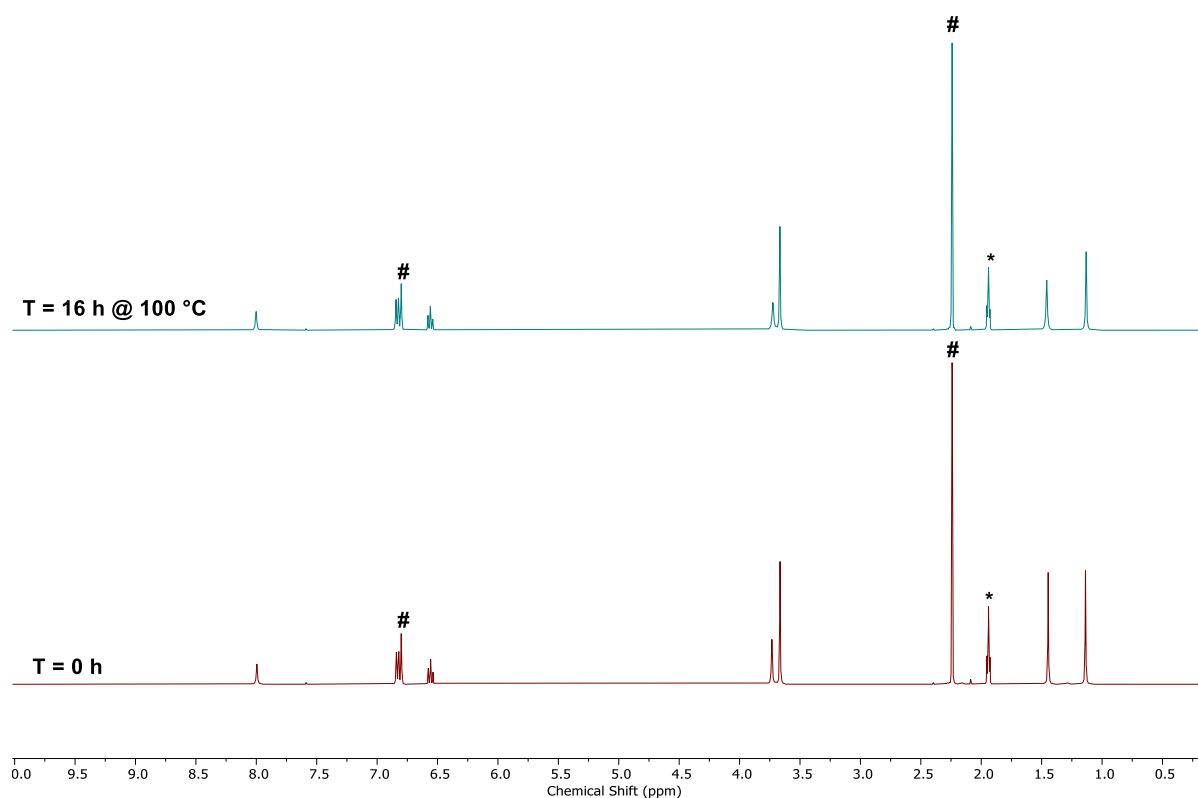
Figure S36. Temperature stability of complex **2**. ^{1}H NMR of complex 2 (400 MHz, MeCN-d_3(*), 298K) before and after heating for 16 hours at 100 °C, with an internal standard (mesitylene, #). No significant change was observed in the NMR integrals, when compared to the internal standard, before and after the heating period.

Figure S37. DOSY NMR spectrum (500 MHz, CDCl3, 298K) of complex **2**. Use of D value obtained from this experiment in the Stokes-Einstein equation yields a solvation radius of 6.0 Å.

Table S7. Data for the ROCOP of PA and CHO with complexes **1 – 4**.[a]

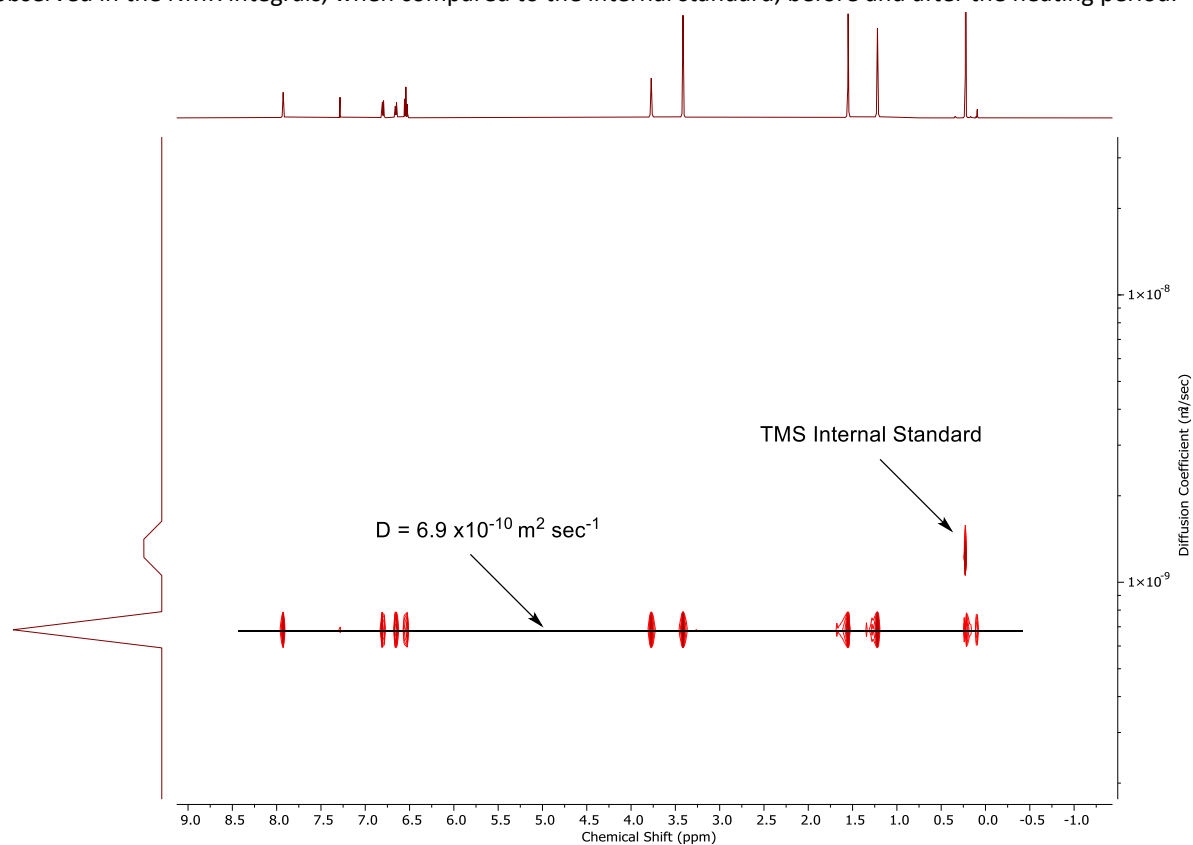| Entry	Catalyst	Time (m)	Conversion (%)	TON[b]	TOF[c] (h⁻¹)	k_{obs} (x10³)[d] (s⁻¹)	$M_{n, GPC}$ [Đ][e] (kg mol⁻¹)	$M_{n, Th.}$[f] (kg mol⁻¹)
1	**1**	15	45	180	720 ± 9	0.91 ± 0.02	9.3 [1.06]	22.1
2	**2**	15	67	268	1072 ± 6	1.50 ± 0.03	14.3 [1.06]	33.0
3	**2**	25	>99	400	-	-	20.1 [1.06]	49.3
4	**3**	15	71	284	1136 ± 6	1.53 ± 0.03	14.4 [1.06]	34.9
5	**4**	15	54	216	875 ± 8	1.18 ± 0.03	10.4 [1.05]	26.6

[a] Conditions: [Cat]:[PA]:[CHO] = 1:400:2000, T = 100 °C. [b]Turnover number (TON) = number of moles of anhydride consumed/number of moles of catalyst. Determined by ¹H NMR through comparison of resonances associated with PA (8.10 – 7.85 ppm) and PCHPE (7.65 – 7.30 ppm). [c] Turnover Frequency (TOF) = TON/time (hours). [d] Observed rate constant for a linear fit of the data (See Figure 2, B), without error weighting. [e] Determined by GPC, in THF at 30 °C, using narrow dispersity polystyrene standards. [f] Theoretical M_n value. Determined through (TON x M_n(repeat unit = 246.26 for PCHPE))/(number of equivalent of catalyst x 2 (as each catalyst contains 2 acetate groups)).
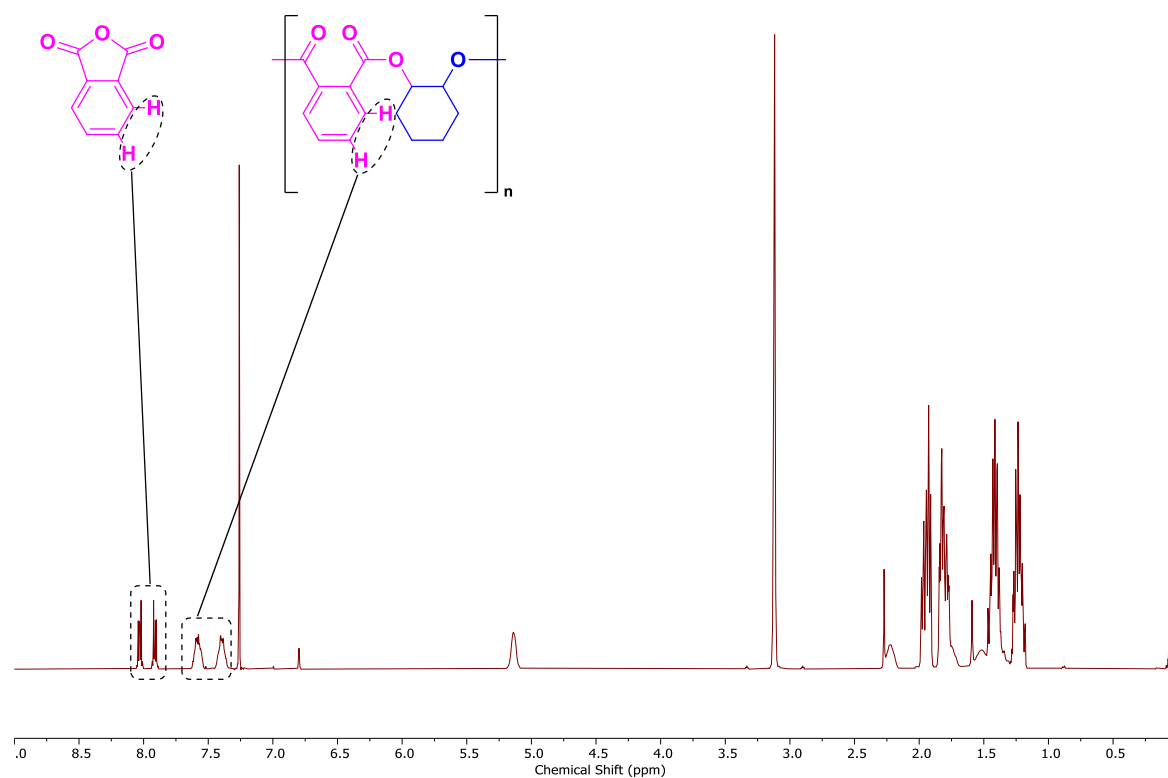
Figure S38. ¹H NMR spectrum (400 MHz, CDCl₃, 298 K) of reaction mixture of CHO and PA. Conversion of PA (%) = ((∫7.65-7.30 ppm)/(∫8.10-7.30 ppm))*100. TON$_{Epoxide}$ = TON$_{Anhydride}$ = Conv.(%)*400.
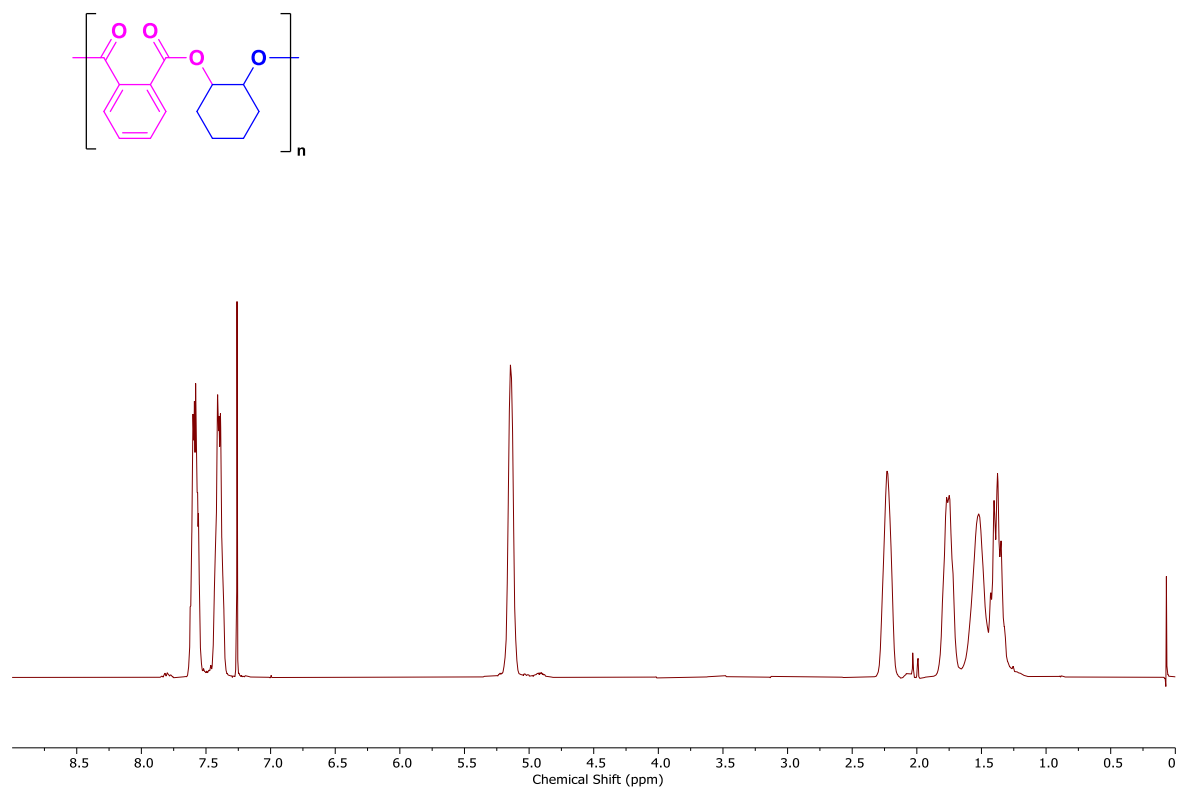
Figure S39. ^{1}H NMR spectrum (400 MHz, CDCl$_3$, 298 K) of purified PCHPE.
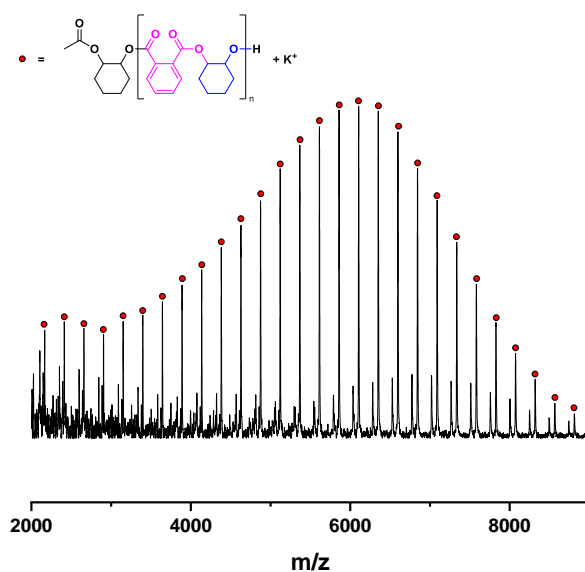

Figure S40. MALDI-ToF spectrum of PCHPE obtained with complex **2.** Observed end group weight = 198.45 g mol^{-1}, calculated end group weight = 197.30 g mol^{-1}. Observed (average) distance between peaks = 246.11 g mol^{-1}, theoretical M$_n$(repeat unit) = 246.26 g mol^{-1}. Minor peaks attributed to minor cyclohexanol initiating species.[11]

Figure S41. ^{1}H NMR spectrum (400 MHz, CDCl$_3$, 298 K) of reaction mixture of CHO and TCA. Conversion of TCA (%) = (($\int$4.90-4.50 ppm/2)/($\int$5.90-5.50 ppm))*100. TON$_{Epoxide}$ = TON$_{Anhydride}$ = Conv.(%)*400. Spectroscopic data is consistent with prior literature reports.[12]

Figure S42. ^{1}H NMR spectrum (400 MHz, CDCl$_3$, 298 K) of reaction mixture of CHO and NBA. Conversion of NBA (%) = ($\int$4.90-4.50 ppm/($\int$6.40-5.90 ppm))*100. TON$_{Epoxide}$ = TON$_{Anhydride}$ = Conv.(%)*400. Spectroscopic data is consistent with prior literature reports.[13]

Figure S43. ^{1}H NMR spectrum (400 MHz, CDCl$_3$, 298 K) of reaction mixture of tBGE and PA. Conversion of PA (%) = ($\int$7.75-7.35 ppm/($\int$8.05-7.35 ppm))*100. TON$_{Epoxide}$ = TON$_{Anhydride}$ = Conv. (%)*400. Spectroscopic data is consistent with prior literature reports.[14]
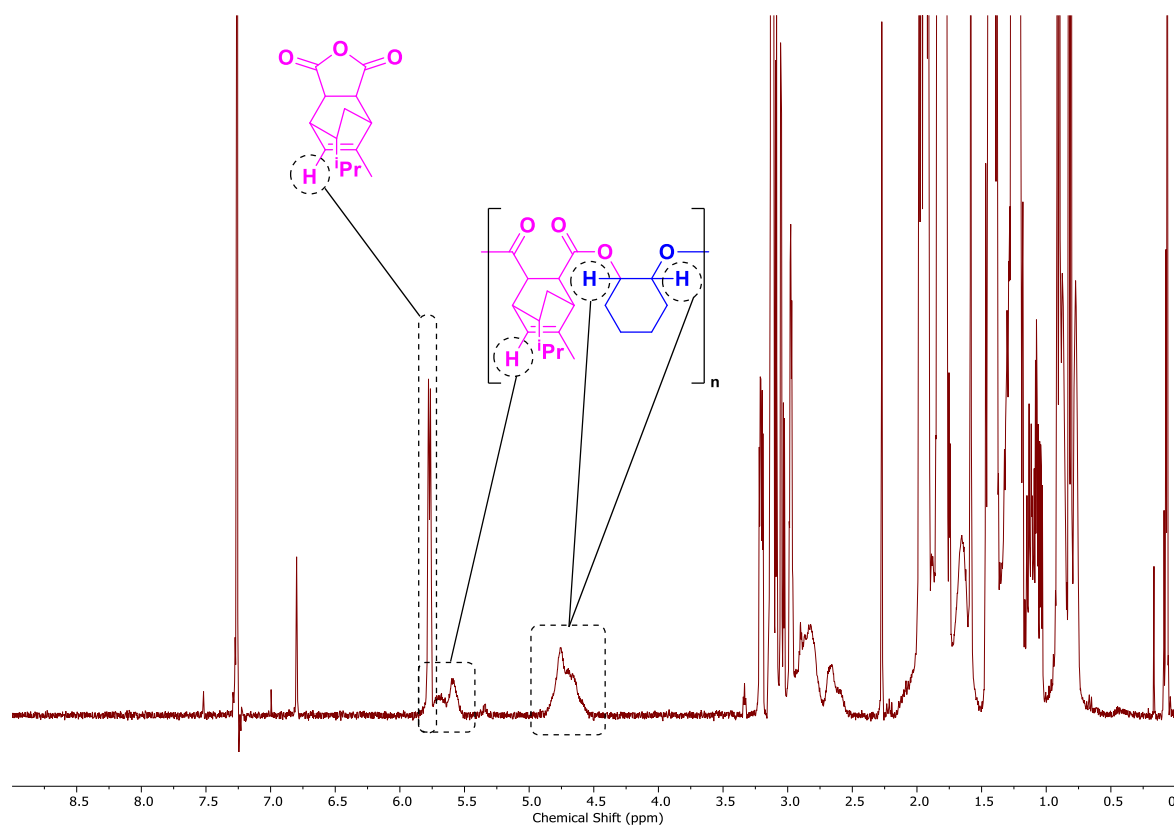

Figure S44. ^{1}H NMR spectrum (400 MHz, CDCl$_3$, 298 K) of reaction mixture of SO and PA. Conversion of PA (%) = ($\int$7.70-7.50 ppm/($\int$8.00-7.90 ppm + $\int$7.70-7.50 ppm))*100. TON$_{Epoxide}$ = TON$_{Anhydride}$ = Conv. (%)*400. Spectroscopic data is consistent with prior literature reports.[14]
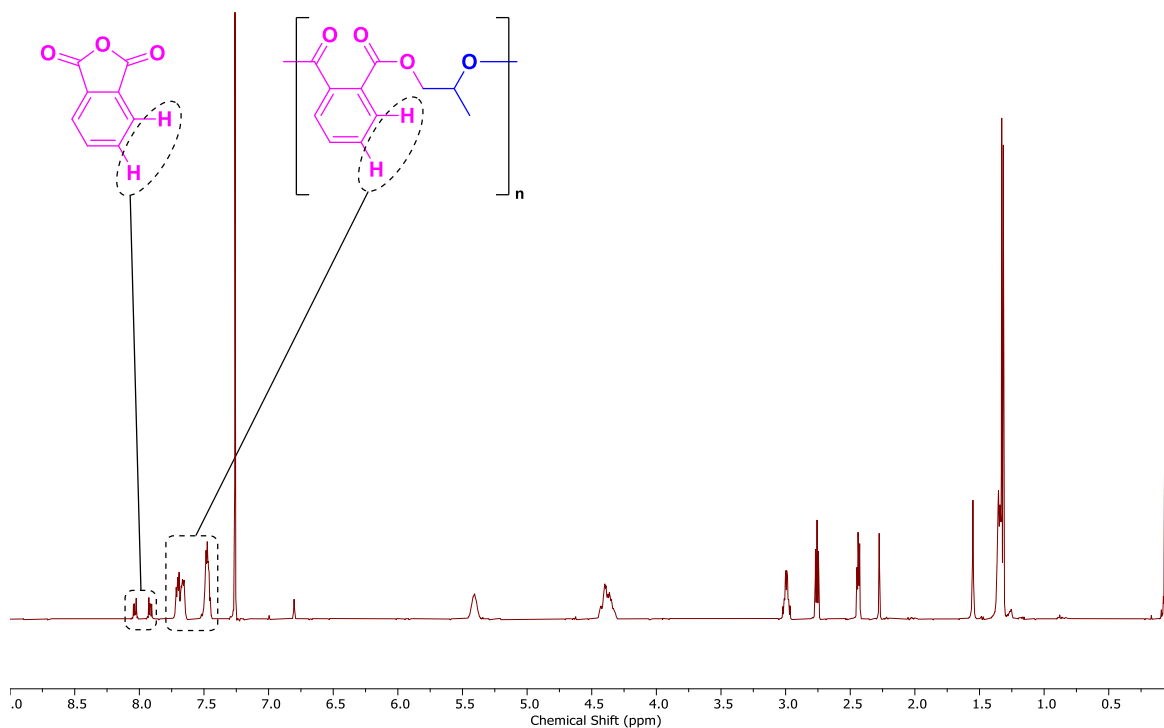
Figure S45. ^{1}H NMR spectrum (400 MHz, CDCl$_3$, 298 K) of reaction mixture of PO and PA. Conversion of PA (%) = ($\int$7.75-7.40 ppm/($\int$8.10-7.40 ppm)*100. TON$_{Epoxide}$ = TON$_{Anhydride}$ = Conv. (%)*400. Spectroscopic data is consistent with prior literature reports.[14]
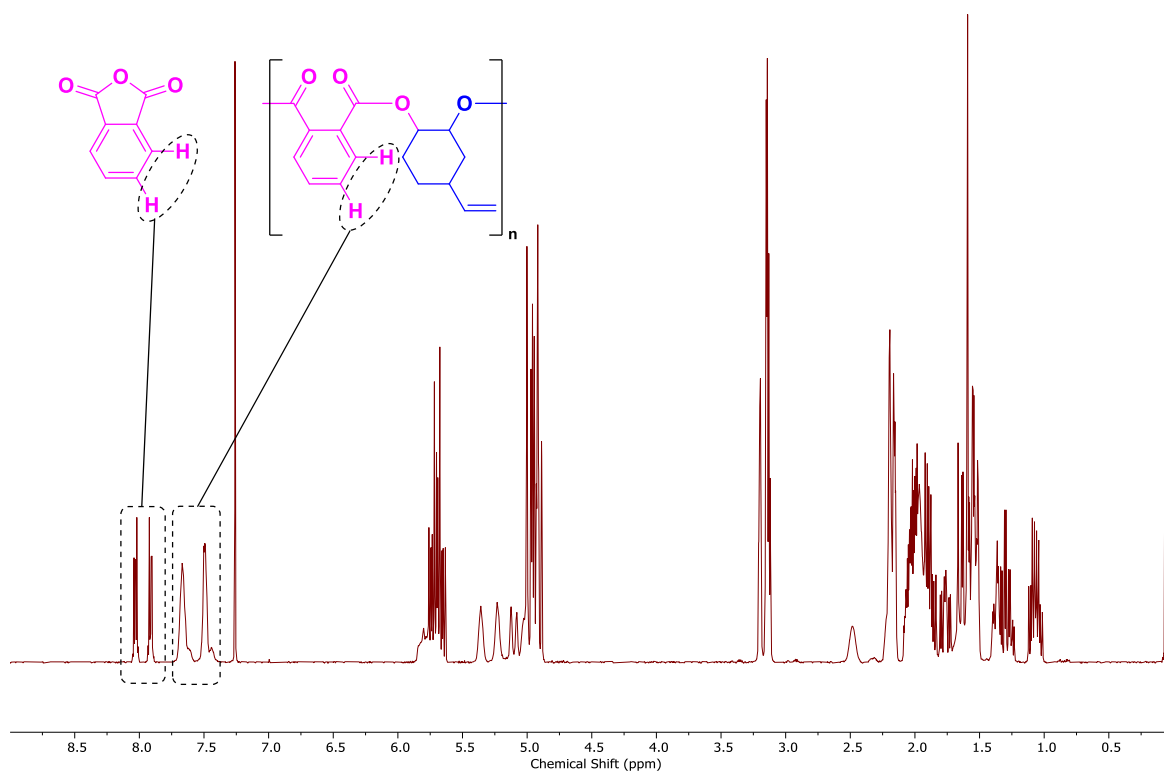
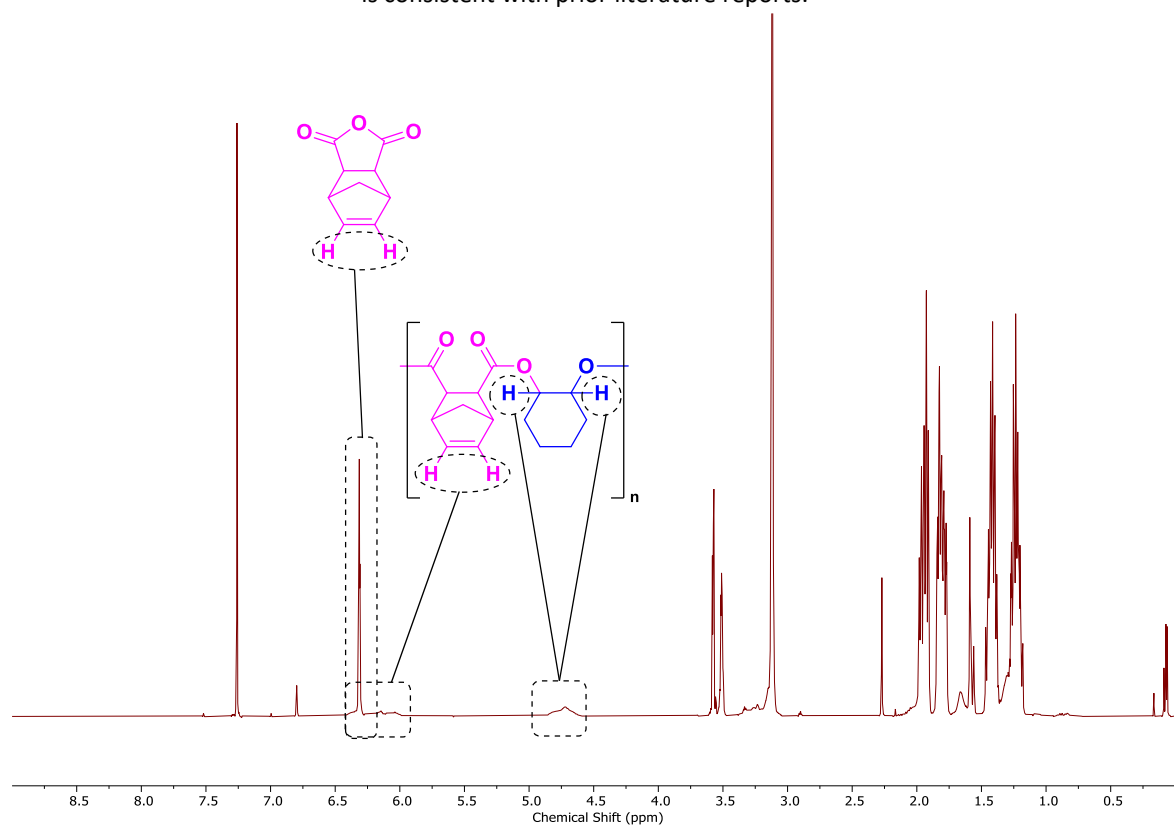**Figure S46.** ^{1}H NMR spectrum (400 MHz, CDCl$_3$, 298 K) of reaction mixture of vCHO and PA. Conversion of PA (%) = ($\int$7.80-7.40 ppm/($\int$8.10-7.40 ppm)*100. TON$_{Epoxide}$ = TON$_{Anhydride}$ = Conv. (%)*400. Spectroscopic data is consistent with prior literature reports.[14]
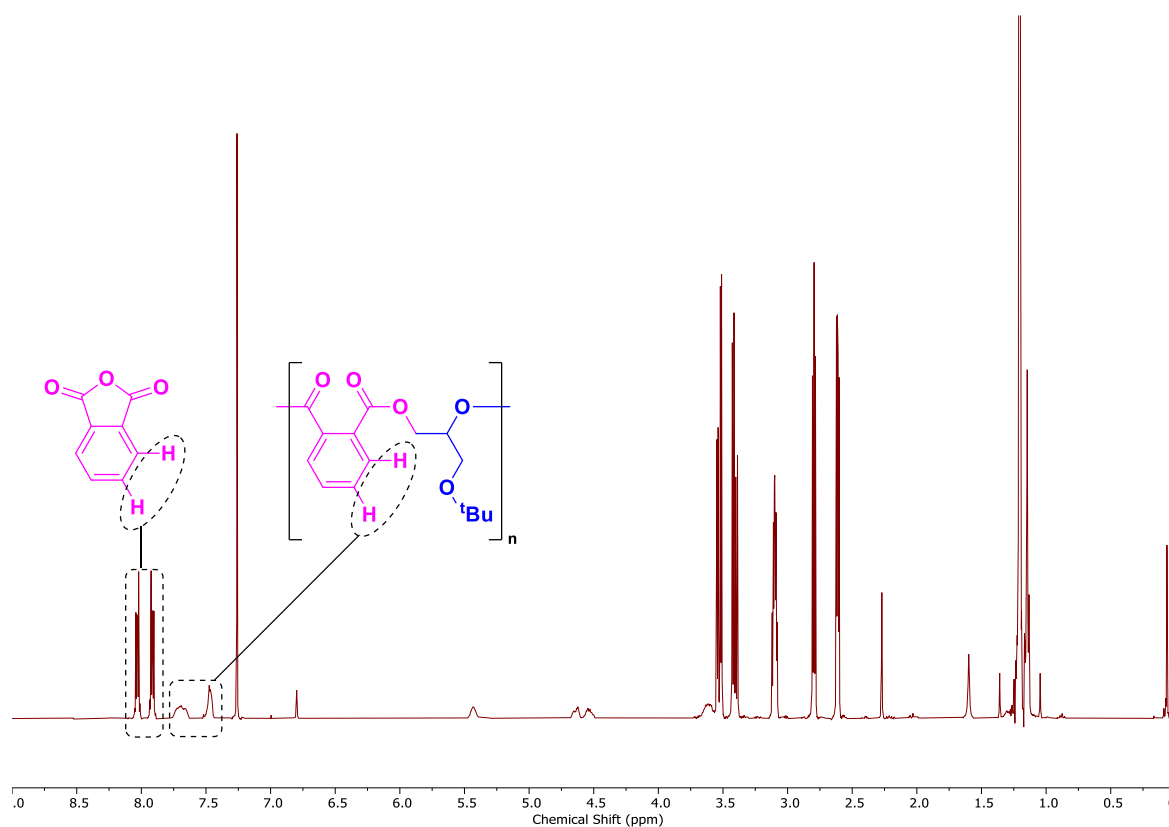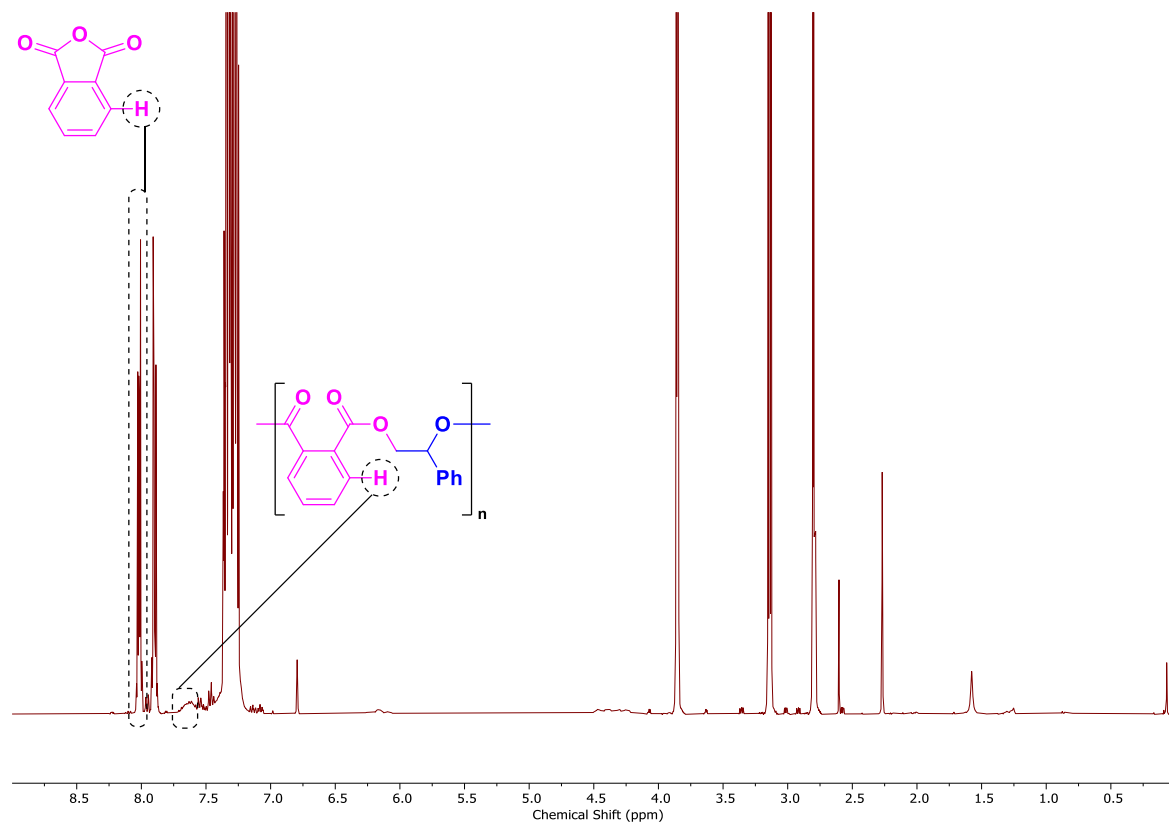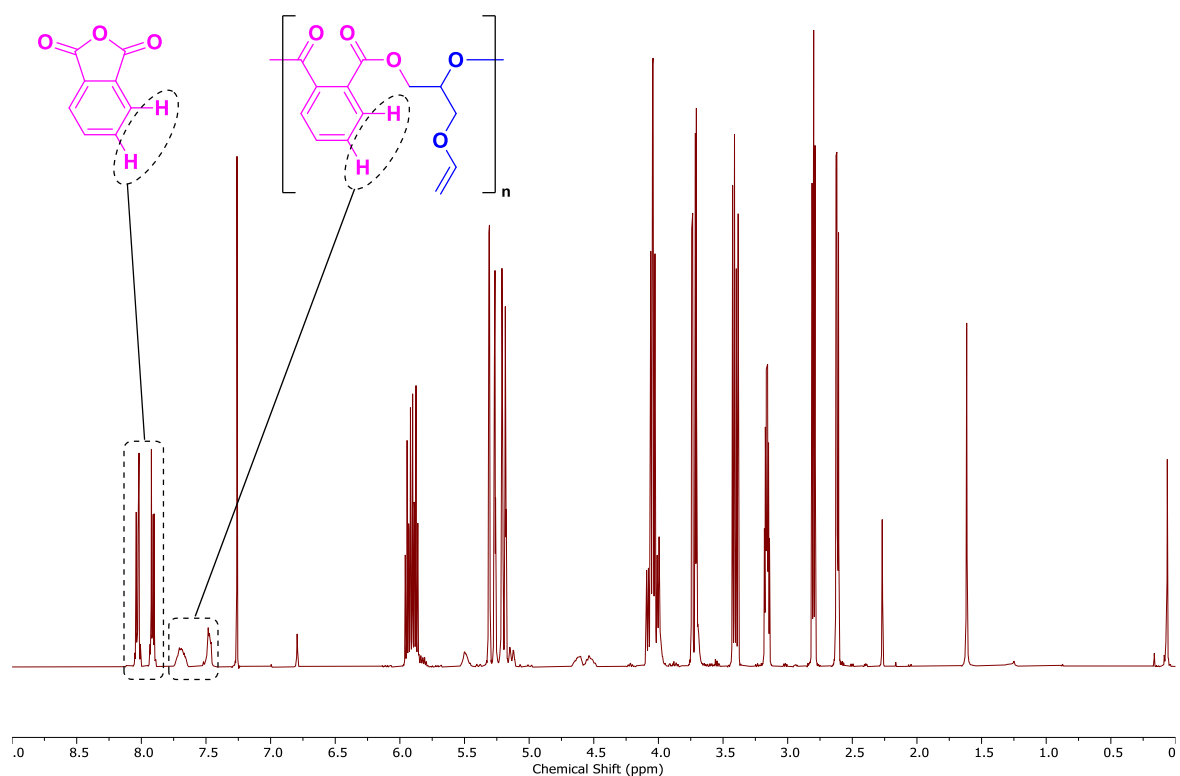
Figure S47. ^{1}H NMR spectrum (400 MHz, CDCl$_3$, 298 K) of reaction mixture of AGE and PA**.** Conversion of PA (%) = ($\int$7.80-7.40 ppm/($\int$8.10-7.40 ppm)*100. TON$_{Epoxide}$ = TON$_{Anhydride}$ = Conv. (%)*400**.** Spectroscopic data is consistent with prior literature reports.[14]

Figure S48. ^1H NMR spectrum (400 MHz, $CDCl_3$, 298 K) of reaction mixture of CHO and CO_2 (1 bar). Conversion of CHO to PCHC (%) = ((∫4.90-4.35 ppm/(∫4.90-4.35 ppm + ∫3.25-3.00 ppm)*100. TON_{PCHC} = Conv.(%)*2000. $Selectivity_{PCHC}$ (%) = (∫4.90-4.35 ppm/(∫4.90-4.35 ppm + ∫4.10-3.90 ppm))*100. Spectroscopic data is consistent with prior literature reports.[12]
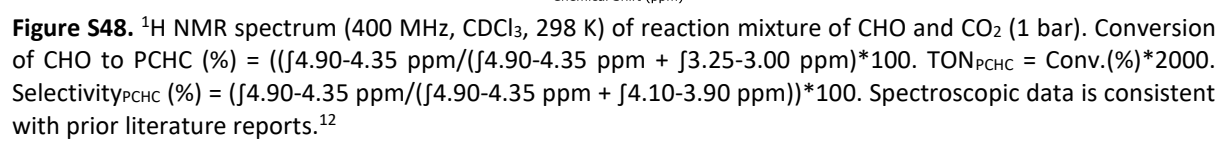
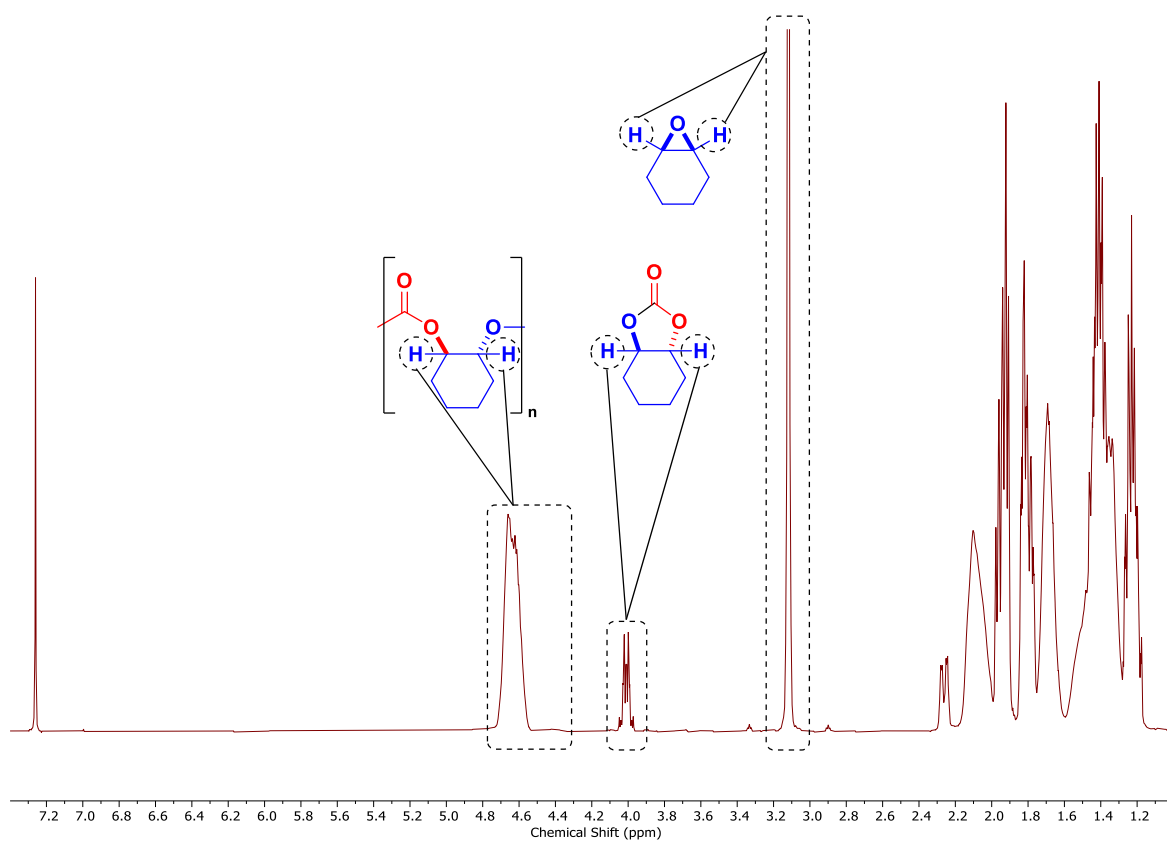**Figure S49.** ^{1}H NMR spectrum (400 MHz, CDCl$_3$, 298 K) of reaction mixture of CHO and CO$_2$ (20 bar). Conversion of CHO to PCHC (%) = (($\int$4.90-4.35 ppm/($\int$4.90-4.35 ppm + $\int$3.25-3.00 ppm)*100. TON$_{PCHC}$ = Conv.(%)*2000. Selectivity$_{PCHC}$ (%) = ($\int$4.90-4.35 ppm/($\int$4.90-4.35 ppm + $\int$4.10-3.90 ppm))*100. Spectroscopic data is consistent with prior literature reports.[12]
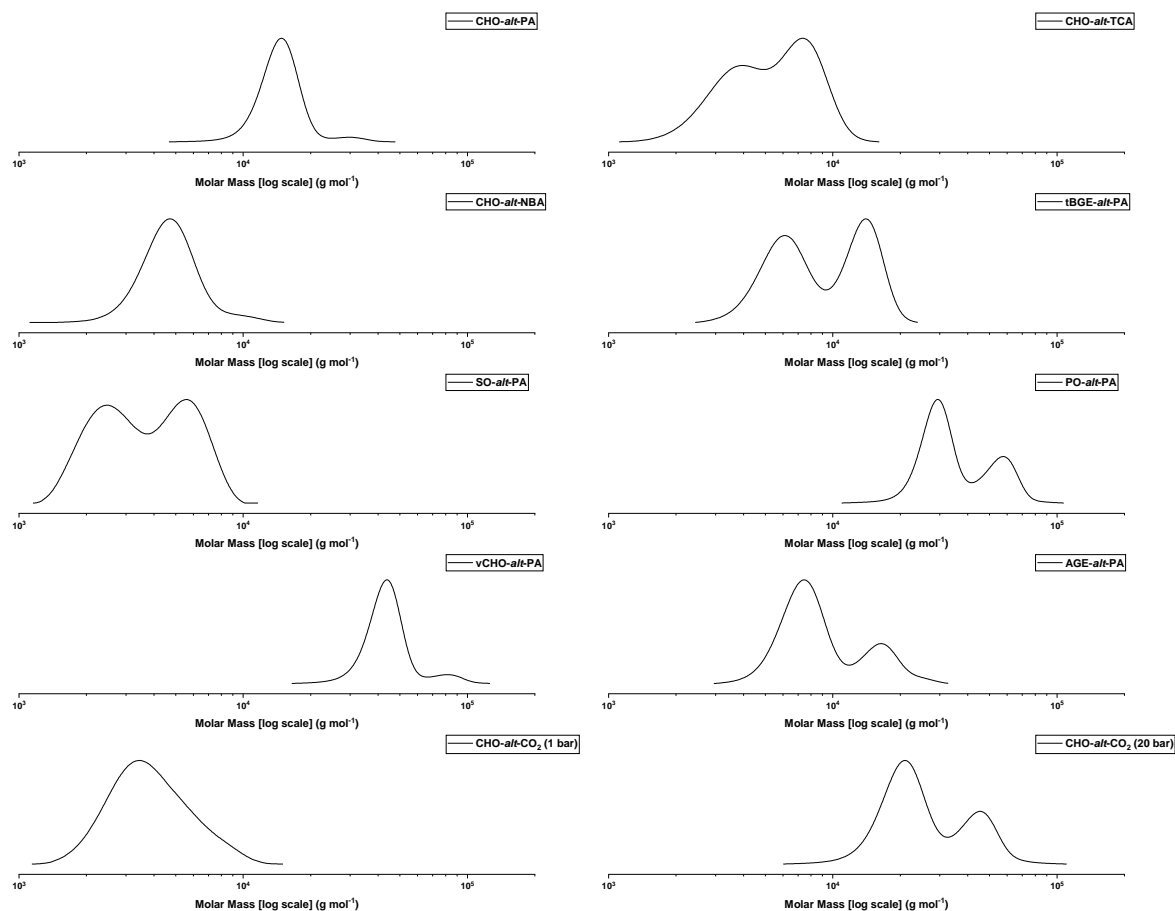
Figure S50. GPC traces for polymers corresponding to Table 2, Entries 1-10. It should be noted that the polymer molecular mass distributions are bimodal, owing to the presence of monofunctional (acetate) and bifunctional (diol or diacid, present as a result of residual H_2O in epoxide or anhydride) initiators.

Table S8. Data for the ROCOP of epoxide and anhydrides with complex **2** at full anhydride conversion. [a]

Entry	Monomer	Time (m)	Conv (%)	TON[b]	$M_{n, GPC}$ [Đ][c] (kg mol^{-1})	$M_{n, Th.}$[d] (kg mol^{-1})
1	CHO / PA	26	>99	400	20.1 [1.06]	49.3
2	CHO / TCA	120	>99	400	13.4 [1.21]	66.4
3	CHO / NBA	120	>99	400	13.5 [1.13]	52.4
4	tBGE / PA[e]	90	90	360	25.5 [1.19]	55.6
5	SO / PA	165	>99	400	14.5 [1.21]	53.6
6	vCHO / PA	75	>99	400	58.3 [1.07]	55.2
7	AGE / PA[e]	85	99	398	27.4 [1.18]	49.6

[a] Conditions: [Cat]:[PA] = 1:400, 1 mL epoxide, [Cat] = 4.9 mmol, T = 100 °C. [b]Turnover number (TON) = number of moles of anhydride consumed/number of moles of catalyst. Determined by ^1H NMR. [c] Determined by GPC, in THF at 30 °C, using narrow dispersity polystyrene standards. [d] Theoretical M_n value. Determined through (TON x M_n(repeat unit))/(number of equivalent of catalyst x 2 (as each catalyst contains 2 acetate groups)). [e] Significant transesterification was observed after full anhydride conversion; data given before full conversion is reached.

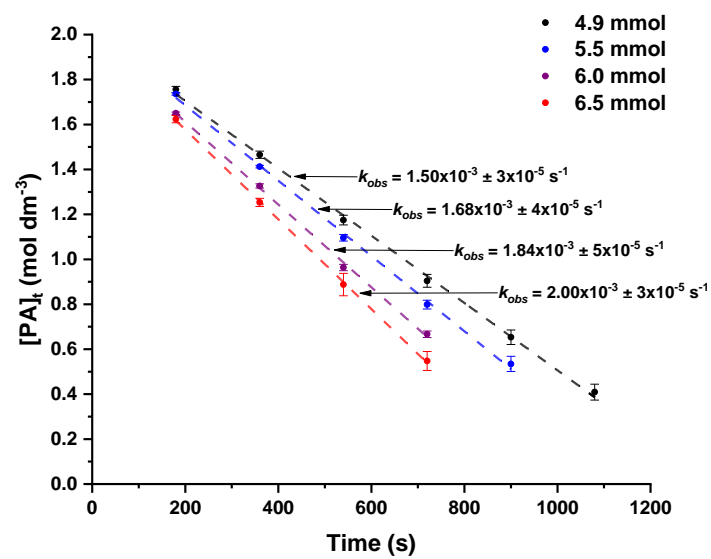**Figure S51.** Plot of $[PA]_t$ *vs*. Time at a range of [**2**]. A linear relationship is observed in all cases. All reactions repeated in triplicate, with average values of $[PA]_t$ plotted and error $\pm \sigma / \sqrt{n}$.
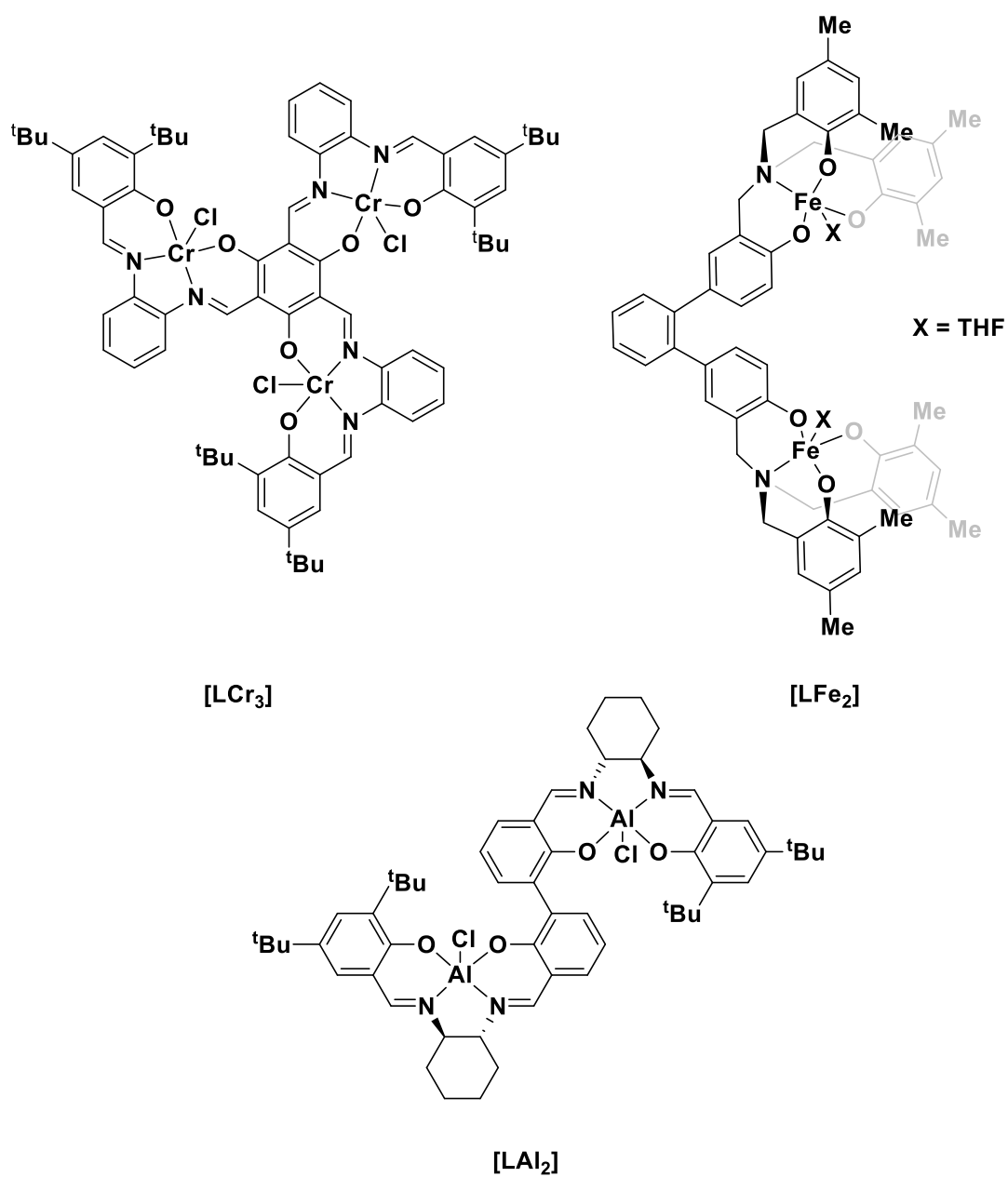
[LCr₃]

[LFe₂]

X = THF

[LAl₂]

Chart S1. Structures of catalysts relating to Table 3, Entries 9, 11 and 14.

Computational Details

Density Functional theory (DFT) calculations were performed using Gaussian16 suite of codes (revision A.03). Geometries were fully optimised without any symmetry or geometry constraints. The nature of all the stationary points as minima or transition states (first-order saddle points) on the potential energy surface was verified by calculations of the vibrational frequency spectrum. All transition states were characterised by precisely one negative frequency corresponding to the intended reaction and were further confirmed by intrinsic reaction coordinate (IRC) calculations.

Free enthalpies were first calculated at 298.15 K and a standard-state concentration in solution of 1 M within the harmonic approximation for vibrational frequencies.

Using the GoodVibes software, free enthalpies were recomputed using Grimme quasi-harmonic approximation, with a cut off frequency of 50 cm^{-1}, and a temperature (T = 373.15 K) and concentration correction applied (at [Cat] = 4.94 mM or [CHO]0 = 9.88 M)).[15, 16]

Geometry optimisations were carried out using ωb97xD functional. The 6-31+G(d,p) basis set was used for C and H atoms, 6-311G+(d) for Al, K, O and N atoms. Solvent effects in cyclohexene oxide were computed using the cpcm continuum model, using modified parameters for THF (eps=16, epsinf=1.867).[17]

Full coordinates for all structures, together with computed energies and vibrational frequency data, are available via the corresponding Gaussian 09 output files, stored in the open-access digital repository: DOI:10.6084/m9.figshare.14955234.

Table S9. Summary of uncorrected computed structures

Structure	G (Hartrees)	ΔG (Kcal mol^{-1})
CHO	-309.679573	-
I	-2715.724047	-
Reference (I + CHO)	-3025.403620	0.0
I$_K$	-3025.402824	+0.5
Pre-TS$_{I-IIK}$	-3025.400396	+2.0
TS$_{I-IIK}$	-3025.348112	+34.8
Post-TS$_{I-IIK}$	-3025.365273	+24.1
II$_K$	-3025.36664	+23.2
I$_{Al}$	-3025.391953	+7.3
Pre-TS$_{I-IIAl}$	-3025.388626	+9.4
TS$_{I-IIAl}$	-3025.365923	+23.7
II$_{Al}$ (/post-TS$_{I-IIAl}$)	-3025.407460	-2.4

^{a} ωb97xD/C H O= 6-31+g(d,p)/K Al = 6-311+g(d)/solvent = modified THF eps=16 epsinf=1.867.

Table S10. Correction computed structures

Structure	Corrections					
	T^b		T + [Cat]^c		T + [CHO]^d	
	G (Hartrees)	ΔG (Kcal mol^{-1})	G (Hartrees)	ΔG (Kcal mol^{-1})	G (Hartrees)	ΔG (Kcal mol^{-1})
CHO	-309.6890640	-	-309.6912960	-	-309.6823140	-
I	-2715.742497	-	-2715.744729	-	-2715.735747	-
Reference	-3025.431561	**0.0**	-3025.436025	**0.0**	-3025.418061	**0.0**
I$_K$	-3025.42225	+5.8	-3025.424482	+7.2	-3025.415500	+1.6
Pre-TS$_{I-IIK}$	-3025420565	+6.9	-3025.422797	+8.3	-3025.413815	+2.7
TS$_{I-IIK}$	-3025.367957	+39.9	-3025.370189	+41.3	-3025.361207	+35.7
Post-TS$_{I-IIK}$	-3025.384582	+29.5	-3025.386814	+30.9	-3025.377832	+25.2
II$_K$	-3025.38668	+28.2	-3025.388912	+29.6	-3025.379930	+23.9
I$_{Al}$	-3025.411441	+12.6	-3025.413673	+14.0	-3025.404691	+8.4
Pre-TS$_{I-IIAl}$	-3025.408603	+14.4	-3025.410835	+15.8	-3025.401853	+10.2
TS$_{I-IIAl}$	-3025.385207	+29.1	-3025.387438	+30.5	-3025.378457	+24.9
II$_{Al}$	-3025.42782	+2.3	-3025.430052	+3.7	-3025.421070	+1.9

^{a} ωb97xD/C H O= 6-31+g(d,p)/K Al = 6-311+g(d)/solvent = modified THF eps=16 epsinf=1.867. ^{b} Temperature correction, T = 373.15 K. ^{c} Catalyst concentration = 4.94 mM. ^{d} Epoxide (CHO) concentration = 9.88 M.
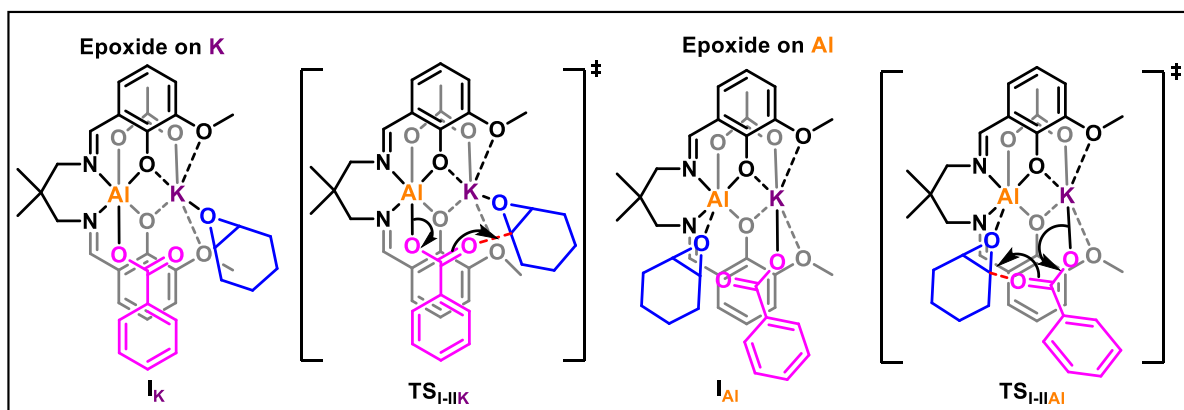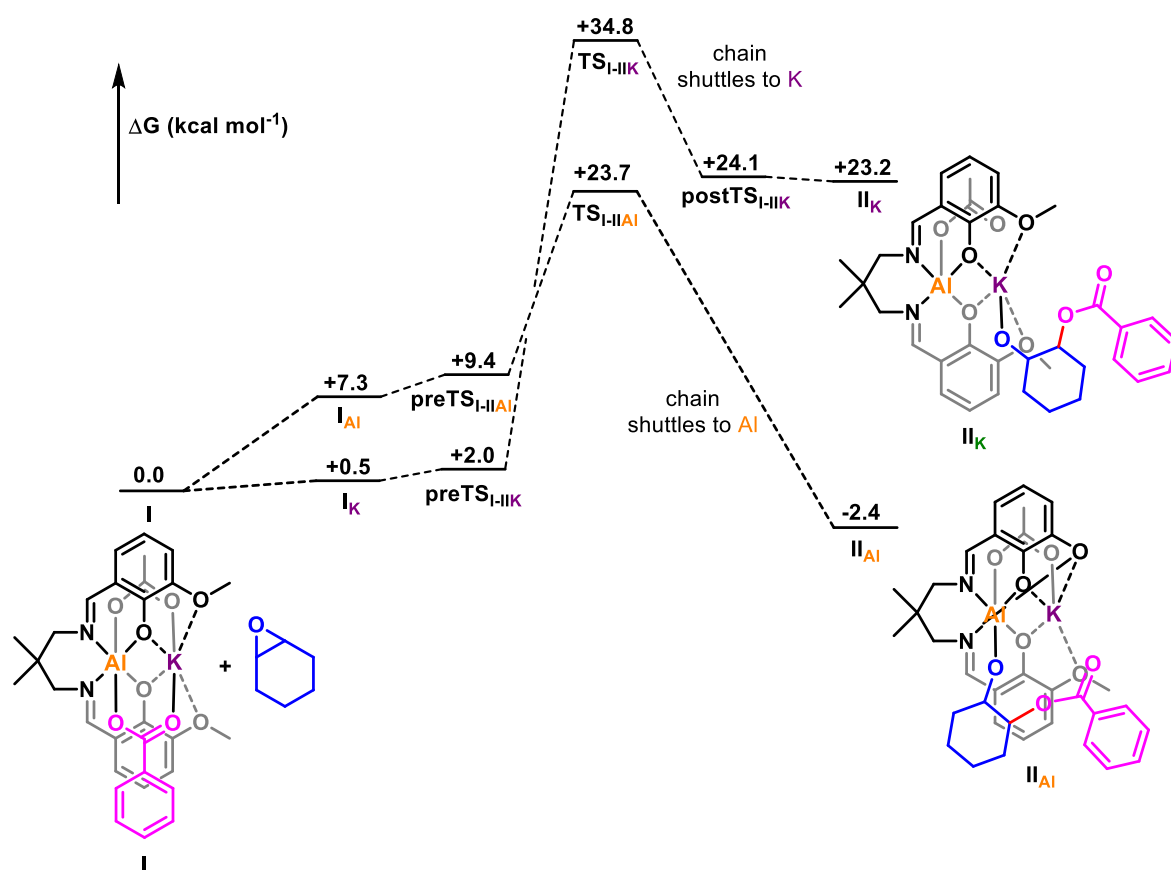
Figure S52. Computed Reaction Profile for epoxide ring-opening. ωb97xD/C H O= 6-31+g(d,p)/K Al = 6-311+g(d)/solvent = modified THF eps=16 epsinf=1.867 (cpcm).

Figure S53. IRC for TS$_{\text{I-IIk}}$ showing connected intermediates either side.. Key bond being formed shown. Maxpoints=50, maxcycle=40, stepsize=20

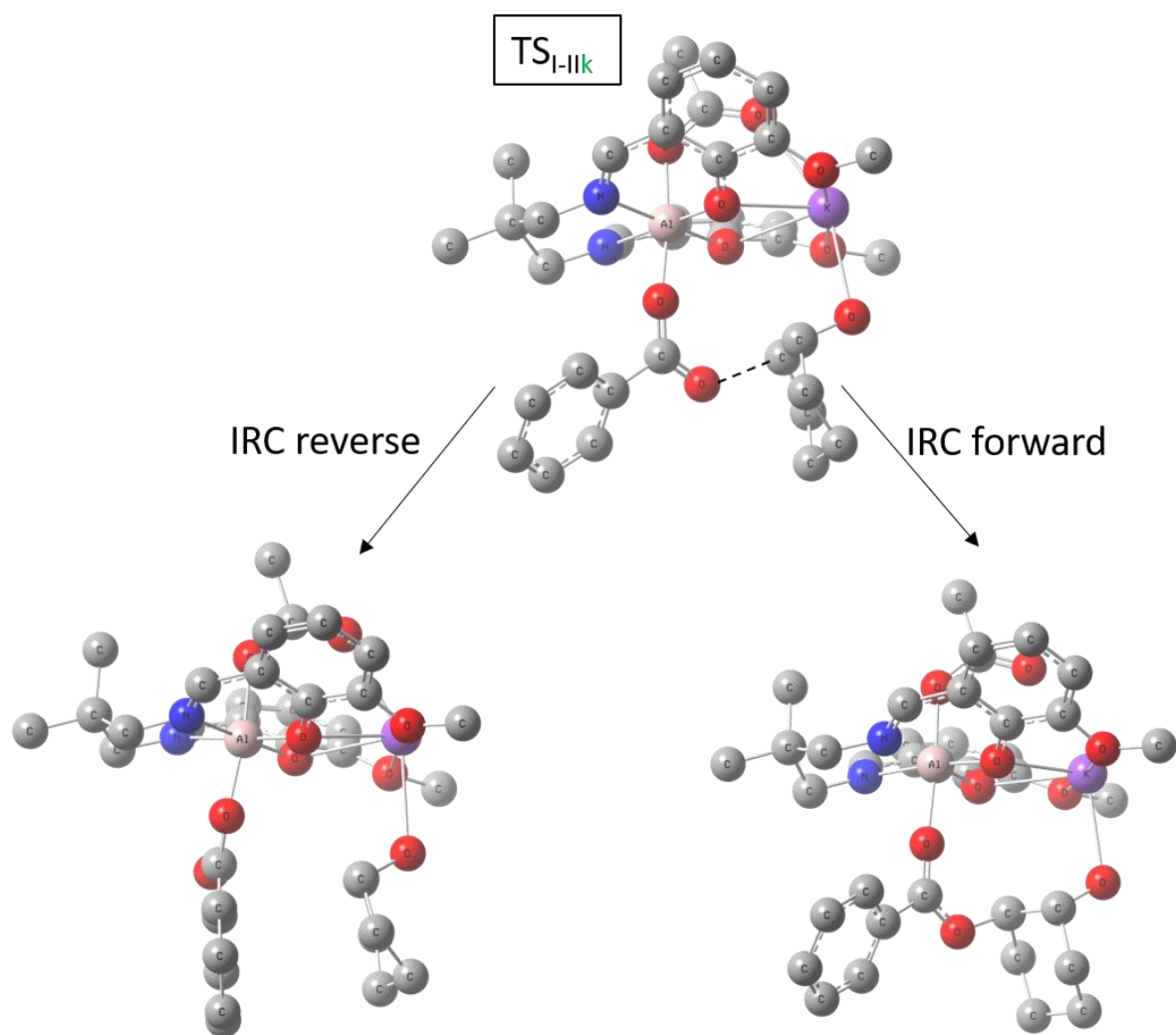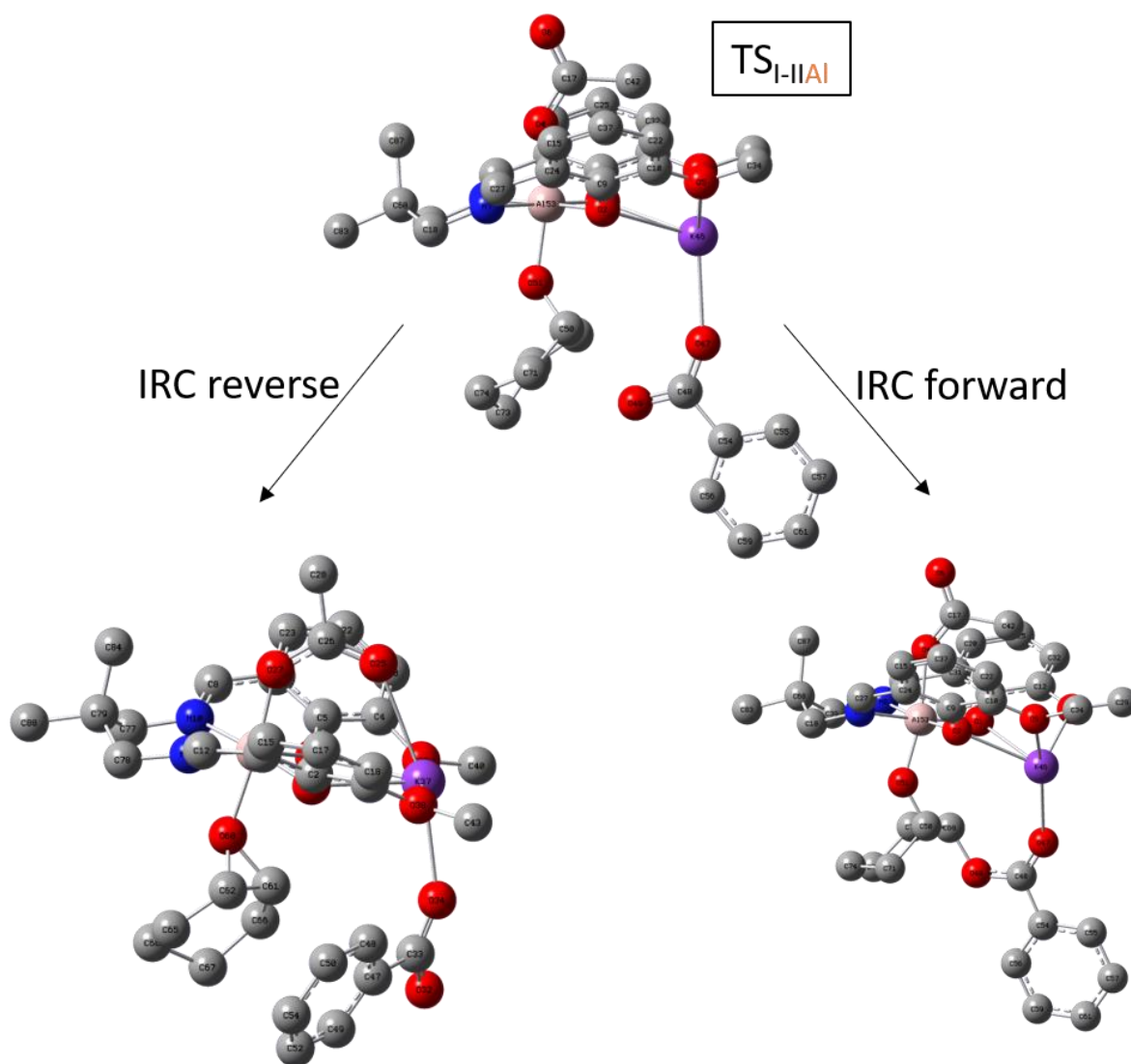**Figure S54.** IRC for TS$_{I-IIAl}$ showing connected intermediates either side. Maxpoints=50, maxcycle=40, stepsize=20
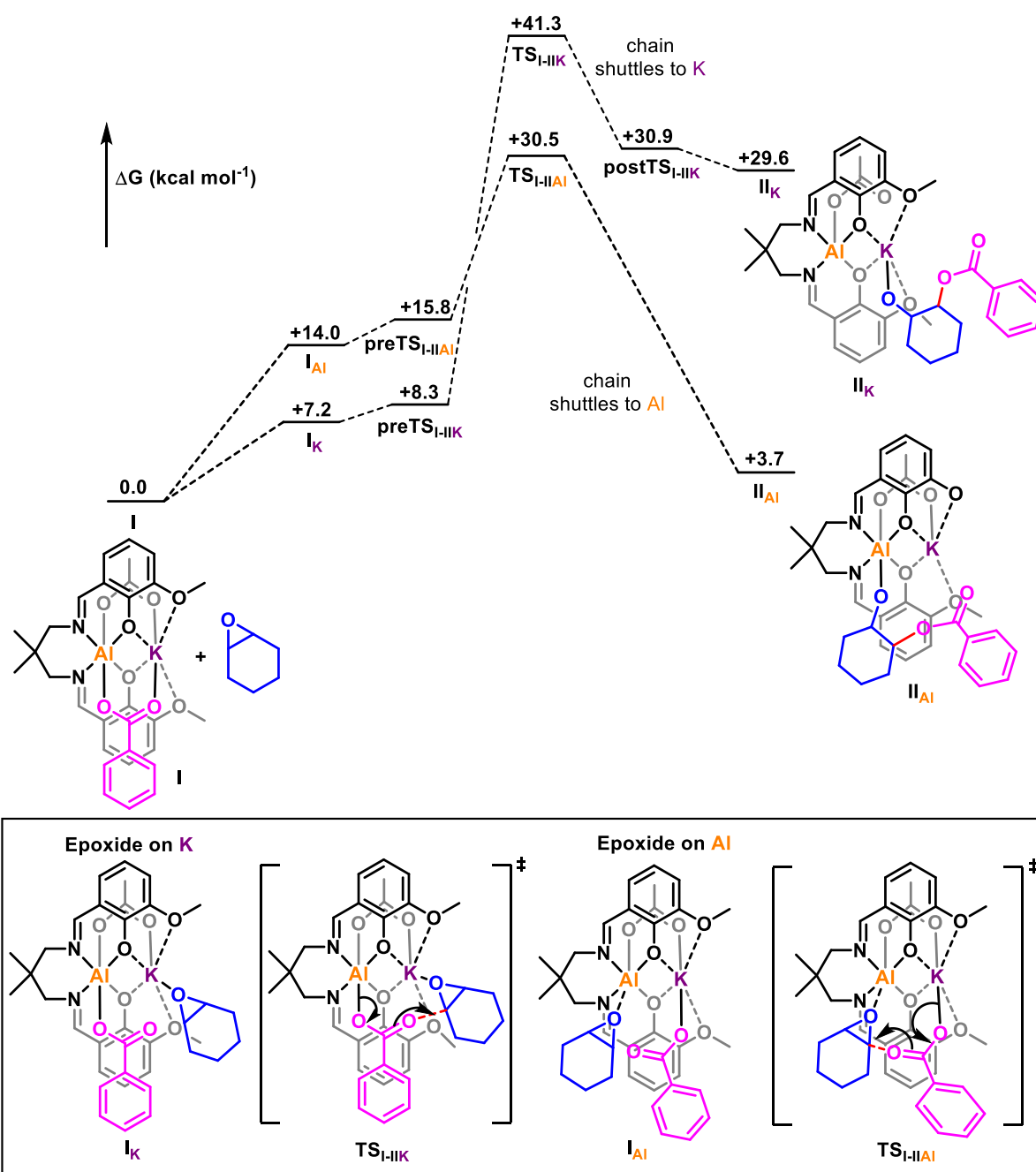
Figure S55. Computed Pathways for lowest free enthalpy TS. Reaction profile showing key intermediates and transitions states computed with temperature corrections and accounting for catalyst concentration.
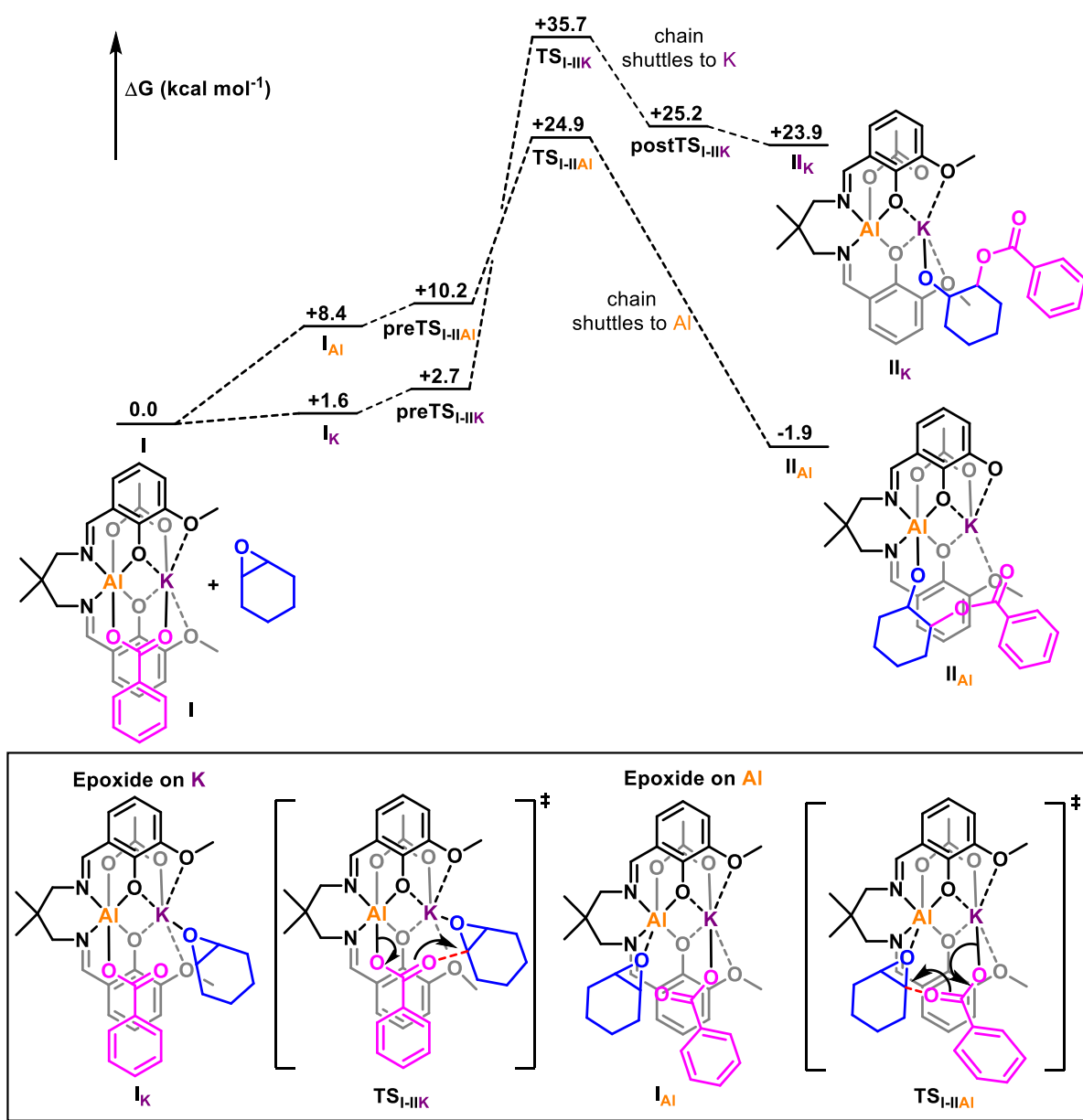
Figure S56. Computed Pathways for lowest free enthalpy TS**.** Reaction profile showing key intermediates and transitions states computed with temperature corrections and accounting for excess epoxide.

References

1.   Dakshinamoorthy, D.; Weinstock, A. K.; Damodaran, K.; Iwig, D. F.; Mathers, R. T., Diglycerol-based polyesters: melt polymerization with hydrophobic anhydrides. *ChemSusChem* **2014,** *7* (10), 2923-9.

2.   Thevenon, A.; Garden, J. A.; White, A. J.; Williams, C. K., Dinuclear Zinc Salen Catalysts for the Ring Opening Copolymerization of Epoxides and Carbon Dioxide or Anhydrides. *Inorg. Chem.* **2015,** *54* (24), 11906-15.

3.   Artus, G. R. J.; Rauch, M. U.; Herrman, W. A., Multiple Bonds between Main Group Elements and Transition Metals. 153.1 Rhenium(V) Oxo Complexes with Tetradentate Schiff Bases: Structural Considerations. *Inorg. Chem.* **1996,** *35*, 1988-1991.

4.   Cosier, J.; Glazer, A. M., A nitrogen-gas-stream cryostat for general X-ray diffraction studies. *J. Appl. Cryst.* **1986,** *19*, 105-107.

5.   CrysAlisPRO, Oxford Diffraction /Agilent Technologies UK Ltd, Yarnton, England.

6.   Sheldrick, G. M., Crystal structure refinement with SHELXL. *Acta Cryst.* **2015,** *C71*, 3-8.

7.   a) SHELXTL v5.1, Bruker AXS, Madison, WI, 1998. b) Sheldrick, G. M., SHELXT − Integrated SpaceGroup and Crystal-Structure Determination. *Acta. Cryst.* **2015,** *A71*, 3-8.

8.   Dolomanov, O. V.; Bourhis, L. J.; Gildea, R. J.; Howard, J. A. K.; Puschmann, H., OLEX2: a complete structure solution, refinement and analysis program. *J. Appl. Cryst.* **2009,** *42*, 339-341.

9.   Diment, W. T.; Stosser, T.; Kerr, R. W. F.; Phanopoulos, A.; Durr, C. B.; Williams, C. K., Ortho-vanillin derived Al(iii) and Co(iii) catalyst systems for switchable catalysis using epsilon-decalactone, phthalic anhydride and cyclohexene oxide. *Catal. Sci. Technol.* **2021,** *11* (5), 1737-1745.

10.   Du, H.; Pang, X.; Yu, H.; Zhuang, X.; Chen, X.; Cui, D.; Wang, X.; Jing, X., Polymerization of rac-Lactide Using Schiff Base Aluminum Catalysts: Structure, Activity, and Stereoselectivity. *Macromolecules* **2007,** *40* (6), 1904-1913.

11.   Deng, J.; Ratanasak, M.; Sako, Y.; Tokuda, H.; Maeda, C.; Hasegawa, J. Y.; Nozaki, K.; Ema, T., Aluminum porphyrins with quaternary ammonium halides as catalysts for copolymerization of cyclohexene oxide and CO2: metal-ligand cooperative catalysis. *Chem. Sci.* **2020,** *11* (22), 5669-5675.

12.   Rosetto, G.; Deacy, A. C.; Williams, C. K., Mg(ii) heterodinuclear catalysts delivering carbon dioxide derived multi-block polymers. *Chemical Science* **2021**.

13.   Abel, B. A.; Lidston, C. A. L.; Coates, G. W., Mechanism-Inspired Design of Bifunctional Catalysts for the Alternating Ring-Opening Copolymerization of Epoxides and Cyclic Anhydrides. *J. Am. Chem. Soc.* **2019,** *141* (32), 12760-12769.

14.   Li, H.; Luo, H. T.; Zhao, J. P.; Zhang, G. Z., Well-Defined and Structurally Diverse Aromatic Alternating Polyesters Synthesized by Simple Phosphazene Catalysis. *Macromolecules* **2018,** *51* (6), 2247-2257.

15.   Luchini, G.; Alegre-Requena, J. V.; Funes-Ardoiz, I.; Paton, R. S., GoodVibes: automated thermochemistry for heterogeneous computational chemistry data. *F1000Research* **2020,** *9*.

16.   Grimme, S., Supramolecular binding thermodynamics by dispersion-corrected density functional theory. *Chem. Eur. J.* **2012,** *18* (32), 9955-64.

17.   Scalmani, G.; Frisch, M. J., Continuous surface charge polarizable continuum models of solvation. I. General formalism. *J. Chem. Phys.* **2010,** *132* (11), 114110.